



ELSEVIER

Nuclear Physics B 487 [FS] (1997) 529–632

NUCLEAR
PHYSICS B

New renormalization group results for scaling of self-avoiding tethered membranes

Kay Jörg Wiese¹, François David^{2,3}*Service de Physique Théorique, C.E.A. Saclay, F-91191 Gif-sur-Yvette Cedex, France*

Received 12 August 1996; accepted 10 October 1996

Abstract

The scaling properties of self-avoiding polymerized two-dimensional membranes are studied via renormalization group methods based on a multilocal operator product expansion. The renormalization group functions are calculated to second order. This yields the scaling exponent ν to order ε^2 . Our extrapolations for ν agree with the Gaussian variational estimate for large space dimension d and are close to the Flory estimate for $d = 3$. The interplay between self-avoidance and rigidity at small d is briefly discussed.

PACS: 68.10.-m; 05.70.-Fh; 11.10.Gh; 11.25.-w

Keywords: Renormalization; Non-local field theories; Self-avoiding tethered membranes; Scaling; Polymerized membranes

1. Introduction

The statistical properties of polymerized flexible membranes are an interesting subject [1], which is still only partially understood. These objects, also called tethered membranes, are two-dimensional generalizations of polymers (one-dimensional flexible chains). It is expected that such two-dimensional membranes exhibit a larger variety of behavior than polymers, when the temperature and the elastic properties of the membranes are varied. One reason is the following: simple dimensional analysis shows that for two-dimensional films, the bending rigidity modulus has the dimension of a pure energy and is therefore marginally relevant (in the sense of the renormalization

¹ E-mail: wiese@amoco.saclay.cea.fr

² E-mail: david@amoco.saclay.cea.fr

³ Physique Théorique CNRS.

group) [2]. Moreover, two-dimensional membranes may have internal shear elasticity and this separates two very different classes of flexible membranes: fluid membranes with zero shear modulus and crystalline (or tethered) membranes with non-zero shear modulus [3].

In this paper, we consider tethered membranes. As long as one takes into account only the local elastic forces (i.e. bending rigidity, compression and shear moduli), numerical simulations and analytical calculations point towards a consistent and relatively well understood picture [4,5,42,6–8]. For high rigidity or equivalently low temperature, the membrane is in a flat phase with an average orientation and a classical “fractal” dimension $d_F = 2$. The roughness properties of this flat phase are nevertheless non-trivial, due to the non-linear coupling between undulation modes and phonons. For low rigidity or equivalently high temperature, the membrane is in a crumpled phase, without any global orientation. In this phase the statistics of the surface is Gaussian (at large length scales) and its fractal dimension is infinite ($d_F = \infty$). The two phases are separated by a crumpling transition, which occurs for a finite bending rigidity (or equivalently a non-zero temperature). Numerical simulations and some of the analytical calculations indicate that this transition is continuous and characterized by non-trivial critical exponents.

The above results do not take into account steric interactions, that is local self-avoidance and thus concern “phantom surfaces”. For membranes ($D = 2$) these interactions must be relevant for the crumpled phase (at large length scales), whatever the bulk dimension d of space is, since the fractal dimension of phantom surfaces is then infinite. They are expected to be strongly relevant for physical membranes in three-dimensional space ($d = 3$). This is in contrast with polymers, where steric interactions are relevant only for $d \leq 4$ and lead to a swollen phase in dimensions $1 < d < 4$ with $1 < d_F < 2$.

The study of the effect of self-avoidance for tethered membranes is in fact much more difficult than for polymers. Most of the studies rely on numerical simulations, which find evidence for a flat phase in three dimensions [9,19]. Some experiments have been performed using thin sheets of graphite oxide, but the results are contradictory. In [24] but not in [25] a swollen crumpled phase is found.

In order to study theoretically self-avoiding membranes, one can use standard approximations, such as the Flory approach or variational methods. A more systematic renormalization group approach has been initiated in [27,28]. This approach is inspired from the direct renormalization method used for polymers [29]. It is a perturbative method and it has been used to calculate the fractal exponent $\nu^* = 2/d_F$ at first order in an ε -expansion [27,28,30]. An important problem has been to check the internal consistency of this renormalization method and to extend it properly to all orders in perturbation theory. This has been completed by B. Duplantier, E. Guitter and one of the authors in [31] (a detailed proof might be released soon [32]), who have shown that the model of self-avoiding membranes of [27,28], although corresponding to a *non-local* field theory, is renormalizable in perturbation theory. This result establishes the validity of the $\mathcal{O}(\varepsilon)$ calculations and gives a systematic formalism to extend these calculations to higher orders.

In this paper we present for the first time in full details the renormalization group calculation at second order for the model of self-avoiding tethered membranes and discuss the results obtained by this approach. A short presentation of the main results has already appeared in [33].

This study is interesting for several reasons:

- (1) It provides an explicit realization of the renormalization formalism of [31]. In particular these calculations illustrate nicely how subdominant divergences are organized.
- (2) The calculation is a non-trivial task. As usual in renormalization theory, there is a long way from existence and convergence theorems to actual calculations, but additional difficulties are present here. In particular, beyond first order, the amplitudes (which are called manifold integrals and generalize in a non-trivial way Feynman integrals in the Schwinger representation to non-integer dimensions $0 < D < 2$) cannot be calculated analytically and in fact describe distributions. One must rely on numerical estimates for these integrals.
- (3) It leads to the first estimates at order $\mathcal{O}(\varepsilon^2)$ for the fractal exponent $\nu^* = 2/d_F$. This allows to check the validity of the $\mathcal{O}(\varepsilon)$ estimates, as well as the consistency of the extrapolation methods used to extract these estimates. Indeed, direct calculations for two-dimensional membranes are impossible, but the model is extended to “membranes” with internal dimension $0 < D < 2$, thus interpolating between polymers ($D = 1$) and membranes ($D = 2$). Perturbative calculations lead to an ε -expansion, where the ε -parameter is given by

$$\varepsilon = \varepsilon(D, d) = 2D - d \frac{(2 - D)}{2}. \quad (1.1)$$

D is the internal dimension of the membrane and d the dimension of bulk space (in which the membrane fluctuates). Using the ε -expansion one may start a-priori from any point (D_0, d_0) such that $\varepsilon(D_0, d_0) = 0$ to extrapolate to (for instance) the physical point $(D = 2, d = 3)$. In [30] an extrapolation scheme was used for $\mathcal{O}(\varepsilon)$ calculations. We shall need and will develop more systematic extrapolation schemes for $\mathcal{O}(\varepsilon^2)$ calculations and we shall discuss their respective advantages.

- (4) Finally, the calculations can be performed for membranes ($D = 2$) in a space with arbitrary dimension d and we can compare explicitly our $\mathcal{O}(\varepsilon^2)$ results for ν^* with other predictions. It turns out that our estimates are quite reliable for large d and in remarkable agreement with the result of a Gaussian variational estimate. We shall explain this fact and argue that this feature persists at higher order in perturbation theory. For smaller d the results are less stable, but still good and in reasonable agreement with Flory estimates (we have no good explanation for this fact).

The paper is organized as follows.

In Section 2 the continuous model of self-avoiding tethered membranes of [27,28] is introduced. It is a generalization of the Edwards model for polymers. We recall the basic results of [31,32] concerning the structure of the perturbative expansion for the model,

the nature of the short distance, or ultra-violet (UV), divergences and their relation with the so-called multilocal operator product expansion (MOPE).

In Section 3 we recall the renormalization of the model at first order in perturbation theory (one loop), give the explicit expressions for the counterterms in the “minimal subtraction scheme” used in this paper and derive the renormalization group functions $\beta(b)$ and $\nu(b)$ at one loop. The results are of course not new, but this fixes the method and the notations used throughout the paper.

In Section 4 we analyze the UV divergences at second order (two loops), and obtain the expressions for the two-loop counterterms, in terms of singular parts of integrals of MOPE coefficients. First the UV-singular configurations (divergent and subdivergent diagrams) are identified (Subsection 4.1), then the leading UV divergences (poles in $1/\varepsilon^2$) are obtained and their exponentiation (predicted by renormalization group) checked (Subsection 4.2). This allows to obtain the subleading divergences (poles in $1/\varepsilon$), whose residues give the renormalization group functions at two loops (Subsection 4.3). We then express these residues as combinations of convergent integrals involving MOPE coefficients (Subsection 4.4).

The next seven sections are devoted to the explicit calculation of these integrals. In Section 5 we briefly introduce some basic analytical methods used in the calculations, which have been developed in [34]. These are: (1) the definition of the “distance measure” which allows to define properly the integration over non-integer dimensional space \mathbb{R}^D ($0 < D < 2$); (2) the expression of the residue of the UV poles in $(1/\varepsilon)$ as a boundary term in the distance integrals; (3) the “conformal mapping” technique, which allows to map different domains of integration and leads to crucial simplifications.

Sections 6, 7 and 8 are devoted to the numerical calculation of the three diagrams which contribute to the coupling constant renormalization. In all cases, we start from the corresponding MOPE coefficients and determine explicitly the integrals which have to be computed (this is in general not straightforward). Then we evaluate numerically these integrals for values of $1 < D < 2$ (the internal dimension of the membrane). We have in general to decompose the domain of distance integration into several pieces, called sectors, and to find ad hoc changes of variables in each sector. In addition, this requires an adaptive Monte Carlo integration routine, first developed in [34], in order to master the rapid variations of the integrand. For the diagram of Section 7 there are additional subtleties, arising from the fact that the measure of integration is then a distribution, with non-integrable singularities on some boundary of the integration domain, which have to be treated by a finite part prescription. For each diagram we compute analytically its $D \rightarrow 1$ limit. This provides a check of the numerics. Secondly for $D = 1$ our model reduces to the Edwards model for polymers, for which two-loop calculations have already been performed by several authors and which give an additional check of our calculations.

Sections 9, 10 and 11 are devoted to the numerical calculation of the three diagrams which contribute to the field renormalization and are organized in a similar way.

In Section 12 we use these two-loop results to calculate critical exponents for self-avoiding membranes. First we recall how the renormalization group functions at two

loops are related to the counterterms that we have calculated (Subsection 12.1) and thus obtain the ε^2 term for the fractal exponent ν^* . Then as explained above, we have to set up extrapolation methods to extrapolate from the ε -expansion to the physical case $D = 2$. We generalize and systematize the extrapolation method proposed by Hwa [30], and use our new schemes to evaluate ν^* for membrane for various bulk space dimensions $2 \leq d < \infty$ (Subsection 12.2). In Subsection 12.3 our results are compared with that of the Gaussian variational method. We argue that ν^* , as obtained from the (properly resummed) ε -expansion, must coincide with the variational estimate ν_{var} for large d and we propose a new ε -expansion for ν^* which coincides with ν_{var} at order ε^0 and which is shown to give very good results for large d . In Subsection 12.4 we compare our results for ν^* with that of the Flory method and consider a similar new ε -expansion around ν_{Flory} . The results of all the two-loop extrapolations for ν^* are summarized in Subsection 12.5. Finally we briefly discuss the case of other scaling exponents for self-avoiding membranes, namely the correction to scaling exponent ω and the contact exponent θ_2 (Subsection 12.6), as well as the fractal exponent ν^θ for membranes at the tri-critical θ -point, which has been already calculated at order ε . In Subsection 12.8 we briefly summarize the main results from numerical simulations as well as experimental data. We also present a heuristic argument which explains why both in numerical simulations and experiments self-avoiding tethered membranes are found in a flat phase (Subsection 12.9).

Conclusions and future prospects are given in Section 13. Several technical points or examples are gathered in the appendices.

2. Definition of the model

We start from the continuous model for a D -dimensional flexible polymerized membrane introduced in [27,28]. This model is a simple extension of the well-known Edwards model for continuous chains. The membrane fluctuates in d -dimensional space. Points in the membrane are labeled by coordinates $x \in \mathbb{R}^D$ and the configuration of the membrane in physical space is described by the field $\mathbf{r} : x \in \mathbb{R}^D \rightarrow \mathbf{r}(x) \in \mathbb{R}^d$. The free energy for a configuration is given by the bare Hamiltonian

$$\mathcal{H}[\mathbf{r}] = \frac{1}{2-D} \int_x \frac{1}{2} (\nabla \mathbf{r}(x))^2 + b \int_x \int_y \tilde{\delta}^d(\mathbf{r}(x) - \mathbf{r}(y)). \quad (2.1)$$

The integral \int_x runs over D -dimensional space and ∇ is the usual gradient operator. The normalizations (hidden in $\frac{1}{2-D}$, \int_x and $\tilde{\delta}^d(\mathbf{r} - \mathbf{r}')$) are chosen in order to simplify the calculations, but are unimportant for the general understanding (see Appendix A). The first term is a Gaussian elastic energy which is known to describe the free “phantom” surface. The interaction term corresponds to a weak repulsive contact interaction (for $b > 0$). The expectation value of physical observables are obtained by performing the average over all field configurations $\mathbf{r}(x)$ with the Boltzmann weight $e^{-\mathcal{H}[\mathbf{r}]}$.

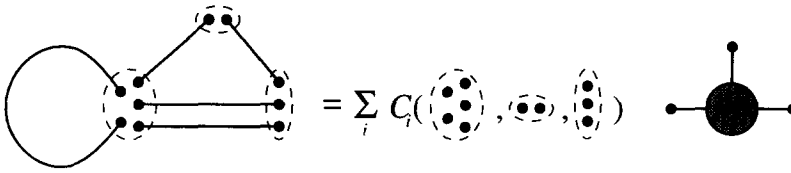


Fig. 2.1. Example of a contraction.

$$b^n \iint \dots \iint \langle \bigcirc \bullet \text{---} \bullet \dots \bullet \text{---} \bullet \rangle_0, \quad (2.9)$$

where the integral runs over the positions of all dipole endpoints. The analysis in [38] shows that UV divergencies appear when some dipole-endpoints approach each other. The divergencies are analyzed via a multilocal operator product expansion (MOPE). The principle is exemplified in Fig. 2.1. One considers n dipoles (here $n = 5$) and one separates the $2n$ endpoints into m separate subsets (here $m = 3$) delimited by the dashed lines. The MOPE describes how the product of these n dipoles behaves when the points inside each of the m subsets are contracted towards a single point z . The result is a sum over multilocal operators $\Phi\{z_1, \dots, z_m\}$, depending on the m points z_1, \dots, z_m , of the form

$$\sum_{\Phi} C_{\Phi} \Phi\{z_1, z_2, \dots, z_m\}, \quad (2.10)$$

where the MOPE-coefficients C_{Φ} depend only on the relative distances $x_i - x_j$ between the dipole endpoint positions x_i inside each subset. This expansion is valid as an operator identity, i.e. inserted in any expectation value and in the limit of small distances between contracted points. As the Hamiltonian (2.1) does not contain any mass-scale, the MOPE coefficients are homogeneous function of the relative positions between the contracted points. The degree of homogeneity is given by simple dimensional analysis. In the case considered here, where n dipoles are contracted to an operator Φ , this degree is simply (for the definition of ν see (2.3))

$$\text{degree}[C_{\Phi}^n] = -n\nu d + [\Phi], \quad (2.11)$$

where $[\Phi]$ is the canonical dimension of the operator Φ and $d(2 - D)/2$ is simply the canonical dimension of the dipole.

In order to evaluate the associated singularity, one has finally to integrate over all relative distances inside each subset. This gives an additional scale factor with degree $D(2n - m)$. A singular configuration, such as depicted in Fig. 2.1, will be UV-divergent if its degree of divergence, defined as $D(2n - m) + \text{deg}[C_{\Phi}^m]$, is negative. It is superficially divergent if the degree is zero and convergent otherwise.

The power-counting analysis of [31,32] shows that at the critical dimension $\varepsilon = 0$ the identity operator \bullet is relevant, while the local operator $\text{---}\text{---}\text{---}$ and the bi-local dipole operator $\bullet \text{---} \bullet$ are marginally relevant. Contractions of n dipoles to \bullet give relevant divergences (negative powers of the short distance cut-off, or poles for some $\varepsilon > 0$),

while contractions towards $\text{---}\nabla$ and $\bullet\text{---}\bullet$ give superficial divergences (logarithms of the cut-off, or poles at $\varepsilon = 0$).

The analysis of the renormalization in [31,32] shows that in order to make perturbation theory UV-finite at $\varepsilon = 0$, one has to add to the Hamiltonian counterterms proportional to all relevant and marginal operators. These counterterms are obtained from the MOPE coefficients, integrated with some IR-cutoff procedure.

3. Renormalization at one-loop order

Let us continue on the concrete example of the one-loop divergences, where we shall also fix our notations for the MOPE coefficients. When the endpoints (x, y) of a single dipole are contracted to a point (taken here to be the center-of-mass $z = (x + y)/2$), the MOPE is

$$\left(\text{dipole} \right) = \left(\text{dipole} \mid \bullet \right) \bullet + \left(\text{dipole} \mid \text{---}\nabla_{\alpha\beta} \right) \text{---}\nabla_{\alpha\beta} + \dots \quad (3.1)$$

with the first MOPE coefficients given explicitly by

$$\begin{aligned} \left(\text{dipole} \mid \bullet \right) &= |x - y|^{-\nu d}, \\ \left(\text{dipole} \mid \text{---}\nabla_{\alpha\beta} \right) &= -\frac{1}{2} |x - y|^{-\nu(d+2)} (x - y)_\alpha (x - y)_\beta \end{aligned} \quad (3.2)$$

and where $\text{---}\nabla_{\alpha\beta}$ denotes the local tensor operator

$$\text{---}\nabla_{\alpha\beta} = \frac{1}{2} \partial_\alpha \mathbf{r} \partial_\beta \mathbf{r}. \quad (3.3)$$

The integral over the relative distance $x - y$ for

$$\left(\text{dipole} \mid \text{---}\nabla_{\alpha\beta} \right)$$

is at $\varepsilon = 0$ logarithmically divergent.

The simplest contraction to a dipole is when two dipoles collapse. The corresponding MOPE coefficient is

$$\left(\text{two dipoles} \mid \bullet\text{---}\bullet \right) = (|x|^{2\nu} + |y|^{2\nu})^{-d/2}, \quad (3.4)$$

where x and y are now the relative distances inside the two subsets. Another possibility is to consider the contraction $\bullet\text{---}\text{dipole}$. But as

$$\left(\begin{array}{c} \text{---} \bullet \text{---} \bullet \text{---} \bullet \text{---} \\ \text{---} \bullet \text{---} \bullet \text{---} \bullet \text{---} \\ \text{---} \bullet \text{---} \bullet \text{---} \bullet \text{---} \end{array} \right) = \left(\begin{array}{c} \text{---} \bullet \text{---} \bullet \text{---} \bullet \text{---} \\ \text{---} \bullet \text{---} \bullet \text{---} \bullet \text{---} \\ \text{---} \bullet \text{---} \bullet \text{---} \bullet \text{---} \end{array} \right) = \left(\begin{array}{c} \text{---} \bullet \text{---} \bullet \text{---} \bullet \text{---} \\ \text{---} \bullet \text{---} \bullet \text{---} \bullet \text{---} \\ \text{---} \bullet \text{---} \bullet \text{---} \bullet \text{---} \end{array} \right) = \left(\begin{array}{c} \text{---} \bullet \text{---} \bullet \text{---} \bullet \text{---} \\ \text{---} \bullet \text{---} \bullet \text{---} \bullet \text{---} \\ \text{---} \bullet \text{---} \bullet \text{---} \bullet \text{---} \end{array} \right) \quad (3.5)$$

this does not give a pole at $\varepsilon = 0$, but a term proportional to the relevant divergence (that we discuss now), times a regular contribution.

In the next step counterterms have to be introduced in order to subtract these divergencies. We have to distinguish between the counterterm for the relevant operator and those for marginal operators. The first one can be defined by analytic continuation, the latter require a subtraction scale. Indeed, the divergence for \bullet is given by the integral

$$\int_{A^{-1} < |x-y| < L} \left(x \begin{array}{c} \text{loop} \\ \text{---} y \end{array} \middle| \bullet \right) = \int_{A^{-1}}^L \frac{dx}{x} x^{D-vd} = \frac{1}{D-\varepsilon} (A^{D-\varepsilon} - L^{\varepsilon-D}) , \quad (3.6)$$

where A is a high-momentum UV-regulator and L a large distance regulator. For $\varepsilon \approx 0$ this is UV-divergent but IR-convergent. The simplest way to subtract this divergence is therefore to replace the dipole operator by

$$X \xrightarrow{\quad} Y \longrightarrow X \cdots \cdots Y, \quad (3.7)$$

where $\bullet_x \cdots \bullet_y = |x - y|^{-vd}$. This amounts to add to the bare Hamiltonian (2.1) the UV-divergent counterterm

$$\Delta\mathcal{H}[r] = -\frac{b}{2} \int_x \int_y |x-y|^{-\nu d}, \quad (3.8)$$

which is a pure number and thus does not change the expectation value of any physical observable. This prescription is sufficient to subtract all relevant UV divergences in the calculation of the renormalization-group functions at two-loop order, that we present in the next sections.

We now treat marginal operators. Let us come back to the MOPE (3.1). The integral over the relative distance of

$$\int_{x=y} \left(\begin{array}{c} \text{loop with two vertices} \\ \text{one vertex is } x, \text{ the other is } y \\ \text{the two vertices are connected by a dashed line} \end{array} \middle| \begin{array}{c} \text{cross with } \alpha\beta \end{array} \right) \begin{array}{c} \text{cross with } \alpha\beta \end{array}$$

is logarithmically divergent at $\varepsilon = 0$. In order to find the appropriate counterterm, we use dimensional regularization, i.e. set $\varepsilon > 0$. An IR-cutoff L , or equivalently a subtraction momentum scale $\mu = L^{-1}$, has to be introduced in order to define the subtraction operation. As a general rule, let us integrate over all distances appearing in the MOPE coefficient, bounded by the subtraction scale $L = \mu^{-1}$. This projects the tensor operator $\bigcirc_{\alpha\beta}$ onto the scalar \bigcirc , times the integral

$$\int_{|x-y|<L} \left(\text{diagram} \right) = \left\langle \text{diagram} \right\rangle_L = L^\varepsilon f(\varepsilon, D). \quad (3.9)$$

Following Refs. [31,32,34] we use a minimal subtraction scheme (MS). The internal dimension of the membrane D is kept fixed and (3.9) is expanded as a Laurent series in ε , which here starts at ε^{-1} . Denoting by $\langle \text{diagram} \rangle_{\varepsilon^p}$ the term of order ε^p of the Laurent expansion of $\langle \text{diagram} \rangle_L$ for $L = 1$, the pure pole part of (3.9) is found to be

$$\left\langle \text{diagram} \right\rangle_{\varepsilon^{-1}} = -\frac{1}{2D} \frac{1}{\varepsilon}. \quad (3.10)$$

It is this pole term that we are going to subtract in the MS scheme. This is done by adding to the Hamiltonian a counterterm

$$\Delta\mathcal{H}[r] = -b \left\langle \text{diagram} \right\rangle_{\varepsilon^{-1}} \int_x \text{diagram}. \quad (3.11)$$

Similarly, the divergence arising from the contraction of two dipoles into a single dipole is subtracted by a counterterm proportional to the single pole of

$$\begin{aligned} \left\langle \text{diagram} \right\rangle_L &= \int_{|x|<L} \int_{|y|<L} \left(\text{diagram} \right) \\ &= \int_{|x|<L} \int_{|y|<L} (|x|^{2\nu} + |y|^{2\nu})^{-d/2}. \end{aligned} \quad (3.12)$$

As a result, the model is UV-finite if we use the renormalized Hamiltonian \mathcal{H}_R

$$\mathcal{H}_R[r] = \frac{Z}{2-D} \int_x \frac{1}{2} (\nabla \mathbf{r}(x))^2 + b Z_b \mu^\varepsilon \int_x \int_y \tilde{\delta}^d(\mathbf{r}(x) - \mathbf{r}(y)), \quad (3.13)$$

instead of the bare Hamiltonian $\mathcal{H}[r]$. Now r and b are the renormalized field and coupling constant, and $\mu = L^{-1}$ is the renormalization momentum scale. The renormalization factors are at one loop

$$Z = 1 - (2-D) \left\langle \text{diagram} \right\rangle_{\varepsilon^{-1}} b + \mathcal{O}(b^2), \quad (3.14)$$

$$Z_b = 1 + \left\langle \text{diagram} \right\rangle_{\varepsilon^{-1}} b + \mathcal{O}(b^2). \quad (3.15)$$

The renormalized theory can be reexpressed in terms of the bare (unrenormalized) theory through

$$\mathbf{r}_0(x) = Z^{1/2} \mathbf{r}(x), \quad b_0 = b Z_b Z^{d/2} \mu^\varepsilon. \quad (3.16)$$

Following the analysis of [31], the renormalization group β -function and the anomalous scaling dimension ν of r are obtained from the variation of the coupling constant and the field with respect to the renormalization scale μ , keeping the bare couplings fixed. They are written in terms of Z and Z_b as

$$\beta(b) = \mu \frac{\partial}{\partial \mu} \bigg|_{b_0} b = \frac{-\varepsilon b}{1 + b \frac{\partial}{\partial b} \ln Z_b + \frac{d}{2} b \frac{\partial}{\partial b} \ln Z}, \quad (3.17)$$

$$\nu(b) = \frac{2-D}{2} - \frac{1}{2} \mu \frac{\partial}{\partial \mu} \bigg|_{b_0} \ln Z = \frac{2-D}{2} - \frac{1}{2} \beta(b) \frac{\partial}{\partial b} \ln Z. \quad (3.18)$$

4. Derivation of the counterterms at two-loop order

4.1. The two-loop counterterms in the MS scheme

In this section we apply the formalism explained above to determine the counterterms which renormalize the theory at second order. If we consider only the bare theory, given by the bare Hamiltonian (2.1), power counting gives the three UV-divergent diagrams (together with their symmetry factors)

$$(a) \frac{1}{2} \text{ (diagram)}, \quad (b) \frac{2}{3} \text{ (diagram)}, \quad (c) 2 \text{ (diagram)} \quad (4.1)$$

which give short distance singularities when the points inside the subsets are contracted to a single point. These singularities give double and single poles at $\varepsilon = 0$. There are two other potentially dangerous diagrams,

$$\text{(diagram)} \quad , \quad \text{(diagram)} \quad . \quad (4.2)$$

These diagrams do not give poles at $\varepsilon = 0$ for reasons similar to what happens with (3.5). Now one has to remember that the model is already renormalized at one-loop, i.e. that we use the renormalized Hamiltonian (3.13), with the counterterms (3.14) and (3.15). As a consequence there are five additional divergent diagrams, which come from the insertion of the one-loop counterterms

$$(d) \quad -2 \mu^{-\varepsilon} \text{ (diagram)} \left\langle \text{diagram} \right| \text{diagram} \rangle_{\varepsilon^{-1}},$$

$$(e) \quad -\mu^{-\varepsilon} \text{ (diagram)} \left\langle \text{diagram} \right| \text{diagram} \rangle_{\varepsilon^{-1}},$$

$$\begin{aligned}
\text{(f)} \quad & -\mu^{-\varepsilon} \left(\text{diagram with two vertices and a loop} \right) \left\langle \text{diagram with one vertex and a loop} \right\rangle_{\varepsilon^{-1}}, \\
\text{(g)} \quad & -2\mu^{-\varepsilon} \left(\text{diagram with two vertices and a loop} \right) \left\langle \text{diagram with one vertex and a loop} \right\rangle_{\varepsilon^{-1}}, \\
\text{(h)} \quad & \frac{1}{2}\mu^{-2\varepsilon} \left(\text{diagram with two vertices and a loop} \right) \left(\left\langle \text{diagram with one vertex and a loop} \right\rangle_{\varepsilon^{-1}} \right)^2.
\end{aligned} \tag{4.3}$$

There are other potentially divergent diagrams, analogous to those depicted in (4.2), which factorize into convergent diagrams.

The first four terms in (4.3) are a combination of a diagram divergent at one-loop order (giving a single pole) times a divergent one-loop counterterm (which gives another single pole). The fifth term is more peculiar: it is the combination of a convergent diagram (which corresponds to a contact term) times two one-loop counterterms (thus giving also a double pole).

Owing to the MOPE, diagrams (a), (e), (f) and (h) give a divergence proportional to the insertion of the local operator $\text{diagram with one vertex and a loop}$. With the notations introduced in the previous section, they can be subtracted by adding a counterterm proportional to the divergent part of the integral of the corresponding MOPE coefficients

$$\begin{aligned}
& \frac{1}{2} \left\langle \text{diagram with two vertices and a loop} \right\rangle_L - \mu^{-\varepsilon} \left\langle \text{diagram with one vertex and a loop} \right\rangle_L \left\langle \text{diagram with two vertices and a loop} \right\rangle_{\varepsilon^{-1}} \\
& - \mu^{-\varepsilon} \left\langle \text{diagram with two vertices and a loop} \right\rangle_L \left\langle \text{diagram with one vertex and a loop} \right\rangle_{\varepsilon^{-1}} \\
& + \frac{1}{2} \mu^{-2\varepsilon} \left\langle \text{diagram with two vertices and a loop} \right\rangle_L \left(\left\langle \text{diagram with one vertex and a loop} \right\rangle_{\varepsilon^{-1}} \right)^2.
\end{aligned} \tag{4.4}$$

Since we use the minimal subtraction scheme, we want to subtract only the double and single poles in ε at $\varepsilon = 0$. To isolate these poles, we have to perform a Laurent expansion of the various terms in (4.4) and to keep the terms of order ε^{-2} and ε^{-1} but to drop the analytic part. Setting the renormalization momentum scale $\mu = L^{-1}$, we obtain the final expression for the renormalization factor Z at two-loop order

$$\begin{aligned}
Z = & 1 - b(2-D) \left\langle \text{diagram with one vertex and a loop} \right\rangle_{\varepsilon^{-1}} \\
& + b^2(2-D) \left[\frac{1}{2} \left\langle \text{diagram with two vertices and a loop} \right\rangle_{\varepsilon^{-2}, \varepsilon^{-1}} \right]
\end{aligned}$$

$$\begin{aligned}
& - \left\langle \text{diagram 1} \mid \text{diagram 2} \right\rangle_{\varepsilon^{-1}, \varepsilon^0} \left\langle \text{diagram 3} \mid \text{diagram 4} \right\rangle_{\varepsilon^{-1}} \\
& - \left\langle \text{diagram 5} \mid \text{diagram 6} \right\rangle_{\varepsilon^{-1}, \varepsilon^0} \left\langle \text{diagram 7} \mid \text{diagram 8} \right\rangle_{\varepsilon^{-1}} \\
& + \frac{1}{2} \left\langle \text{diagram 9} \mid \text{diagram 10} \right\rangle_{\varepsilon^0, \varepsilon^1} \left(\left\langle \text{diagram 11} \mid \text{diagram 12} \right\rangle_{\varepsilon^{-1}} \right)^2 \\
& + \mathcal{O}(b^3).
\end{aligned} \tag{4.5}$$

Here $\langle \mid \rangle_{\varepsilon^{n_1}, \dots, \varepsilon^{n_p}}$ denotes the sum of the terms of order $\varepsilon^{n_1}, \dots, \varepsilon^{n_p}$ in the Laurent expansion of $\langle \mid \rangle_L$, taken at $L = 1$.

Similarly, the diagrams (b), (c), (e) and (f) give a divergence proportional to the bilocal operator $\bullet \text{---} \bullet$. An analogous analysis leads to the following expression for the coupling-constant renormalization factor Z_b at two loops

$$\begin{aligned}
Z_b = & 1 + b \left\langle \text{diagram 1} \mid \text{diagram 2} \right\rangle_{\varepsilon^{-1}} \\
& + b^2 \left[-\frac{2}{3} \left\langle \text{diagram 3} \mid \text{diagram 4} \right\rangle_{\varepsilon^{-2}, \varepsilon^{-1}} \right. \\
& + 2 \left\langle \text{diagram 5} \mid \text{diagram 6} \right\rangle_{\varepsilon^{-1}, \varepsilon^0} \left\langle \text{diagram 7} \mid \text{diagram 8} \right\rangle_{\varepsilon^{-1}} \\
& - 2 \left\langle \text{diagram 9} \mid \text{diagram 10} \right\rangle_{\varepsilon^{-2}, \varepsilon^{-1}} \\
& \left. + 2 \left\langle \text{diagram 11} \mid \text{diagram 12} \right\rangle_{\varepsilon^{-1}, \varepsilon^0} \left\langle \text{diagram 13} \mid \text{diagram 14} \right\rangle_{\varepsilon^{-1}} \right] \\
& + \mathcal{O}(b^3).
\end{aligned} \tag{4.6}$$

4.2. The leading divergences (double poles)

In fact we are interested only in the residues of the single poles, that is into the residues c_1 and f_1 in the Laurent expansion of the counterterms

$$\begin{aligned}
Z &= 1 + \frac{e_1}{\varepsilon} b + \left(\frac{f_1}{\varepsilon} + \frac{f_2}{\varepsilon^2} \right) b^2 + \mathcal{O}(b^3), \\
Z_b &= 1 + \frac{a_1}{\varepsilon} b + \left(\frac{c_1}{\varepsilon} + \frac{c_2}{\varepsilon^2} \right) b^2 + \mathcal{O}(b^3).
\end{aligned} \tag{4.7}$$

Indeed, the finiteness of the renormalization group functions (3.17) and (3.18) implies that the residues of the double poles, f_2 and c_2 , can be expressed in terms of the

one-loop residues e_1 and a_1 .

Let us show explicitly how this happens, since this will be useful in order to subtract efficiently the double poles in the counterterms. From the analysis at one-loop order, we know that

$$\frac{e_1}{\varepsilon} = -(2-D) \left\langle \text{Diagram 1} \middle| \text{Diagram 2} \right\rangle_{\varepsilon^{-1}}, \quad \frac{a_1}{\varepsilon} = \left\langle \text{Diagram 3} \middle| \text{Diagram 4} \right\rangle_{\varepsilon^{-1}} \quad (4.8)$$

and we obtain the one-loop RG functions

$$\beta(b) = -\varepsilon b + b^2 \left(\frac{de_1}{2} + a_1 \right), \quad \nu(b) = \frac{(2-D)}{2} + b \frac{e_1}{2}. \quad (4.9)$$

Inserting these one-loop RG functions into (3.17) and (3.18), yields differential equations for the counterterms Z and Z_b , whose solution is explicitly

$$Z^{(1)} = \left[1 - \frac{b}{\varepsilon} \left(\frac{de_1}{2} + a_1 \right) \right]^{-\frac{2e_1}{d\varepsilon_1 + 2a_1}}, \quad Z_b^{(1)} = \left[1 - \frac{b}{\varepsilon} \left(\frac{de_1}{2} + a_1 \right) \right]^{-\frac{2a_1}{d\varepsilon_1 + 2a_1}}. \quad (4.10)$$

This shows the exponentiation of the leading divergences, i.e. that the residue of the leading pole in ε^{-n} at order b^n is determined by the residue of the simple pole in ε^{-1} at order b . Expanding (4.10) to order b^2 , we obtain

$$Z^{(1)} = 1 + \frac{e_1}{\varepsilon} b + \frac{\tilde{f}_2(\varepsilon)}{\varepsilon^2} b^2 + \mathcal{O}(b^3), \quad Z_b^{(1)} = 1 + \frac{a_1}{\varepsilon} b + \frac{\tilde{c}_2(\varepsilon)}{\varepsilon^2} b^2 + \mathcal{O}(b^3) \quad (4.11)$$

with, in terms of diagrams,

$$\begin{aligned} \frac{\tilde{f}_2(\varepsilon)}{\varepsilon^2} &= -\nu \left\langle \text{Diagram 1} \middle| \text{Diagram 2} \right\rangle_{\varepsilon^{-1}} \\ &\times \left[\left\langle \text{Diagram 3} \middle| \text{Diagram 4} \right\rangle_{\varepsilon^{-1}} - \nu(d+2) \left\langle \text{Diagram 1} \middle| \text{Diagram 2} \right\rangle_{\varepsilon^{-1}} \right] \end{aligned} \quad (4.12)$$

$$\begin{aligned} \frac{\tilde{c}_2(\varepsilon)}{\varepsilon^2} &= \frac{1}{2} \left\langle \text{Diagram 3} \middle| \text{Diagram 4} \right\rangle_{\varepsilon^{-1}} \\ &\times \left[2 \left\langle \text{Diagram 3} \middle| \text{Diagram 4} \right\rangle_{\varepsilon^{-1}} - \nu d \left\langle \text{Diagram 1} \middle| \text{Diagram 2} \right\rangle_{\varepsilon^{-1}} \right]. \end{aligned} \quad (4.13)$$

Both $\tilde{f}_2(\varepsilon)$ and $\tilde{c}_2(\varepsilon)$ contain not only a constant term but also a term linear in ε . The latter is not fixed by the RG functions at one-loop order.

The leading poles of $Z^{(1)}$ and $Z_b^{(1)}$ must be equal to those of Z and Z_b . This implies that

$$f_2 = \tilde{f}_2(\varepsilon) + \mathcal{O}(\varepsilon), \quad c_2 = \tilde{c}_2(\varepsilon) + \mathcal{O}(\varepsilon). \quad (4.14)$$

This is compatible with the explicit expressions (4.5) and (4.6) for Z and Z_b . Indeed, one can directly calculate the double poles in (4.5) and (4.6). The simplest case is diagram (b) in (4.1). A subdivergence occurs when two dipoles are contracted to a single dipole. When this contraction is performed first, the MOPE coefficient factorizes as

$$\left(\text{diagram (b)} \right) \approx \left(\text{diagram (b)} \right) \left(\text{diagram (b)} \right). \quad (4.15)$$

There are three different subdivergences and one finally obtains that the double pole associated with this diagram is given by

$$\begin{aligned} \left\langle \text{diagram (b)} \right\rangle_{\epsilon^{-2}} &= 3 \times \frac{1}{2} \left\langle \text{diagram (b)} \right\rangle_{\epsilon^{-1}} \\ &\times \left\langle \text{diagram (b)} \right\rangle_{\epsilon^{-1}}. \end{aligned} \quad (4.16)$$

The factor $1/2$ comes from the nested integration [35]: the double pole results from the integration over a “sector” where the distances inside the subdiagram are smaller than all the other distances. This will become clear in the explicit calculations of the next sections.

Similarly, let us consider diagram (c) in (4.1). A subdivergence occurs when the single dipole to the right of the diagram is contracted to a point. The MOPE coefficient factorizes as

$$\left(\text{diagram (c)} \right) \approx \left(\text{diagram (c)} \right) \left(\text{diagram (c)} \right). \quad (4.17)$$

Consequently, the double pole for this diagram is

$$\begin{aligned} \left\langle \text{diagram (c)} \right\rangle_{\epsilon^{-2}} &= \frac{1}{2} \left\langle \text{diagram (c)} \right\rangle_{\epsilon^{-1}} \\ &\times \left\langle \text{diagram (c)} \right\rangle_{\epsilon^{-1}}, \end{aligned} \quad (4.18)$$

where the factor $1/2$ again comes from the nested integration.

Finally, let us consider diagram (a) in (4.1). Four sectors contribute to the double pole, which correspond to the subcontractions depicted here

$$\left(\text{diagram (a)} \right) \approx \left(\text{diagram (a)} \right) \left(\text{diagram (a)} \right),$$

$$\left(\text{diagram} \mid \text{operator} \right) \approx \left(\text{diagram} \mid \text{operator} \right) \left(\text{diagram} \mid \text{operator} \right). \quad (4.19)$$

Each of the contractions appears with a combinatorial factor two. The double pole for this diagram is therefore

$$\begin{aligned} \left\langle \text{diagram} \mid \text{operator} \right\rangle_{\varepsilon^{-2}} &= 2 \times \frac{1}{2} \left\langle \text{diagram} \mid \text{operator} \right\rangle_{\varepsilon^{-1}} \left\langle \text{diagram} \mid \text{operator} \right\rangle_{\varepsilon^{-1}} \\ &+ 2 \times \frac{1}{2} \left\langle \text{diagram} \mid \text{operator} \right\rangle_{\varepsilon^{-1}} \left\langle \text{diagram} \mid \text{operator} \right\rangle_{\varepsilon^{-1}}. \end{aligned} \quad (4.20)$$

Inserting (4.16), (4.18) and (4.20) in the explicit expressions for the two-loop counterterms (4.5) and (4.6) we apparently do not obtain for the double poles the results (4.12) and (4.13) predicted by the renormalization group. However, we can make use of the equation of motion to compute the effect of the insertion of the operator operator in the counterterms. In Appendix C we show that

$$\left\langle \text{diagram} \mid \text{operator} \right\rangle_{\varepsilon^{-1}} = -\frac{\nu d}{2} \left\langle \text{diagram} \mid \text{operator} \right\rangle_{\varepsilon^{-1}} + \mathcal{O}(\varepsilon^0), \quad (4.21)$$

$$\begin{aligned} \left\langle \text{diagram} \mid \text{operator} \right\rangle_{\varepsilon^{-1}} &= -\nu(d+2) \left\langle \text{diagram} \mid \text{operator} \right\rangle_{\varepsilon^{-1}} \\ &+ \left\langle \text{diagram} \mid \text{operator} \right\rangle_{\varepsilon^{-1}} \left\langle \text{diagram} \mid \text{operator} \right\rangle_{\varepsilon^0} + \mathcal{O}(\varepsilon^0). \end{aligned} \quad (4.22)$$

Using these identities one recovers (4.12) and (4.13).

4.3. The subleading divergences (single poles)

We can now give the expressions for the residues of the single poles. For the single pole of Z we find

$$\begin{aligned} \frac{f_1}{\varepsilon} &= \frac{(2-D)}{2} \left[\left\langle \text{diagram} \mid \text{operator} \right\rangle_{\varepsilon^{-2}, \varepsilon^{-1}} \right. \\ &+ \left\langle \text{diagram} \mid \text{operator} \right\rangle_{\varepsilon^1} \left(\left\langle \text{diagram} \mid \text{operator} \right\rangle_{\varepsilon^{-1}} \right)^2 \\ &- \left\langle \text{diagram} \mid \text{operator} \right\rangle_{\varepsilon^{-1}} \left\langle \text{diagram} \mid \text{operator} \right\rangle_{\varepsilon^{-1}} \end{aligned}$$

$$\begin{aligned}
& -2 \left\langle \text{diagram 1} \mid \text{diagram 2} \right\rangle_{\varepsilon^0} \left\langle \text{diagram 3} \mid \text{diagram 4} \right\rangle_{\varepsilon^{-1}} \\
& - \left\langle \text{diagram 5} \mid \text{diagram 6} \right\rangle_{\varepsilon^{-1}} \left\langle \text{diagram 7} \mid \text{diagram 8} \right\rangle_{\varepsilon^{-1}} \\
& -2 \left\langle \text{diagram 9} \mid \text{diagram 10} \right\rangle_{\varepsilon^0} \left\langle \text{diagram 11} \mid \text{diagram 12} \right\rangle_{\varepsilon^{-1}} \Bigg] . \tag{4.23}
\end{aligned}$$

One can simplify this expression, since the explicit calculation shows that

$$\left\langle \text{diagram 13} \mid \text{diagram 14} \right\rangle_{\varepsilon^1} = 0, \quad \left\langle \text{diagram 15} \mid \text{diagram 16} \right\rangle_{\varepsilon^0} = 0. \tag{4.24}$$

For the single pole of Z_b the result is

$$\begin{aligned}
\frac{c_1}{\varepsilon} = & \left[-\frac{2}{3} \left\langle \text{diagram 17} \mid \text{diagram 18} \right\rangle_{\varepsilon^{-2}, \varepsilon^{-1}} \right. \\
& + \left\langle \text{diagram 19} \mid \text{diagram 20} \right\rangle_{\varepsilon^{-1}} \left\langle \text{diagram 21} \mid \text{diagram 22} \right\rangle_{\varepsilon^{-1}} \\
& + 2 \left\langle \text{diagram 23} \mid \text{diagram 24} \right\rangle_{\varepsilon^0} \left\langle \text{diagram 25} \mid \text{diagram 26} \right\rangle_{\varepsilon^{-1}} \\
& - 2 \left\langle \text{diagram 27} \mid \text{diagram 28} \right\rangle_{\varepsilon^{-2}, \varepsilon^{-1}} \\
& + \left\langle \text{diagram 29} \mid \text{diagram 30} \right\rangle_{\varepsilon^{-1}} \left\langle \text{diagram 31} \mid \text{diagram 32} \right\rangle_{\varepsilon^{-1}} \\
& \left. + 2 \left\langle \text{diagram 33} \mid \text{diagram 34} \right\rangle_{\varepsilon^0} \left\langle \text{diagram 35} \mid \text{diagram 36} \right\rangle_{\varepsilon^{-1}} \right] . \tag{4.25}
\end{aligned}$$

4.4. Expressing the residues as convergent integrals

The next step is to evaluate the residues f_1 and c_1 , that is to write them as convergent integrals involving combinations of MOPE coefficients. It is convenient not to compute directly f_1 and c_1 , but rather to consider the $\mathcal{O}(\varepsilon^{-1})$ parts of the counterterms that are not already contained in the second-order resummation of the one-loop divergences, as given by (4.12) and (4.13). We thus denote

$$\frac{f_2}{\varepsilon^2} + \frac{f_1}{\varepsilon} = \frac{\tilde{f}_2(\varepsilon)}{\varepsilon^2} + \frac{\tilde{f}_1}{\varepsilon}, \quad \frac{c_2}{\varepsilon^2} + \frac{c_1}{\varepsilon} = \frac{\tilde{c}_2(\varepsilon)}{\varepsilon^2} + \frac{\tilde{c}_1}{\varepsilon}. \tag{4.26}$$

Using $d = 4D/(2 - D) - 2\varepsilon/(2 - D)$ it is easy to extract the $\mathcal{O}(\varepsilon^{-1})$ part of (4.12) and (4.13). With (4.8) we get

$$f_1 = \tilde{f}_1 - \frac{e_1^2}{2(2 - D)}, \quad c_1 = \tilde{c}_1 - \frac{e_1 a_1}{2(2 - D)}. \quad (4.27)$$

Now subtracting (4.12) from (4.5) yields an equivalent explicit expression for \tilde{f}_1

$$\begin{aligned} \frac{\tilde{f}_1}{2 - D} \frac{1}{\varepsilon} = & \frac{1}{2} \left\langle \text{diagram 1} \middle| \cdot \right\rangle_{\varepsilon^{-2}, \varepsilon^{-1}} - \left\langle \text{diagram 2} \middle| \cdot \right\rangle_{\varepsilon^{-1}} \left\langle \text{diagram 3} \middle| \cdot \right\rangle_{\varepsilon^{-2}, \varepsilon^{-1}} \\ & - \frac{\nu(d+2)}{2} \left\langle \text{diagram 4} \middle| \cdot \right\rangle_{\varepsilon^{-1}}^2 + \frac{1}{2} \left\langle \text{diagram 5} \middle| \cdot \right\rangle_{\varepsilon^{-1}}^2 \left\langle \text{diagram 6} \middle| \cdot \right\rangle_{\varepsilon^0} \\ & - \frac{1}{2} \left\langle \text{diagram 7} \middle| \cdot \right\rangle_{\varepsilon^{-1}} \left\langle \text{diagram 8} \middle| \cdot \right\rangle_{\varepsilon^{-1}}. \end{aligned} \quad (4.28)$$

Finally, one has to remember that $\left\langle \dots \middle| \cdot \right\rangle_{\varepsilon^p}$ are the terms of order ε^p of the Laurent series of the integral over distances of the corresponding MOPE coefficient

$$\left\langle \dots \middle| \cdot \right\rangle_L = \int_{\text{distances} \leq L} \left(\dots \middle| \cdot \right)_L. \quad (4.29)$$

Using this fact one obtains the following decomposition:

$$\frac{\tilde{f}_1}{2 - D} \frac{1}{\varepsilon} = \mathcal{F}_1 + \mathcal{F}_2 + \mathcal{F}_3 + \mathcal{O}(\varepsilon^0), \quad (4.30)$$

where each term can be written as a convergent integral. These terms are

$$\begin{aligned} \mathcal{F}_1 = & \frac{1}{2} \left\langle \text{diagram 1} \middle| \cdot \right\rangle_L - \frac{1}{2} \left\langle \text{diagram 2} \middle| \cdot \right\rangle_L \left\langle \text{diagram 3} \middle| \cdot \right\rangle_L \\ & - \frac{1}{2} \left\langle \text{diagram 7} \middle| \cdot \right\rangle_L \left\langle \text{diagram 8} \middle| \cdot \right\rangle_L, \end{aligned} \quad (4.31)$$

$$\begin{aligned} \mathcal{F}_2 = & -\frac{1}{2} \left\langle \text{diagram 4} \middle| \cdot \right\rangle_{\varepsilon^{-1}} \\ & \times \left(\left\langle \text{diagram 3} \middle| \cdot \right\rangle_L + \frac{(2 - D)(d + 2)}{2} \left\langle \text{diagram 5} \middle| \cdot \right\rangle_L \right. \\ & \left. - \left\langle \text{diagram 2} \middle| \cdot \right\rangle_L \left\langle \text{diagram 6} \middle| \cdot \right\rangle_L \right), \end{aligned} \quad (4.32)$$

$$\mathcal{F}_3 = \frac{1}{2} \left(\left\langle \text{diagram 1} \right\rangle_{\varepsilon^{-1}} \left(\left\langle \text{diagram 2} \right\rangle_L - \left\langle \text{diagram 3} \right\rangle_{\varepsilon^{-1}} \right) \right). \quad (4.33)$$

Even if not written explicitly, we will only calculate the residue of $\mathcal{F}_1, \dots, \mathcal{F}_3$ at $L = 1$. Similarly, subtracting (4.13) from (4.6) we obtain for \tilde{c}_1

$$\begin{aligned} \frac{\tilde{c}_1}{\varepsilon} = & - \left\langle \text{diagram 4} \right\rangle_{\varepsilon^{-1}}^2 \\ & + \frac{(2-D)d}{4} \left\langle \text{diagram 5} \right\rangle_{\varepsilon^{-1}} \left\langle \text{diagram 6} \right\rangle_{\varepsilon^{-1}} \\ & + 2 \left\langle \text{diagram 7} \right\rangle_{\varepsilon^{-1}} \left\langle \text{diagram 8} \right\rangle_{\varepsilon^{-1}, \varepsilon^0} \\ & - \frac{2}{3} \left\langle \text{diagram 9} \right\rangle_{\varepsilon^{-2}, \varepsilon^{-1}} - 2 \left\langle \text{diagram 10} \right\rangle_{\varepsilon^{-2}, \varepsilon^{-1}} \\ & + 2 \left\langle \text{diagram 11} \right\rangle_{\varepsilon^{-1}} \left\langle \text{diagram 12} \right\rangle_{\varepsilon^{-1}, \varepsilon^0} \end{aligned} \quad (4.34)$$

that we decompose as

$$\frac{\tilde{c}_1}{\varepsilon} = \mathcal{C}_1 + \mathcal{C}_2 + \mathcal{C}_3 + \mathcal{O}(\varepsilon^0), \quad (4.35)$$

with

$$\mathcal{C}_1 = -\frac{2}{3} \left\langle \text{diagram 13} \right\rangle_L + \left\langle \text{diagram 14} \right\rangle_L^2, \quad (4.36)$$

$$\begin{aligned} \mathcal{C}_2 = & -2 \left\langle \text{diagram 15} \right\rangle_L \\ & + \left\langle \text{diagram 16} \right\rangle_L \left\langle \text{diagram 17} \right\rangle_L, \end{aligned} \quad (4.37)$$

$$\begin{aligned} \mathcal{C}_3 = & \left\langle \text{diagram 18} \right\rangle_{\varepsilon^{-1}} \left(\left\langle \text{diagram 19} \right\rangle_L \right. \\ & \left. + \frac{(2-D)d}{4} \left\langle \text{diagram 20} \right\rangle_{\varepsilon^{-1}} \right). \end{aligned} \quad (4.38)$$

The coefficients \mathcal{C}_1 , \mathcal{C}_2 and \mathcal{C}_3 can like \mathcal{F}_1 , \mathcal{F}_2 and \mathcal{F}_3 be expressed as convergent integrals and will be calculated in the next sections.

5. General strategy and technical tools

In this section we give a brief overview over the analytical tools involved in the calculation of the Feynman-diagrams. These are the measure (Subsection 5.1), the procedure to extract the residue and the conformal mapping (Subsection 5.2).

5.1. Analytic continuation of the measure

We first define the explicit form for the integration measure in non-integer dimension D , that will be used in the calculations. We use the general formalism of distance geometry [37], which has been already used to construct other, but equivalent, representation for such measures.

The general problem is to integrate a function $f(x_1, \dots, x_N)$, which is invariant under Euclidean displacements (and therefore depends only on the $N(N-1)/2$ relative distances $|x_i - x_j|$ between these points) over the $N-1$ first points (the last point is fixed, using translational invariance) in \mathbb{R}^D for non-integer D . In order to define the integration, let us take $D \geq N-1$ and integer. For $i < N$ we denote by $y_i = x_i - x_N$ the i th distance vector and by y_i^a its a th component ($a = 1, \dots, D$).

The integral over y_1 is simple: Using rotation invariance, we fix y_1 to have only the $a = 1$ component non-zero. The measure becomes

$$\int d^D y_1 = S_D \int_0^\infty dy_1^1 (y_1^1)^{D-1}, \quad y_1 = (y_1^1, 0, \dots, 0), \quad (5.1)$$

where S_D is the volume of the unit sphere in \mathbb{R}^D , defined by

$$S_D = 2 \frac{\pi^{D/2}}{\Gamma(D/2)}. \quad (5.2)$$

We now fix y_2 to have only $a = 1$ and $a = 2$ as non-zero components. The integral over y_2 consists of the integration along the direction fixed by y_1 and the integration in the orthogonal space \mathbb{R}^{D-1} :

$$\int d^D y_2 = S_{D-1} \int_{-\infty}^\infty dy_2^1 \int_0^\infty dy_2^2 (y_2^2)^{D-2}, \quad y_2 = (y_2^1, y_2^2, 0, \dots, 0). \quad (5.3)$$

For the j th point, one proceeds recursively to integrate first over the hyperplane defined by y_1, \dots, y_{j-1} and then the orthogonal complement:

$$\int d^D y_j = S_{D-j+1} \prod_{a < j} \int_{-\infty}^\infty dy_j^a \int_0^\infty dy_j^j (y_j^j)^{D-j}, \quad y_j = (y_j^1, \dots, y_j^j, 0, \dots, 0). \quad (5.4)$$

The final result for an integral over all configurations of N points is

$$\int \prod_{j=1}^{N-1} d^D y_j = S_D S_{D-1} \cdots S_{D-N+2} \prod_{j=1}^{N-1} \left(\prod_{a=1}^{j-1} \int_{-\infty}^{\infty} dy_j^a \int_0^{\infty} dy_j^j (y_j^j)^{D-j} \right). \quad (5.5)$$

This expression for the measure, now written in terms of the $N(N-1)$ variables y_j^a , can be analytically continued to non-integer D . For $D \leq N-1$ this measure is not integrable when some $y_j^a = 0$. For D not integer, the integration is defined through the standard finite-part prescription. This means that the measure (5.5) becomes a distribution.

Let us make this explicit on the example of $N = 3$ points, following Refs. [37,34]. The measure is then

$$S_D S_{D-1} \int_0^{\infty} dy_1^1 (y_1^1)^{D-1} \int_{-\infty}^{+\infty} dy_2^2 \int_0^{\infty} dy_2^1 (y_2^1)^{D-2}. \quad (5.6)$$

It is well defined and integrable for $D > 1$. For $D = 1$ the integral over y_2^2 diverges logarithmically at $y_2^2 \rightarrow 0$, but this singularity is canceled by the zero of S_{D-1} and the measure becomes

$$2 \int_0^{\infty} dy_1^1 \int_{-\infty}^{+\infty} dy_2^1 \int_0^{\infty} dy_2^2 \delta(y_2^2) = \int_{\mathbf{R}} dy_1 \int_{\mathbf{R}} dy_2 \quad (5.7)$$

thus it reduces to the measure for two points on a line. For $0 < D < 1$ the integral over y_2^2 diverges at $y_2^2 \rightarrow 0$, but this divergence is treated by a finite part prescription.

For integrals over $N > 3$ points, a finite part prescription has already to be used for $D < 2$. This will be shown explicitly later. The expression (5.5) is equivalent to the measures defined in [37].

5.2. Extraction of the residue

We now explain how we extract the residue of the pole at $\varepsilon = 0$ for the example of the one-loop counterterms. Note from (3.1) that

$$\left\langle \text{diagram} \right\rangle_L = -\frac{1}{2D} \int_{x < L} x^{D-\nu d} = -\frac{1}{2D} \frac{1}{\varepsilon} L^\varepsilon. \quad (5.8)$$

We used the normalization of the measure

$$\int_x = \frac{1}{S_D} \int d^D x, \quad S_D = 2 \frac{\pi^{D/2}}{\Gamma(D/2)} \quad (5.9)$$

which was chosen to simplify the calculations (see Appendix A). The residue can most easily be extracted by applying $L \frac{\partial}{\partial L}$ to (5.8). This yields

$$\varepsilon \left\langle \left(\text{diagram: a circle with two dots inside, connected by a vertical line} \right) \middle| \text{diagram: a cross} \right\rangle_L = -\frac{1}{2D} L \int_{x=L} x^{D-\nu d} = -\frac{1}{2D} L^\varepsilon. \quad (5.10)$$

So the residue of (5.8) is

$$\varepsilon \left\langle \left(\text{diagram: a circle with two dots inside, connected by a vertical line} \right) \middle| \text{diagram: a cross} \right\rangle_{\varepsilon^{-1}} = \lim_{\varepsilon \rightarrow 0} L \frac{\partial}{\partial L} \left\langle \left(\text{diagram: a circle with two dots inside, connected by a vertical line} \right) \middle| \text{diagram: a cross} \right\rangle_L = -\frac{1}{2D}. \quad (5.11)$$

We can apply this recipe to the second one-loop counterterm:

$$\left\langle \left(\text{diagram: two circles with two dots each, connected by a vertical line} \right) \middle| \text{diagram: a cross} \right\rangle_L = \int_{x < L} \int_{y < L} \left(\text{diagram: two circles with two dots each, connected by a vertical line} \right) \quad (5.12)$$

since it is also proportional to L^ε . We thus have to calculate

$$L \frac{\partial}{\partial L} \left\langle \left(\text{diagram: two circles with two dots each, connected by a vertical line} \right) \middle| \text{diagram: a cross} \right\rangle_L = L \left[\int_{x < y=L} + \int_{y < x=L} \right] (x^{2\nu} + y^{2\nu})^{-d/2}. \quad (5.13)$$

We now introduce a general method which is very useful to manipulate and simplify such integrals. It relies on (global) conformal transformations in position space and is called conformal mapping of sectors. It has first been introduced in [34], where a geometric interpretation can be found. We will explain the method on a concrete example and then state the general result.

Let us consider the second integral on the r.h.s. of (5.13)

$$L \int_{y < x=L} (x^{2\nu} + y^{2\nu})^{-d/2} = L \int_0^\infty \frac{dx}{x} x^D \int_0^\infty \frac{dy}{y} y^D (x^{2\nu} + y^{2\nu})^{-d/2} \delta(x-L) \Theta(y < x). \quad (5.14)$$

Now two changes of variables are performed: The first one

$$x \rightarrow \tilde{x}, \quad x = \tilde{x} y L^{-1} \quad (5.15)$$

leads to

$$L^{1-D+\nu d} \int_0^\infty \frac{d\tilde{x}}{\tilde{x}} \tilde{x}^D \int_0^\infty \frac{dy}{y} y^{2D-\nu d} (\tilde{x}^{2\nu} + L^{2\nu})^{-d/2} \delta(\tilde{x} y L^{-1} - L) \Theta(L < \tilde{x}). \quad (5.16)$$

The second one

$$y \rightarrow \tilde{y}, \quad y = \tilde{y} \tilde{x}^{-1} L \quad (5.17)$$

finally gives

$$L^{1+\varepsilon} \int_0^\infty \frac{d\tilde{x}}{\tilde{x}} \tilde{x}^{D-\varepsilon} \int_0^\infty \frac{d\tilde{y}}{\tilde{y}} \tilde{y}^D (\tilde{x}^{2\nu} + \tilde{y}^{2\nu})^{-d/2} \delta(\tilde{y} - L) \Theta(\tilde{y} < \tilde{x}). \quad (5.18)$$

Replacing the second integral on the r.h.s. of (5.13) by (5.18) gives

$$L \frac{\partial}{\partial L} \left\langle \text{diagram} \right\rangle_L = L^{1+\varepsilon} \int_0^\infty \frac{dx}{x} x^D \int_0^\infty \frac{dy}{y} y^D (x^{2\nu} + y^{2\nu})^{-d/2} \\ \times \max(x, y)^{-\varepsilon} \delta(y - L). \quad (5.19)$$

Now one distance (here y) is fixed, whereas the integral over the other distance (here x) runs from 0 to ∞ . The former constraint $\max(x, y) = L$ has been transformed into the factor $\max(x, y)^{-\varepsilon}$ times the constraint $y = L$.

Before generalizing this formula, we shall show how it can be used in practice. The residue in $\frac{1}{\varepsilon}$ (which determines the corresponding one-loop counterterm) is given by the simple formula ($d_c(D) = 4D/(2 - D)$):

$$\varepsilon \left\langle \text{diagram} \right\rangle_{\varepsilon^{-1}} = \int_0^\infty \frac{dx}{x} x^D (x^{2\nu} + 1)^{-d_c(D)/2} = \frac{1}{2 - D} \frac{\Gamma\left(\frac{D}{2 - D}\right)^2}{\Gamma\left(\frac{2D}{2 - D}\right)}. \quad (5.20)$$

The subleading term can analogously be calculated by expanding $(x^{2\nu} + 1)^{-(d - d_c(D))/2}$ and $\max(x, y)^\varepsilon$ in ε . We obtain the convergent integral representation

$$\left\langle \text{diagram} \right\rangle_{\varepsilon^0} = \int_0^\infty \frac{dx}{x} x^D \left(\frac{1}{2 - D} \ln(x^{2\nu} + 1) - \ln(\max(x, 1)) \right). \quad (5.21)$$

This method extends to the integrals which appear in the counterterms associated to the contraction of any number of points. In general we have to compute integrals over $N(N - 1)$ distances x, y, \dots , of the form

$$I(\varepsilon) = \int_{\max(x, y, \dots) \leq L} f(x, y, \dots) \quad (5.22)$$

with a homogeneous function f such that the integral has a conformal weight (dimension in L) κ . For the integrals which appear in n -loop diagrams, this weight is simply

$$\kappa = n\varepsilon. \quad (5.23)$$

The integral over the distances is defined by the D -dimensional measure (5.5). The residue is extracted from the dimensionless integral

$$J(\varepsilon) = L^{-\kappa} L \frac{\partial}{\partial L} I(\varepsilon) = n\varepsilon L^{-\kappa} I(\varepsilon) \\ = L \int_{\max(x, y, \dots) = L} f(x, y, \dots) \max(x, y, \dots)^{-\kappa}. \quad (5.24)$$

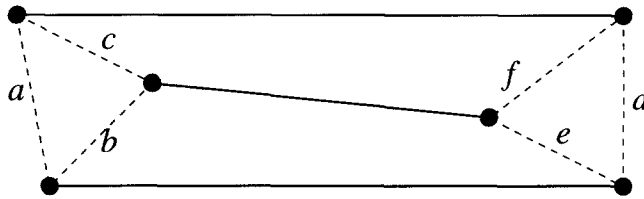


Fig. 6.1. The distances in (6.2).

The domain of integration can be decomposed into “sectors”, for instance

$$\{\dots < y < x = L\}, \{\dots < x < y = L\}, \quad (5.25)$$

and we can map these different sectors onto each other by global conformal transformations. For instance we can rewrite the integral (5.24)

$$J(\varepsilon) = L \int_{x=L} f(x, y, \dots) \max(x, y, \dots)^\kappa = L \int_{y=L} f(x, y, \dots) \max(x, y, \dots)^\kappa. \quad (5.26)$$

The constraint on the maximum of the distances is replaced by the constraint on a (arbitrarily chosen) distance.

This mapping of sectors is one of the basic tools used in the following to explicitly calculate the two-loop diagrams.

6. Coupling constant renormalization, first graph

6.1. The counterterm

We are now going to calculate the first diagram of Section 4. It contributes to the coupling-constant renormalization in two-loop order and is

$$-\frac{3}{2}\mathcal{C}_1 = \left\langle \left(\text{diagram} \right) \middle| \text{diagram} \right\rangle_L - \frac{3}{2} \left\langle \left(\text{diagram} \right) \middle| \text{diagram} \right\rangle_L^2. \quad (6.1)$$

With the distances labeled as in Fig. 6.1, the first MOPE coefficient is

$$\begin{aligned} & \left(\left(\text{diagram} \right) \middle| \text{diagram} \right) \\ &= \left[\frac{1}{4} \left(\sqrt{a^{2\nu} + d^{2\nu}} + \sqrt{b^{2\nu} + e^{2\nu}} + \sqrt{c^{2\nu} + f^{2\nu}} \right) \right. \\ & \quad \times \left(\sqrt{b^{2\nu} + e^{2\nu}} + \sqrt{c^{2\nu} + f^{2\nu}} - \sqrt{a^{2\nu} + d^{2\nu}} \right) \\ & \quad \times \left. \left(\sqrt{a^{2\nu} + d^{2\nu}} + \sqrt{c^{2\nu} + f^{2\nu}} - \sqrt{b^{2\nu} + e^{2\nu}} \right) \right] \end{aligned}$$

$$\times \left(\sqrt{a^{2\nu} + d^{2\nu}} + \sqrt{b^{2\nu} + e^{2\nu}} - \sqrt{c^{2\nu} + f^{2\nu}} \right) \Big]^{-d/2}. \quad (6.2)$$

The derivation of this expression can be found in Appendix B. Recall that the factorization of the divergences, which are subtracted in (6.1), is

$$\left(\text{diagram} \right) \approx \left(\text{diagram} \right) \left(\text{diagram} \right). \quad (6.3)$$

We therefore represent the MOPE coefficients associated to the second term in (6.1) as

$$\begin{aligned} & -\frac{3}{2} \left(\text{diagram} \right) \left(\text{diagram} \right) \\ &= -\frac{1}{2} (a^{2\nu} + d^{2\nu})^{-d/2} (b^{2\nu} + e^{2\nu})^{-d/2} - \frac{1}{2} (a^{2\nu} + d^{2\nu})^{-d/2} (c^{2\nu} + f^{2\nu})^{-d/2} \\ & \quad - \frac{1}{2} (b^{2\nu} + e^{2\nu})^{-d/2} (c^{2\nu} + f^{2\nu})^{-d/2}. \end{aligned} \quad (6.4)$$

There are three subdivergencies subtracted due to the three possible contractions and a factor $1/2$ due to symmetry, i.e. due to the nested contraction.

We can now proceed to calculate the diagram (6.1), which is of order $1/\varepsilon$ and not of order $1/\varepsilon^2$ as the single terms. To do so, let us consider the integral $I(L)$, which is defined as the integral of the MOPE coefficients, with all mutual distances appearing in Fig. 6.1 restricted to be smaller than L :

$$\begin{aligned} I(L) &= \int \int \int \int \int \int_{a,b,c,d,e,f < L} \left(\text{diagram} \right) \\ & \quad - \frac{3}{2} \left(\text{diagram} \right) \left(\text{diagram} \right). \end{aligned} \quad (6.5)$$

Note that $I(L)$ is *not* exactly equal to (6.1). However, we shall show below that the leading term, i.e. the pole in $1/\varepsilon$ in which we are interested, is the same.

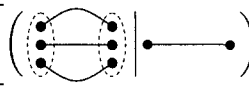

$I(L)$ has the following Laurent expansion:

$$I(L) = L^{2\varepsilon} \left(\frac{a}{\varepsilon} + \mathcal{O}(\varepsilon^0) \right). \quad (6.6)$$

We now apply the operator $L \frac{\partial}{\partial L}$ to $I(L)$ to extract the residue a in $1/\varepsilon$. We obtain an integral similar to (6.5) with the constraint that $\max(a, b, c, d, e, f) = L$. Using the trick of conformal mapping explained before, we can rewrite this as an integral with the constraint that one of the distances (for instance a) is equal to L and that the other can vary freely. We thus obtain the integral

$$J(L) = L \frac{\partial}{\partial L} I(L)$$

$$\begin{aligned}
&= L \iiint\limits_{b,c,d,e,f} \max(a, b, c, d, e, f)^{-2\varepsilon} \left[\left(\text{diagram 1} \right) \right. \\
&\quad \left. - \frac{3}{2} \left(\text{diagram 2} \right) \left(\text{diagram 3} \right) \right]. \quad (6.7)
\end{aligned}$$

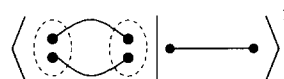
We know that the only divergencies, which lead to poles in $1/\varepsilon$, could appear in (6.7) when a pair of distances, i.e. (a, d) , (b, e) or (c, f) simultaneously tends to 0. But by construction these divergences cancel between the first and the second terms of the integrand. So, the integrand in (6.7) has only integrable singularities at short distances and we can perform the limit $d \rightarrow d_c$, i.e. $\varepsilon \rightarrow 0$ inside the integral in order to compute

$$J(L)|_{\varepsilon=0} = 2a. \quad (6.8)$$

This convergent integral can be calculated numerically by the methods developed in [34]. We shall explicit this calculation later.

The next problem we have to treat is that in (6.5) we subtracted a counterterm that we had chosen by convenience. It is however not the counterterm in (6.1), which is fixed by our renormalization prescription at one-loop order. The latter can be written as

$$\left\langle \text{diagram 1} \right\rangle_L^2 = \iiint\limits_{a,b,d,e < L; c,f} (a^{2\nu} + d^{2\nu})^{-d/2} (b^{2\nu} + e^{2\nu})^{-d/2}. \quad (6.9)$$



The difference between (6.9) and the counterterm in (6.5) is that the integration over c and f is *not* restricted. To evaluate the residue for the true counterterm, we apply the operator $L \frac{\partial}{\partial L}$ to (6.9) and get an integral with the constraint that $\max(a, b, d, e) = L$. We now use the trick of conformal mapping to transform this integral into an integral with the constraint $a = L$ as in (6.7). This yields

$$L \iiint\limits_{b,c,d,e,f} (a^{2\nu} + d^{2\nu})^{-d/2} (b^{2\nu} + e^{2\nu})^{-d/2} \max(a, b, d, e)^{-2\varepsilon}. \quad (6.10)$$

This expression has to be compared to the corresponding counterterm in (6.7). The difference between these two counterterms is

$$\begin{aligned}
&\iiint\limits_{b,c,d,e,f} (a^{2\nu} + d^{2\nu})^{-d/2} (b^{2\nu} + e^{2\nu})^{-d/2} \\
&\quad \times (\max(a, b, d, e)^{-2\varepsilon} - \max(a, b, c, d, e, f)^{-2\varepsilon}). \quad (6.11)
\end{aligned}$$

A priori this term is $\mathcal{O}(\varepsilon^0)$ and might contribute to the residue. We state that this term is $\mathcal{O}(\varepsilon)$, thus subdominant and does not contribute to the counterterm. To prove this we set $L = 1$ and we develop $\max(\dots)^{-2\varepsilon}$ in powers of ε . This expansion is licit over the

domain of integration, since $\max(\dots) \geq 1$ and since the integral is convergent at large distances. This implies that (6.11) is equivalent to

$$2\varepsilon \int \int \int \int \int_{b,c,d,e,f} (a^{2\nu} + d^{2\nu})^{-d/2} (b^{2\nu} + e^{2\nu})^{-d/2} \times [\ln(\max(a, b, c, d, e, f)) - \ln(\max(a, b, d, e))] \quad (6.12)$$

when $\varepsilon \rightarrow 0$. Poles of the integral in $1/\varepsilon$ might appear if $b, e \rightarrow 0$ simultaneously. In that case however $c \rightarrow a$ and $d \rightarrow f$ so that the difference in the last factor in (6.12) vanishes. The last integral in (6.12) is therefore convergent, implying that (6.11) = $\mathcal{O}(\varepsilon)$ and that $I(L) + 3/2\mathcal{C}_1 = \mathcal{O}(\varepsilon^0)$. Therefore the use of (6.5) instead of (6.1) to compute the residue of the pole is justified.

Such a phenomenon is not peculiar to this diagram. In the other diagrams that we shall calculate similar simplifications occur when dealing with the counterterms, which allow to take the same constraints over the distances for the two-loop diagram and for the counterterms associated with one-loop subdivergences. We call this property the “two-loop miracle”. (A generalization to the calculation of higher order diagrams is possible.)

6.2. Numerical calculation

We now want to calculate the residue $J(L)$, given by the integral (6.7), numerically. This calculation will be performed for values of D in the interval $1 < D < 2$. As we already discussed, the integral representation (6.7) suffers from additional divergences for $D < 1$, which come from the fact that the measure over three points becomes a distribution, and which must be treated by a finite part prescription. This will not be done here, since it turns out to be sufficient to calculate the diagrams for $1 < D < 2$ in order to have good estimates for the critical exponent of membranes.

The calculation is considerably simplified by using the symmetries of the diagram and by integrating over one of the equivalent sectors only. First of all, one can suppose that $\max(a, b, c) > \max(d, e, f)$. Furthermore an ordering of a, b and c is introduced: $a > b > c$. This gives rise to a symmetry factor $2 \times 6 = 12$. In order to eliminate all divergencies, also d, e and f have to be ordered. We assume that $d > e > f$ but then have to sum over all permutations of d, e and f . Denoting by

$$g(a, b, c, d, e, f) = \left(\begin{array}{c} \text{diagram 1} \end{array} \right) - \frac{3}{2} \left(\begin{array}{c} \text{diagram 2} \end{array} \right) \left(\begin{array}{c} \text{diagram 3} \end{array} \right) \quad (6.13)$$

as in (6.2) and (6.4), we get

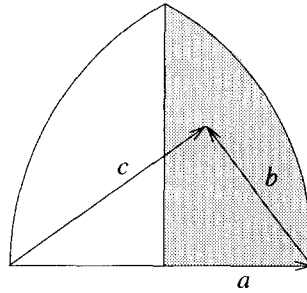


Fig. 6.2. The half-sector used for the numerical integration.

$$\begin{aligned}
 J(L)|_{\epsilon=0} &= \int_{a=1, b, c, d, e, f} g(a, b, c, d, e, f) \\
 &= 12 \int_{\substack{a=1 > b > c \\ a > d > e > f}} g(a, b, c, d, e, f) + g(a, b, c, e, f, d) + g(a, b, c, f, d, e) \\
 &\quad + g(a, b, c, f, e, d) + g(a, b, c, e, d, f) + g(a, b, c, d, f, e). \quad (6.14)
 \end{aligned}$$

We can furthermore divide the remaining integral into two sectors where either $b < e$ or $b > e$. There will always be an integrable divergence in the smaller distance which has to be treated by an appropriate variable transformation. As in [34] we parametrize the integral over b as

$$\begin{aligned}
 \int_b &= \frac{S_{D-1}}{S_D} \int_{-\infty}^{\infty} db_1 \int_0^{\infty} db_2 b_2^{D-2}, \quad (6.15) \\
 a &= 1, \quad b = \sqrt{b_1^2 + b_2^2}, \quad c = \sqrt{(1 - b_1)^2 + b_2^2},
 \end{aligned}$$

restricted to the domain where $b < c < a$ (see Fig. 6.2): There are singularities for $b_1 \rightarrow 0$ and for $b_2 \rightarrow 0$. They are disentangled by switching to radial and angular coordinates. In these coordinates the singularities can be eliminated by the following parametrization:

$$\int_b = \frac{1}{D - \sigma} \frac{1}{D - 1} \frac{\pi}{2} \frac{S_{D-1}}{S_D} \int_0^1 d\beta \beta^{\frac{2-D}{D-1}} \sin(\alpha)^{D-2} \int_0^1 dt b^\sigma \Theta(1 - b) \Theta(c - b), \quad (6.16)$$

where

$$\alpha = \frac{\pi}{2} \beta^{\frac{1}{D-1}}, \quad (6.17)$$

$$b = t^{\frac{1}{D-\sigma}}, \quad (6.18)$$

$$\sigma = \begin{cases} 2D - 2, & e < b \\ 0, & e > b \end{cases}. \quad (6.19)$$

$$c = \sqrt{b^2 + 1 - 2b \cos(\alpha)}. \quad (6.20)$$

The change of variables from the angle α to β , (6.17), generates a factor $\beta^{(2-D)/(D-1)}$ which exactly cancels the singularity for $\alpha \rightarrow 0$ from the measure, i.e. $\sin(\alpha)^{D-2}$. The other variable transformations are constructed in a similar way.

Furthermore there is the integral over d and e ,

$$\int_d \int_e = \int_d d^D \int_{e'} \quad \text{with} \quad e' = \frac{e}{d}. \quad (6.21)$$

Therefore we write

$$\int_{d < a} d^D = \frac{1}{2D} \int_0^1 dr, \quad d = r^{1/2D}. \quad (6.22)$$

The remaining integral over e' is parametrized in analogy to the integral over b as

$$\begin{aligned} \int_{e'} &= \frac{1}{D-\tau} \frac{1}{D-1} \frac{\pi}{2} \frac{S_{D-1}}{S_D} \int_0^1 d\delta \delta^{\frac{2-D}{D-1}} \sin(\gamma)^{D-2} \\ &\quad \times \int_0^1 dt (e')^\tau \Theta(d-f) \Theta(f-e), \end{aligned} \quad (6.23)$$

where

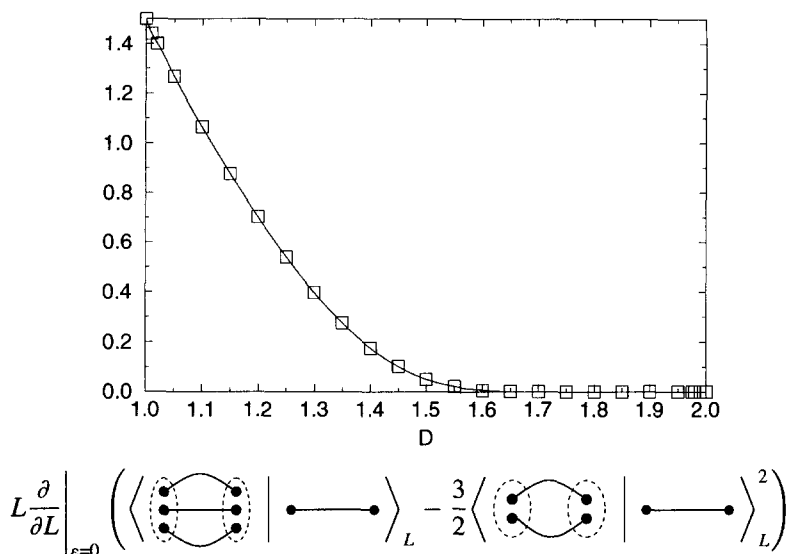
$$\gamma = \frac{\pi}{2} \delta^{\frac{1}{D-1}}, \quad (6.24)$$

$$e = d s^{\frac{1}{D-\tau}}, \quad (6.25)$$

$$\tau = \begin{cases} 0, & e < b \\ 2D-2, & e > b \end{cases}, \quad (6.26)$$

$$f = \sqrt{d^2 + e^2 - 2ed \cos(\gamma)}. \quad (6.27)$$

With these variable transformations, the integrand is bounded. This does not mean that the numerical integration is easy. The main problem is that the integral is localized in some small domain, in which the integrand (with all the factors of the measure and from the variable transformations) is about 100 or 1000 times its mean value, whereas it is much smaller in large domains of integration. A genuine adaptive Monte Carlo (AMC) routine has to be used. It is described in our earlier publication [34]. The idea is to divide the domain of integration into subboxes and to try to integrate each subbox using standard Monte Carlo (MC) integration with few sample points. The MC routine gives an estimate for the integral and for the standard deviation from this value. If the latter is too large, the box is divided into smaller subboxes and the procedure is repeated.



D		D	
1.00	1.5	1.55	$2.16 \times 10^{-2} \pm 2 \times 10^{-3}$
1.01	$1.441 \pm 5 \times 10^{-3} \pm 4 \times 10^{-3}$	1.60	$7.07 \times 10^{-3} \pm 6 \times 10^{-5}$
1.02	$1.399 \pm 5 \times 10^{-3}$	1.65	$1.61 \times 10^{-3} \pm 1 \times 10^{-5}$
1.05	$1.268 \pm 5 \times 10^{-3}$	1.70	$2.17 \times 10^{-4} \pm 2 \times 10^{-6}$
1.10	$1.065 \pm 5 \times 10^{-3}$	1.75	$1.23 \times 10^{-5} \pm 2 \times 10^{-7}$
1.15	$0.876 \pm 4 \times 10^{-3}$	1.80	$1.55 \times 10^{-7} \pm 2 \times 10^{-9}$
1.20	$0.702 \pm 4 \times 10^{-3}$	1.85	$1.07 \times 10^{-10} \pm 2 \times 10^{-12}$
1.25	$0.543 \pm 3 \times 10^{-3}$	1.90	$4.72 \times 10^{-17} \pm 6 \times 10^{-19}$
1.30	$0.399 \pm 2 \times 10^{-3}$	1.95	$3.99 \times 10^{-36} \pm 6 \times 10^{-36}$
1.35	$0.275 \pm 2 \times 10^{-3}$	1.975	$2.81 \times 10^{-74} \pm 3 \times 10^{-76}$
1.40	$0.176 \pm 2 \times 10^{-3}$	1.98	$2.33 \times 10^{-93} \pm 2 \times 10^{-95}$
1.45	$0.1022 \pm 7 \times 10^{-4}$	1.99	$6.89 \times 10^{-189} \pm 1 \times 10^{-189}$
1.50	$5.16 \times 10^{-2} \pm 4 \times 10^{-4}$	2.00	0

Fig. 6.3. Numerical results for the diagram (6.7). The first error in the table is the statistical error, the second the systematic error. The latter is only given if it can not be neglected.

This algorithm was implemented recursively using the computer language C. For details see Ref. [34]. The AMC routine gives an estimate of the integral and of its statistical error. A systematic error also appears, which is more difficult to estimate. It comes from the domain of small angular variables, where the numerical precision of the workstation is no longer sufficient and it appears to be the most important for $D \rightarrow 1$, as can be seen from (6.16). It can be estimated by counting exceptions of the floating-point unit and comparing it to known integrals. For (6.7), the systematic error is negligible. Its treatment will be discussed for the diagrams, where its contribution is important. The results for (6.7) were obtained within some hours on a workstation and are listed in Fig. 6.3. The numerical results nicely fit with the analytical value for $D = 1$, discussed in the next section.

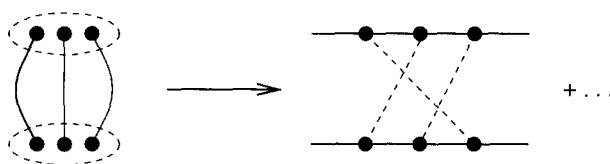


Fig. 6.4. Connection between the MOPE coefficient and the diagrams in polymer theory.

We checked the numerical integration routine. This check is provided by integrating the function

$$g(a, b, c, d, e, f) = (a^2 + b^2 + c^2 + d^2 + e^2 + f^2)^{-2D} \quad (6.28)$$

which has conformal weight $\kappa = 0$ and by comparing to the analytical solution

$$\int_{a=1, b, c, d, e, f} g(a, b, c, d, e, f) = \frac{\Gamma(D/2)^4}{8 \cdot 3^D \Gamma(2D)}. \quad (6.29)$$

This test ensures that the integration can be done for $1 < D < 2$.

6.3. Analytical calculation for $D \rightarrow 1$

To check the numerical calculation, we want to evaluate (6.7) for $D = 1$. This calculation can be performed analytically.

Some subtleties have to be taken care of in order to understand the calculation which follows. We remarked that in (6.7) the factor $\max(a, b, c, d, e, f)^{-2\varepsilon}$ could be dropped without changing the result as the contribution to the integral is finite in any subdomain. For the following calculation we shall drop this factor but shall not take the limit $d \rightarrow d_c$ as we only can calculate the diagram and its counterterms separately. Single terms will thus have divergencies in $1/\varepsilon$, which are treated by a finite part integration prescriptions, and which have to cancel at the end. Through this change only the sum of all terms but not each single term has a meaning in the limit $\varepsilon \rightarrow 0$, that we take at the end.

For $D \rightarrow 1$ the measure localizes on a line. This introduces different orderings of the distances, which are topologically inequivalent. (For an example see Fig. 6.4.) Two types of diagrams appear for $D \rightarrow 1$. There are either the “untwisted” diagrams (Fig. 6.5) or the “twisted” diagrams (Fig. 6.6). We remark that the second diagram in Fig. 6.5 is untwisted as it can be transformed into the first one by simply exchanging the orientation of the lower line. With the same reasoning one deduces that the four diagrams in Fig. 6.6 are topologically equivalent.

Let us start to calculate the untwisted diagram (without the counterterm). We note that $d = 4 - 2\varepsilon$. We find



Fig. 6.5. The two untwisted diagrams.

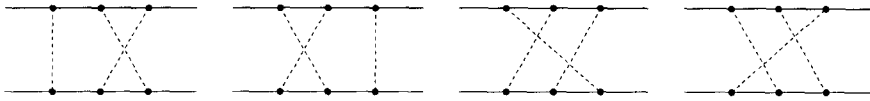


Fig. 6.6. The four twisted diagrams.

$$\begin{aligned}
 & \text{Diagram: } \begin{array}{c} \text{Top line: } \bullet \quad \bullet \quad \bullet \quad \bullet \\ \text{Bottom line: } \bullet \quad \bullet \quad \bullet \quad \bullet \\ \text{Dashed lines: } (1,2), (2,3), (3,4), (4,1) \end{array} \\
 &= \int_a \int_d \int_e (ab + ae + bd + ed)^{-d/2} \\
 &= \int_a \int_d \int_e (a + d)^{-d/2} (b + e)^{-d/2} = 0. \quad (6.30)
 \end{aligned}$$

The fact that the last integral is zero is a well-known property of the finite part integration of a homogeneous function (here $\int_a \int_d (a + d)^{-d/2} = 0$).

The counterterms are

$$\int_a \int_d \int_e (a + d)^{-d/2} (b + e)^{-d/2} = 0, \quad (6.31)$$

$$\begin{aligned}
 \int_a \int_d \int_e (a + d)^{-d/2} (c + f)^{-d/2} &= \int_a \int_d \int_e (a + d)^{-d/2} (1 + a + d + e)^{-d/2} \\
 &= \frac{1}{8} \frac{1}{\varepsilon} + \frac{1}{8} + \mathcal{O}(\varepsilon), \quad (6.32)
 \end{aligned}$$

$$\begin{aligned}
 \int_a \int_d \int_e (b + e)^{-d/2} (c + f)^{-d/2} &= \int_a \int_d \int_e (1 + e)^{-d/2} (1 + a + d + e)^{-d/2} \\
 &= -\frac{1}{8} \frac{1}{\varepsilon} - \frac{3}{8} + \mathcal{O}(\varepsilon). \quad (6.33)
 \end{aligned}$$

So together these terms add up to

$$6 \left(\text{Diagram: } \begin{array}{c} \text{Top line: } \bullet \quad \bullet \quad \bullet \quad \bullet \\ \text{Bottom line: } \bullet \quad \bullet \quad \bullet \quad \bullet \\ \text{Dashed lines: } (1,2), (2,3), (3,4), (4,1) \end{array} - \frac{1}{2} \sum \text{counter terms} \right) = \frac{3}{4} + \mathcal{O}(\varepsilon). \quad (6.34)$$

The factor 6 is the combinatorial factor.

The twisted diagram is given by

$$\begin{aligned}
 & \text{Diagram: } \begin{array}{c} \text{Top line: } \bullet \quad \bullet \quad \bullet \quad \bullet \\ \text{Bottom line: } \bullet \quad \bullet \quad \bullet \quad \bullet \\ \text{Dashed lines: } (1,2), (2,3), (3,4), (4,1) \end{array} \\
 &= \int_a \int_d \int_f (ab + af + ad + bd + df)^{-d/2} \\
 &= \int_a \int_d \int_f (a + af + ad + d + df)^{-d/2} \\
 &= \frac{1}{8} \frac{1}{\varepsilon} + \frac{3}{8} + \mathcal{O}(\varepsilon). \quad (6.35)
 \end{aligned}$$

The counterterms are

$$\begin{aligned}
 \int_a \int_d \int_f (a+d)^{-d/2} (b+e)^{-d/2} &= \int_a \int_d \int_f (a+d)^{-d/2} (1+d+f)^{-d/2} \\
 &= \frac{1}{8} \frac{1}{\varepsilon} + \frac{1}{4} + \mathcal{O}(\varepsilon), \quad (6.36)
 \end{aligned}$$

$$\begin{aligned}
 \int_a \int_d \int_f (a+d)^{-d/2} (c+f)^{-d/2} &= \int_a \int_d \int_f (a+d)^{-d/2} (1+a+f)^{-d/2} \\
 &= \frac{1}{8} \frac{1}{\varepsilon} + \frac{1}{4} + \mathcal{O}(\varepsilon), \quad (6.37)
 \end{aligned}$$

$$\begin{aligned}
 \int_a \int_d \int_f (b+e)^{-d/2} (c+f)^{-d/2} &= \int_a \int_d \int_f (1+f+d)^{-d/2} (1+a+f)^{-d/2} \\
 &= \frac{1}{8} + \mathcal{O}(\varepsilon). \quad (6.38)
 \end{aligned}$$

These terms add up to

$$12 \left(\text{diagram} - \frac{1}{2} \sum \text{counter terms} \right) = \frac{3}{4} + \mathcal{O}(\varepsilon). \quad (6.39)$$

The factor 12 again is the combinatorial factor.

The final result which has to be compared to the numerics thus is (cf. (6.7)):

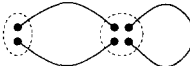
$$J(L=1)|_{D=1} = \frac{3}{2}. \quad (6.40)$$

7. Coupling constant renormalization, second graph

7.1. Derivation of an analytical expression

The next diagram that has to be calculated is (4.37):

$$\begin{aligned}
 I(L) = -\frac{1}{2} \mathcal{C}_2 &= \left\langle \text{diagram} \mid \text{diagram} \right\rangle_L \\
 &\quad - \frac{1}{2} \left\langle \text{diagram} \mid \text{diagram} \right\rangle_L \left\langle \text{diagram} \mid \text{diagram} \right\rangle_L. \quad (7.1)
 \end{aligned}$$

The second term on the r.h.s. subtracts the subdivergence, when first the single dipole on the r.h.s. of  is contracted. In this case the MOPE is

$$\left(\text{diagram} \mid \text{diagram} \right) \approx \left(\text{diagram} \mid \text{diagram} \right) \left(\text{diagram} \mid \text{diagram} \right). \quad (7.2)$$

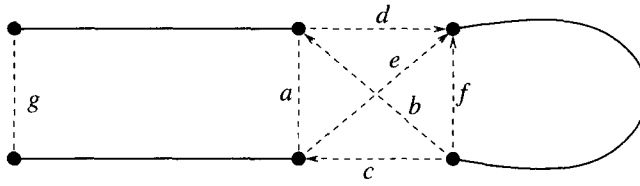


Fig. 7.1. The distances in (7.1).

Note that the MOPE (7.2) has a tensorial structure and that a counterterm like

$$\left(\begin{array}{c} \text{diagram} \end{array} \right) \left(\begin{array}{c} \text{diagram} \end{array} \right) \quad (7.3)$$

would subtract the pole term from the integral but would not be sufficient to make the integral convergent. With the distances as noted in Fig. 7.1 the MOPE coefficients are

$$\left(\begin{array}{c} \text{diagram} \end{array} \right) = \left[(g^{2\nu} + a^{2\nu}) f^{2\nu} - \frac{1}{4} (b^{2\nu} - c^{2\nu} + e^{2\nu} - d^{2\nu})^2 \right]^{-d/2} \quad (7.4)$$

$$\begin{aligned} & \left(\begin{array}{c} \text{diagram} \end{array} \right) \left(\begin{array}{c} \text{diagram} \end{array} \right) \\ &= \frac{d}{2} \nu^2 (g^{2\nu} + a^{2\nu})^{-d/2-1} f^{-\nu(d+2)} (b f b^{-D} - c f c^{-D})^2 \\ &= \frac{d}{2} \nu^2 (g^{2\nu} + a^{2\nu})^{-d/2-1} f^{-\nu(d+2)} (e f e^{-D} - d f d^{-D})^2, \end{aligned} \quad (7.5)$$

where two equivalent formulations were given.

For scalar products we always use the convention that the vectors involved start from the same point, i.e. we *define* (cf. Fig. 7.1)

$$b f = \frac{1}{2} (b^2 + f^2 - d^2). \quad (7.6)$$

A relevant counterterm, which we did not explicitly write in C_2 , appears too. It is canceled by

$$\left(\begin{array}{c} \text{diagram} \end{array} \right) = (g^{2\nu} + a^{2\nu})^{-d/2} f^{-\nu d}. \quad (7.7)$$

We state and will show below that

$$I(L) = \int_{a,b,c,d,e,f,g < L} \left(\begin{array}{c} \text{diagram} \end{array} \right) - \left(\begin{array}{c} \text{diagram} \end{array} \right)$$

$$\begin{aligned}
& - \left(\text{diagram 1} \mid \text{diagram 2} \right) \left(\text{diagram 3} \mid \text{diagram 4} \right) \Theta(f < \max(a, d, e, g)) \\
& + \mathcal{O}(\varepsilon^0),
\end{aligned} \tag{7.8}$$

where we used the second version of the counterterm in (7.5).

To compute the residue of the single pole, we apply $L\partial/\partial L$ to this expression and map onto $c = L = 1$:

$$\begin{aligned}
J(L) &= L \frac{\partial}{\partial L} I(L) = \int \int \int \int \int \int_{c=1; a, b, d, e, f, g} \max(a, b, c, d, e, f, g)^{-2\varepsilon} \\
&\times \left(\left[(g^{2\nu} + a^{2\nu}) f^{2\nu} - \frac{1}{4} (b^{2\nu} - c^{2\nu} + e^{2\nu} - d^{2\nu})^2 \right]^{-d/2} - (g^{2\nu} + a^{2\nu})^{-d/2} f^{-\nu d} \right. \\
&\left. - \frac{d}{2} \nu^2 (g^{2\nu} + a^{2\nu})^{-d/2-1} f^{-\nu(d+2)} (e f e^{-D} - d f d^{-D})^2 \Theta(f < \max(a, d, e, g)) \right).
\end{aligned} \tag{7.9}$$

We check that this expression is integrable everywhere, as is indeed the case and can be seen by a (generalized) Taylor expansion.

We then have to explain that

$$\begin{aligned}
& \int_{a, d, e, g < L; f} \left(\text{diagram 1} \mid \text{diagram 2} \right) \left(\text{diagram 3} \mid \text{diagram 4} \right) \Theta(f < \max(a, d, e, g)) \\
&= \int_{a, d, e, g < L; f} \left(\text{diagram 1} \mid \text{diagram 2} \right) \left(\text{diagram 3} \mid \text{diagram 4} \right) \Theta(f < \max(a, d, e, g)) \\
&= \frac{1}{2} \left\langle \text{diagram 1} \mid \text{diagram 2} \right\rangle_L \left\langle \text{diagram 3} \mid \text{diagram 4} \right\rangle_L.
\end{aligned} \tag{7.10}$$

The first equality is due to symmetry. The second stems from the so-called nested integration. We see this explicitly as follows:

$$\begin{aligned}
& \int_{a, d, e, g < L; f} \left(\text{diagram 1} \mid \text{diagram 2} \right) \left(\text{diagram 3} \mid \text{diagram 4} \right) \Theta(f < \max(a, d, e, g)) \\
&= \int_{a, d, e, g < L} \left(\text{diagram 1} \mid \text{diagram 2} \right) \left\langle \text{diagram 3} \mid \text{diagram 4} \right\rangle_L \left(\frac{\max(a, d, e, g)}{L} \right)^e,
\end{aligned} \tag{7.11}$$

where we used the fact that for any l

$$\left\langle \text{diagram} \right\rangle_l \sim l^\varepsilon. \quad (7.12)$$

The whole integral scales like $L^{2\varepsilon}$, so that we can apply $\frac{L}{2\varepsilon} \frac{\partial}{\partial L}$ to (7.11) without changing it. Doing so we obtain that (7.11) equals

$$\frac{L}{2\varepsilon} \int_{\max(a,d,e,g)=L} \left(\text{diagram} \right) \left(\frac{\max(a,d,e,g)}{L} \right)^\varepsilon \times \left\langle \text{diagram} \right\rangle_L. \quad (7.13)$$

The factor $(\max(a,d,e,g)/L)^\varepsilon$ is equal to unity and the integral is our usual expression for the residue of $\left\langle \text{diagram} \right\rangle_L$. Taking all this together we obtain

$$\frac{1}{2} \left\langle \text{diagram} \right\rangle_L \left\langle \text{diagram} \right\rangle_L. \quad (7.14)$$

This proves the desired result. The reader can verify that this is a general feature of these so-called nested contractions. If the largest distance in the subdiagram is restricted to be smaller than the largest distance that remains after complete contraction of the subdiagram, then the so restricted integral is $1/2$ times the product of the subdiagram and the diagram which rests after contraction. This demands of course that both of them scale like L^ε , where L is the IR cutoff. The reader will be able to generalize this rule for a scaling with other exponents, which would be necessary in higher order calculations.

The subtle point which we still have to check is that the changes in the domain of integration of the marginal counterterm from (7.1) to (7.8) do not change the residue, i.e. that again the “two-loop-miracle” appears. Analogously to Section 6.1 we write down the difference, apply $L\partial/\partial L$ to this expression and map onto $c = 1$. We obtain

$$\begin{aligned} & \frac{d}{2} \nu^2 \iiint \int \int \int \int_{a,b,d,e,f,g} (\max(a,b,c,d,e,f,g)^{-2\varepsilon} - \max(a,d,e,f,g)^{-2\varepsilon}) \\ & \times (g^{2\nu} + a^{2\nu})^{-d/2-1} f^{-\nu(d+2)} (ef e^{-D} - df d^{-D})^2 \Theta(f < \max(a,d,e,g)). \end{aligned} \quad (7.15)$$

We would like to develop $(\max(a,b,c,d,e,f,g)^{-2\varepsilon} - \max(a,b,c,f,g)^{-2\varepsilon})$ for ε small and show that the corrections are of order ε . This might be wrong, if and only if this expression does not vanish at points where the integral has a pole. For $f \rightarrow 0$ it vanishes. The limit $a, g \rightarrow 0$ is a bit more subtle as the difference does not vanish. However, in this case $(ef e^{-D} - df d^{-D})^2$ is of order a^2 so that no pole in the integration over a and g appears.

Let us now perform in (7.9) the limit $d \rightarrow d_c$, i.e. $\varepsilon \rightarrow 0$. Then we would like to integrate over g analytically. This is not possible due to the Θ -function. We therefore modify this constraint from $\Theta(f < \max(a,d,e,g))$ to $\Theta(f < d)$. Note that the modified counterterm still successfully subtracts the marginal subdivergence. We obtain

$$\begin{aligned}
\tilde{J}(L) = & \int \int \int \int \int \int \int \int \left(\left[(g^{2\nu} + a^{2\nu}) f^{2\nu} - \frac{1}{4} (b^{2\nu} - c^{2\nu} + e^{2\nu} - d^{2\nu})^2 \right]^{-d_c/2} \right. \\
& - (g^{2\nu} + a^{2\nu})^{-d_c/2} f^{-\nu d_c} \\
& \left. - \frac{d_c}{2} \nu^2 (g^{2\nu} + a^{2\nu})^{-d_c/2-1} f^{-\nu(d_c+2)} (e f e^{-D} - d f d^{-D})^2 \Theta(f < d) \right).
\end{aligned} \tag{7.16}$$

Of course this change affects the result and we shall calculate the difference in Section 7.7. The modified counterterm has another useful property, which justifies its choice: The Θ -function is not affected by the **R**-operation discussed in the next section.

Now the integration over g can be performed. The result is

$$\tilde{J}(L) = \int \int \int \int \int F(a, b, c, d, e, f) \tag{7.17}$$

with

$$\begin{aligned}
F(a, b, c, d, e, f) = & \frac{1}{2-D} \frac{\Gamma\left(\frac{D}{2-D}\right)^2}{\Gamma\left(\frac{2D}{2-D}\right)} \\
& \times \left\{ f^{-D} \left(a^{2\nu} f^{2\nu} - \frac{1}{4} (b^{2\nu} - c^{2\nu} + e^{2\nu} - d^{2\nu})^2 \right)^{-d_c/4} - a^{-D} f^{-2D} \right. \\
& \left. - \frac{D}{2} \nu a^{-2} f^{-2-D} \Theta(f < d) (e f e^{-D} - d f d^{-D})^2 \right\}.
\end{aligned} \tag{7.18}$$

7.2. Improvement of the measure

For $c = 1$ the measure, given by (5.5) and (A.1), simplifies to an integral over the vectors a and f :

$$\frac{S_{D-1} S_{D-2}}{S_D^2} \int_{-\infty}^{\infty} da_1 \int_0^{\infty} da_2 a_2^{D-2} \int_{-\infty}^{\infty} df_1 \int_{-\infty}^{\infty} df_2 \int_0^{\infty} df_3 f_3^{D-3} F(a, b, c, d, e, f). \tag{7.19}$$

For $D < 2$ the measure defined in (7.19) is a distribution and suffers from a relevant divergence for $f_3 \rightarrow 0$. Geometrically these are configurations where the tetrahedron spanned by a, b, \dots, f has volume 0, i.e. is restricted to a plane. A finite part prescription has to be applied in order to make the measure finite. This was first discussed in [34].

One may think of implementing this prescription by subtracting the singularity. This method however imposes at least numerical difficulties. It is better to eliminate the

singularity by a partial integration with respect to f_3 , which is mathematically equivalent [34]. As only d , e and f depend on f_3 , the integral

$$\text{f.p.} \int_0^\infty df_3 f_3^{D-3} F(a, b, c, d, e, f) \quad (7.20)$$

can be converted to

$$\begin{aligned} & \frac{1}{2-D} \int_0^\infty df_3 f_3^{D-2} \frac{\partial}{\partial f_3} F(a, b, c, d, e, f) \\ &= \frac{1}{2-D} \int_0^\infty df_3 f_3^{D-1} \mathbf{R} F(a, b, c, d, e, f), \end{aligned} \quad (7.21)$$

where \mathbf{R} is defined via

$$\mathbf{R} = \frac{1}{d} \frac{\partial}{\partial d} + \frac{1}{e} \frac{\partial}{\partial e} + \frac{1}{f} \frac{\partial}{\partial f}. \quad (7.22)$$

The strength of the divergences for $a \rightarrow 0$ or $f \rightarrow 0$ is unchanged. It is important to remark that this trick cannot be used to eliminate the relevant divergences when $a \rightarrow 0$ or $f \rightarrow 0$. It works for the divergence in f_3 , because the integrand does not directly depend on f_3 but on d , e and f , which themselves depend on f_3 . So the derivation of F with respect to f_3 does not produce a factor $1/f_3$ but factors $1/d$, $1/e$ and $1/f$, which are not singular for $f_3 \rightarrow 0$. Explicitly

$$\begin{aligned} \mathbf{R} F(a, b, c, d, e, f) &= \frac{1}{2-D} \frac{\Gamma\left(\frac{D}{2-D}\right)^2}{\Gamma\left(\frac{2D}{2-D}\right)} \\ &\times \left\{ -D f^{-2-D} \left(a^{2\nu} f^{2\nu} - \frac{1}{4} (b^{2\nu} - c^{2\nu} + e^{2\nu} - d^{2\nu})^2 \right)^{-d_c/4} \right. \\ &\quad - D f^{-D} \left(a^{2\nu} f^{2\nu} - \frac{1}{4} (b^{2\nu} - c^{2\nu} + e^{2\nu} - d^{2\nu})^2 \right)^{-d_c/4-1} \\ &\quad \times \left(a^{2\nu} f^{-D} - \frac{1}{2} (b^{2\nu} - c^{2\nu} + e^{2\nu} - d^{2\nu}) (e^{-D} - d^{-D}) \right) \\ &\quad + 2D a^{-D} f^{-2D-2} \\ &\quad + (2+D) \frac{D\nu}{2} a^{-2} f^{-4-D} \Theta(d > f) (e f e^{-D} - d f d^{-D})^2 \\ &\quad - D \nu a^{-2} f^{-2-D} \Theta(d > f) (e f e^{-D} - d f d^{-D}) \\ &\quad \left. \times (2e^{-D} - 2d^{-D} - D e f e^{-D-2} + D d f d^{-D-2}) \right\}. \end{aligned} \quad (7.23)$$

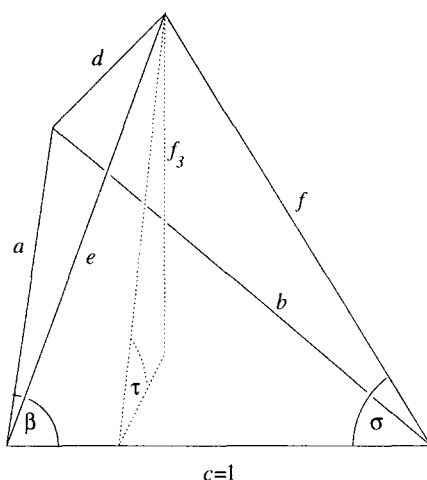


Fig. 7.2. Parametrization of the tetrahedron.

Note that $\mathbf{R}\Theta(f < d) = 0$ whereas $\mathbf{R}\Theta(f < \max(a, d, e))$ gives contributions proportional to e.g. $\delta(a - f)$ which had to be treated separately. This justifies our choice of the modified bound of the counterterm in (7.16).

7.3. Parametrization of the measure

The main singularities for small distances appear for a or f small. We therefore want to parametrize the measure with the help of these distances. The divergences for small volume of the tetrahedron spanned by a, \dots, f , $a \rightarrow 0$ or $f \rightarrow 0$ shall be treated by a parametrization in angles as by this way small distance and small volume singularities are best disentangled. We have chosen the parametrization indicated in Fig. 7.2. One triangle is spanned by c and a with an angle β between them, another by c and f , where the corresponding angle is σ . The angle between the planes spanned by these two triangles is τ . The distances as functions of a, f and β, σ, τ are

$$\begin{aligned} b &= \sqrt{a^2 + 1 - 2a \cos \beta}, \\ e &= \sqrt{f^2 + 1 - 2f \cos \sigma}, \\ d &= \sqrt{(a \cos \beta - 1 + f \cos \sigma)^2 + (a \sin \beta - f \sin \sigma \cos \tau)^2 + (f \sin \tau \sin \sigma)^2}, \end{aligned} \quad (7.24)$$

The integrals over a and f run from 0 to ∞ , the integrals over β, σ and τ over the interval $[0, \pi]$. As we do not want to map all the points that are far away, we have to find a reparametrization of the measure which behaves for $a \rightarrow 0$ like a^γ and for $a \rightarrow \infty$ like a^ω , by this way eliminating the principle divergences. If u is equally distributed we can use

$$a = u^{\frac{1}{D-\gamma}} (1 - u)^{\frac{1}{D-\omega}}. \quad (7.25)$$

The integral over β will be parametrized as

$$\beta = \begin{cases} \frac{\pi}{2} (2\alpha)^{\frac{1}{D-1}} & \alpha \leq 0.5 \\ \pi - \frac{\pi}{2} (2 - 2\alpha)^{\frac{1}{D-1}} & \alpha > 0.5 \end{cases} . \quad (7.26)$$

The integral over f (note that the factor f_3^2 came from the partial integration with respect to f_3)

$$\int df_1 df_2 df_3 f_3^{D-3} (f_3^2) \quad (7.27)$$

can be written as

$$\int df f^{D-1} \int d\sigma (\sin \sigma)^D \int d\tau (\sin \tau)^{D-1} (f^2) . \quad (7.28)$$

We change variables from f to v :

$$f = v^{\frac{1}{D-\gamma}} (1-v)^{\frac{1}{D-\omega}} . \quad (7.29)$$

Furthermore we choose in the same spirit as for β

$$\sigma = \begin{cases} \frac{\pi}{2} (2\eta)^{\frac{1}{D+1}} & \eta \leq 0.5 \\ \pi - \frac{\pi}{2} (2 - 2\eta)^{\frac{1}{D+1}} & \eta > 0.5 \end{cases} \quad (7.30)$$

and

$$\tau = \begin{cases} \frac{\pi}{2} (2\zeta)^{\frac{1}{D}} & \zeta \leq 0.5 \\ \pi - \frac{\pi}{2} (2 - 2\zeta)^{\frac{1}{D}} & \zeta > 0.5 \end{cases} . \quad (7.31)$$

So the complete integral over four points is

$$\begin{aligned} & \frac{S_{D-1} S_{D-2}}{S_D^2} \frac{\pi^3}{(2-D)(D-1)D(D+1)} \\ & \times \int_0^1 du a^D \left(\frac{1}{D-\gamma} \frac{1}{u} + \frac{1}{\omega-D} \frac{1}{1-u} \right) \int_0^1 d\alpha \min(2\alpha, 2-2\alpha)^{\frac{2-D}{D-1}} (\sin \beta)^{D-2} \\ & \times \int_0^1 dv f^D \left(\frac{1}{D-\gamma} \frac{1}{v} + \frac{1}{\omega-D} \frac{1}{1-v} \right) \int_0^1 d\eta \min(2\eta, 2-2\eta)^{\frac{-D}{D+1}} (\sin \sigma)^D \\ & \times \int_0^1 d\zeta \min(2\zeta, 2-2\zeta)^{\frac{1-D}{D}} (\sin \tau)^{D-1} f^2 \mathbf{RF}(a, b, 1, d, e, f) . \end{aligned} \quad (7.32)$$

Another way of parametrizing consists in replacing the integral over the vectors a and f by the integral over the vectors a and d . This parametrization is especially useful to

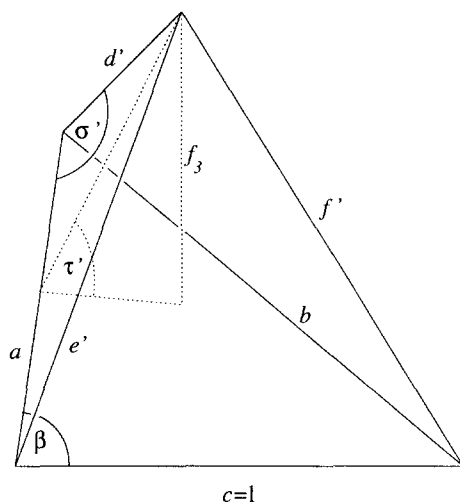


Fig. 7.3. Alternative parametrization of the tetrahedron.

eliminate divergences, when a and f simultaneously go to infinity. It will be used for the integration over one of the sectors in the next section. The new formulas are given here, a prime indicating new angles and distances as can be deduced from Fig. 7.3 σ' and τ' obey the same relations as σ and τ . For d' we use the same variable transformation as before for f :

$$d' = v^{\frac{1}{D-\gamma}} (1-v)^{\frac{1}{D-\omega}}. \quad (7.33)$$

The other new distances are

$$e' = \sqrt{a^2 + d'^2 - 2ad' \cos \sigma'}, \quad (7.34)$$

$$f' = \sqrt{(d' \sin \sigma' \sin \tau')^2 + (d' \cos \sigma' - a + \cos \beta)^2 + (\sin \beta - d' \sin \sigma' \cos \tau')^2}. \quad (7.35)$$

For the integrand (7.23), the exponents γ and ω are found by performing a (generalized) Taylor expansion:

$$\gamma = 0, \quad (7.36)$$

$$\omega = 2D. \quad (7.37)$$

7.4. Decomposition into sectors

Although the measure absorbs the principal singularities it cannot handle all of them. There remains e.g. a singularity for $b \rightarrow 0$ and $e \rightarrow 0$. Two methods may be applied to handle the remaining integrable singularities. The first consists in using the second measure of Subsection 7.3. The second is to map again some parts of the domain of

integration. Thereby we face the problem that the measure is no longer symmetric in the distances, as we have changed it in order to eliminate the relevant singularity for $f_3 \rightarrow 0$. In order to restore this symmetry, we rewrite the integral (7.32) as

$$\begin{aligned} & \frac{S_{D-1} S_{D-2}}{S_D^2} \frac{\pi^3}{(2-D)(D-1)D(D+1)} \\ & \times \int du a^{D+2} \left(\frac{1}{D-\gamma} \frac{1}{u} + \frac{1}{\omega-D} \frac{1}{1-u} \right) \int d\alpha \min(2\alpha, 2-2\alpha)^{\frac{2-D}{D-1}} (\sin \beta)^D \\ & \times \int dv f^{D+2} \left(\frac{1}{D-\gamma} \frac{1}{v} + \frac{1}{\omega-D} \frac{1}{1-v} \right) \int d\eta \min(2\eta, 2-2\eta)^{\frac{2-D}{D-1}} (\sin \sigma)^D \\ & \times \int d\zeta \min(2\zeta, 2-2\zeta)^{\frac{1-D}{D}} (\sin \tau)^{D-1} T(a, b, c, d, e, f), \end{aligned} \quad (7.38)$$

with

$$T(a, b, c, d, e, f) = \frac{1}{(2\Delta(a, b, c))^2} \mathbf{R}F(a, b, c, d, e, f), \quad (7.39)$$

and where

$$\Delta(a, b, c) = \frac{1}{2} ac \sin(\beta) = \frac{1}{4} \sqrt{(a+b+c)(a+b-c)(b+c-a)(c+a-b)}$$

is the area of the triangle spanned by a , b and c . This is, except for the geometric prefactor, the invariant measure in $D+2$ dimensions. The integrand now is conformal invariant, as follows directly from Eqs. (5.22) to (5.26).

The sectors are decomposed as follows:

- (1) $(a < 2 \text{ or } f < 2)$ and $(b > \frac{1}{2} \text{ or } e > \frac{1}{2})$.

This sector is convergent: $F(a, b, c, d, e, f)$ is integrated directly, using the simple measure (7.32).

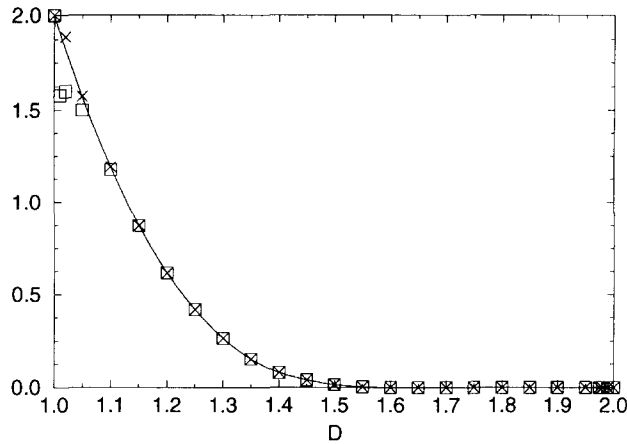
- (2) $a > 2$ and $f > 2$.

The measure (7.32) does not eliminate the singularity, when both a and f simultaneously go to ∞ . The easiest way to integrate this sector is to use the second measure (7.33) ff. of Section 7.3.

The divergences of the integrand could also be eliminated by a mapping. This however induces new singularities due to the measure (the term $1/(2\Delta(a, b, c))^2$ in T , Eq. (7.39)). This would not be the case, if we had not been forced to use the trick of integrating the measure by parts.

- (3) $b < \frac{1}{2}$ and $e < \frac{1}{2}$.

In this sector the mapping can be used successfully: a has to be exchanged with b and e with f . We get $T(b, a, c, d, f, e)$ with $a < \frac{1}{2}$ and $f < \frac{1}{2}$. This is integrated using the measure (7.38).



D		D		D	
1.00	2	1.30	$2.52 \times 10^{-1} \pm 4 \times 10^{-3}$	1.70	$3.9 \times 10^{-4} \pm 2 \times 10^{-4}$
1.01	$1.56 \pm 0.02 + 0.36$	1.35	$1.62 \times 10^{-1} \pm 3 \times 10^{-3}$	1.75	$4.2 \times 10^{-5} \pm 3 \times 10^{-6}$
1.02	$1.56 \pm 0.02 + 0.25$	1.40	$9.88 \times 10^{-2} \pm 2 \times 10^{-3}$	1.80	$2.0 \times 10^{-6} \pm 3 \times 10^{-7}$
1.05	$1.42 \pm 0.02 + 0.07$	1.45	$5.62 \times 10^{-2} \pm 2 \times 10^{-3}$	1.85	$1.3 \times 10^{-8} \pm 3 \times 10^{-9}$
1.10	1.06 ± 0.02	1.50	$2.91 \times 10^{-2} \pm 6 \times 10^{-4}$	1.90	$8.6 \times 10^{-13} \pm 3 \times 10^{-13}$
1.15	0.775 ± 0.009	1.55	$1.35 \times 10^{-2} \pm 3 \times 10^{-4}$	1.95	$1.7 \times 10^{-25} \pm 2 \times 10^{-25}$
1.20	0.547 ± 0.007	1.60	$5.20 \times 10^{-3} \pm 2 \times 10^{-4}$	1.98	$< 10^{-48}$
1.25	0.379 ± 0.005	1.65	$1.61 \times 10^{-3} \pm 5 \times 10^{-5}$	2.00	0

Fig. 7.4. Numerical results for the integral of (7.23). The first error is the statistical error, the second an estimate for the correction due to the systematic error, which becomes important for $D \rightarrow 1$, cf. the text. In the plot, the boxes are the uncorrected, the crosses the corrected results.

7.5. Numerical calculations

The numerical calculations are difficult. We refer the interested reader to the discussion in Section 6.2 and for more details to Ref. [34], Section 6. Here we only give the result, see Fig. 7.4. The extrapolation for $D \rightarrow 1$ is consistent with the analytic result 2, found in Subsection 7.6.

We however want to discuss our estimate of the systematic error. It is a general phenomenon that our algorithm fails to correctly integrate for integrals over four points in the limit $D \rightarrow 1$. This is due to problems in the domain $a_2 \rightarrow 0$ and $f_2 \rightarrow 0$ and thus occurs even for integrals which are well behaved at small and large distances. An example of such a function is

$$F(a, b, c, d, e, f) = (a^2 + b^2 + c^2 + d^2 + e^2 + f^2)^{-3D/2}, \quad (7.40)$$

which is analytically integrated to give

$$\frac{1}{S_D^2} \frac{\Gamma(\frac{D}{2})}{\Gamma(\frac{3D}{2})} \left(\frac{\pi}{4}\right)^D. \quad (7.41)$$

Table 7.1

Numerical results for the integral of (7.40)

D		D		D	
1.01	0.770 ± 0.002	1.05	0.951 ± 0.002	1.15	0.999 ± 0.002
1.02	0.843 ± 0.002	1.10	0.993 ± 0.002	1.20	0.999 ± 0.002

The ratio of the numerically and analytically calculated values is displayed in Table 7.1. As these factors should be independent of the integral which has to be performed, we use them to correct the numerical results.

7.6. The limit $D \rightarrow 1$

In the limit $D \rightarrow 1$, (7.17) can again be calculated analytically. This calculation is interesting as it reveals the connection to standard polymer theory and the fact that $\langle \text{diagram} \rangle_L$ decomposes into three topologically different and non-equivalent diagrams. As in Eq. (7.17) we keep $c = 1$ fixed. By a direct calculation it can be verified that the measure indeed reduces to an integral over a line. On this line two points, the endpoints of c , are already fixed. Then there are 12 different possibilities to distribute the last two points. They still can be separated into four topological inequivalent classes A, B, C and D, cf. Fig. 7.5. These are the four standard diagrams arising in polymer theory. In each of these classes the line with $c = 1$ may be chosen to be the line connecting (12), (14), (23) or (34). Readers more familiar with Feynman diagrams arising in the framework of a scalar field theory may recover the three corresponding diagrams after a de Gennes transformation [40]. They contribute to the renormalization of the φ^4 interaction at $d = 4$ and are represented on the r.h.s. Diagrams in one class can be mapped onto each other by the now well-known mapping of sectors. One subtlety however has to be taken into account. The marginal counterterm in Eq. (7.18) is not invariant by this mapping. In order to perform the integration only over one sector in every class, the symmetrized version will be used:

$$\begin{aligned}
 F(a, b, c, d, e, f) = & f^{-1} \left(af - \frac{1}{4}(b - c + e - d)^2 \right)^{-1} - a^{-1} f^{-2} \\
 & - \frac{1}{16} a^{-2} f^{-3} \left[(\Theta(f < c) + \Theta(f < b)) (bfb^{-1} - cfc^{-1})^2 \right. \\
 & \left. + (\Theta(f < d) + \Theta(f < e)) (efe^{-1} - dfd^{-1})^2 \right]. \quad (7.42)
 \end{aligned}$$

The diagrams give

$$\begin{aligned}
 \text{diagram} &= \frac{1}{4} \int_1^\infty da \int_1^\infty df \frac{1}{f(af - 1)} - \frac{1}{af^2} - \frac{1}{16} \frac{1}{a^2 f} \Theta(a - 1 - f) \\
 &= \frac{1}{4} - \frac{1}{16} \ln(2), \quad (7.43)
 \end{aligned}$$

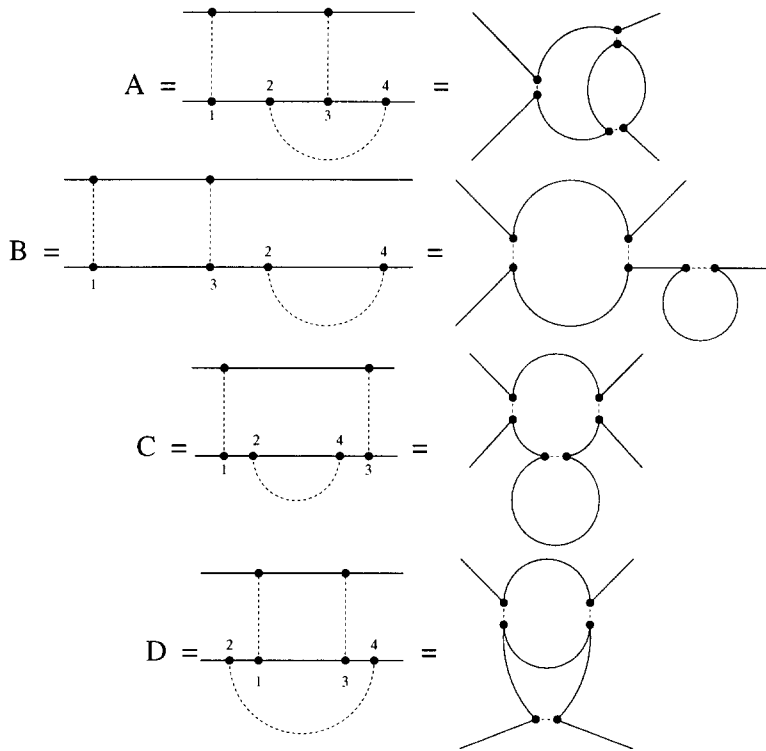


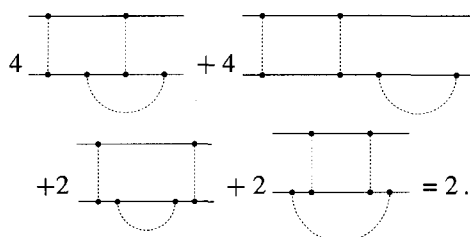
Fig. 7.5. The four topological inequivalent classes A, B, C and D and the equivalent diagrams in the $n \rightarrow 0$ limit of scalar φ^4 theory.

$$\begin{aligned}
 & \text{Diagram A} = \frac{1}{4} \int_0^\infty da \int_0^\infty df \frac{1}{af^2} - \frac{1}{af^2} - 0 \\
 & = 0,
 \end{aligned} \tag{7.44}$$

$$\begin{aligned}
 & \text{Diagram B} = \frac{1}{4} \int_0^\infty dd \int_0^\infty df \left[\frac{1}{f^2(1+d)} - \frac{1}{(1+f+d)f^2} \right. \\
 & \quad \left. - \frac{1}{4(1+f+d)^2 f} (2 + \Theta(f < 1) + \Theta(f < d)) \right] \\
 & = \frac{1}{4} + \frac{1}{8} \ln(2),
 \end{aligned} \tag{7.45}$$

$$\begin{aligned}
 & \text{Diagram C} = \frac{1}{4} \int_1^\infty df \int_0^{f-1} da \frac{1}{af(f-a)} - \frac{1}{af^2} \\
 & = \frac{1}{4}.
 \end{aligned} \tag{7.46}$$

Taking care of the combinatorial factor 4 for the sectors A and B and of the factor 2 for C and D, the final result is



$$4 + 4 + 2 + 2 = 2. \quad (7.47)$$

7.7. The correction for the unusual marginal counterterm

We recall that $\tilde{J}(L)$, given in Eq. (7.16) and which we calculated numerically, was not exactly the counterterm $J(L)$ but was modified in order to simplify the calculations. We still have to calculate the difference $J(L) - \tilde{J}(L)$, which also contributes to the counterterm:

$$J(L) - \tilde{J}(L) = \frac{\nu^2 d}{2} \int_{c=1; a, b, d, e, f, g} (a^{2\nu} + g^{2\nu})^{-d/2-1} f^{-\nu(d+2)} (\mathbf{bfb}^{-D} - \mathbf{cfc}^{-D})^2 \\ \times [\Theta(f < c) - \Theta(f < \max(a, b, c, g))] \max(a, b, c, f, g)^{-2\varepsilon}. \quad (7.48)$$

First of all, the integral over f is performed. Since

$$\int_{f < l} (\mathbf{bfb}^{-D} - \mathbf{cfc}^{-D})^2 f^{-\nu(d+2)} = \frac{1}{D} (\mathbf{bb}^{-D} - \mathbf{cc}^{-D})^2 \frac{l^\varepsilon}{\varepsilon} \quad (7.49)$$

we get

$$J(L) - \tilde{J}(L) = \frac{\nu^2 d}{2D} \int_{a=1; b, c, g} (a^{2\nu} + g^{2\nu})^{-d/2-1} (\mathbf{bb}^{-D} - \mathbf{cc}^{-D})^2 \\ \times \frac{1}{\varepsilon} [c^\varepsilon - \max(a, b, c, g)^\varepsilon] \max(a, b, c, f, g)^{-2\varepsilon} \\ = \frac{2-D}{2} \int_{a=1; b, c, g} (a^{2\nu} + g^{2\nu})^{-d/2-1} (\mathbf{bb}^{-D} - \mathbf{cc}^{-D})^2 \\ \times [\ln(c) - \ln(\max(a, b, c, g))] + \mathcal{O}(\varepsilon). \quad (7.50)$$

Since $(\mathbf{bb}^{-D} - \mathbf{cc}^{-D})^2$ is symmetric under the exchange of \mathbf{b} and \mathbf{c} , this can still be written as

$$\begin{aligned}
J(L) - \tilde{J}(L) &= \frac{2-D}{2} \int_{a=1; b, c, g} (a^{2\nu} + g^{2\nu})^{-d_c/2-1} \\
&\quad \times (b^{2-2D} + c^{2-2D} + (a^2 - b^2 - c^2)b^{-D}c^{-D})^2 \\
&\quad \times \left[\frac{1}{2} \ln(bc) - \ln(\max(a, b, c, g)) \right] + \mathcal{O}(\varepsilon). \quad (7.51)
\end{aligned}$$

Numerical integration

The domain of integration has to be split into the two sectors where either b or c is the smallest distance. These two sectors are equivalent, so the integral will be performed over $b < c$ only. The integral is furthermore split into the integral over the radial and the angular coordinate. We use the following change of variables:

$$b = u^{\frac{1}{D-\gamma_b}} (1-u)^{\frac{1}{D-\omega_b}}, \quad (7.52)$$

$$\omega_b = \frac{3}{2}D < 2D, \quad (7.53)$$

$$\gamma_b = 2D - 2, \quad (7.54)$$

$$\beta = \begin{cases} \frac{\pi}{2} (2\alpha)^{\frac{1}{D-1}} & \alpha \leq 0.5 \\ \pi - \frac{\pi}{2} (2-2\alpha)^{\frac{1}{D-1}} & \alpha > 0.5 \end{cases}, \quad (7.55)$$

$$c = \sqrt{b^2 + 1 - 2b \cos(\beta)}. \quad (7.56)$$

This gives

$$\begin{aligned}
\int_b &= \frac{\pi}{D-1} \frac{S_{D-1}}{S_D} \int_0^1 d\alpha \min(2\alpha, 2-2\alpha)^{\frac{2-D}{D-1}} \sin(\beta)^{D-2} \\
&\quad \times \int_0^1 du \left(\frac{1}{D-\gamma_b} \frac{1}{u} + \frac{1}{\omega_b-D} \frac{1}{1-u} \right) b^D. \quad (7.57)
\end{aligned}$$

The integral over g is independently parametrized as

$$g = v^{\frac{1}{D-\gamma_g}} (1-v)^{\frac{1}{D-\omega_g}}, \quad (7.58)$$

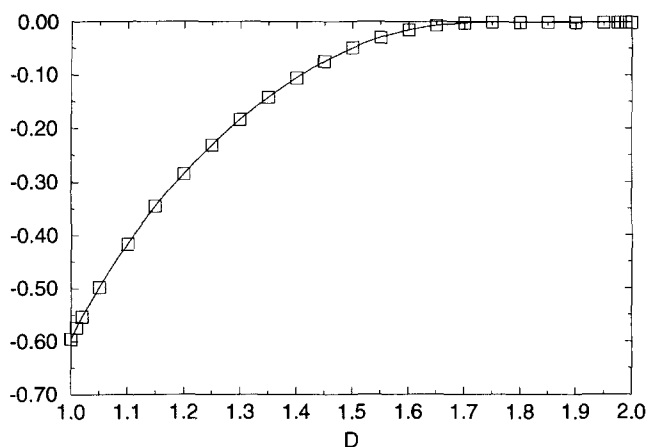
$$\omega_g = 1 + D < 2 + D, \quad (7.59)$$

$$\gamma_g = 0. \quad (7.60)$$

This implies

$$\int_g = \int_0^1 dv \left(\frac{1}{D-\gamma_g} \frac{1}{v} + \frac{1}{\omega_g-D} \frac{1}{1-v} \right) g^D. \quad (7.61)$$

The results of the numerical calculations are given in Fig. 7.6.



D		D		D		D	
1.00	-0.596573590	1.20	-2.85×10^{-1}	1.50	-4.96×10^{-2}	1.80	-2.94×10^{-5}
1.01	-5.75×10^{-1}	1.25	-2.31×10^{-1}	1.55	-2.97×10^{-2}	1.85	-3.51×10^{-7}
1.02	-5.55×10^{-1}	1.30	-1.84×10^{-1}	1.60	-1.56×10^{-2}	1.90	-4.05×10^{-11}
1.05	-4.98×10^{-1}	1.35	-1.42×10^{-1}	1.65	-6.64×10^{-3}	1.95	-4.01×10^{-23}
1.10	-4.16×10^{-1}	1.40	-1.06×10^{-1}	1.70	-2.08×10^{-3}	1.98	-2.50×10^{-59}
1.15	-3.46×10^{-1}	1.45	-7.50×10^{-2}	1.75	-3.90×10^{-4}	2.00	0

Fig. 7.6. Numerical results for Eq. (7.51). The error is $\pm 10^{-3}$ relative.

The limit $D \rightarrow 1$

For $D = 1$ the integral can again be performed analytically. We get

$$\begin{aligned}
 & \int_0^\infty dg \int_0^1 db (1+g)^{-3} (\ln(b) - \ln(\max(1, g))) \\
 &= \int_0^\infty dg (1+g)^{-3} \int_0^1 db \ln(b) - \int_1^\infty dg (1+g)^{-3} \ln(g) \\
 &= -\frac{1}{4} - \frac{1}{2} \ln(2) = -0.5965735903.
 \end{aligned} \tag{7.62}$$

8. Complementary contribution for the renormalization of the coupling constant

We still have to calculate C_3 , Eq. (4.38):

$$C_3 = \left\langle \left(\text{diagram 1} \right) \middle| \text{diagram 2} \right\rangle_{e^{-1}} \left(\left\langle \left(\text{diagram 3} \right) \middle| \text{diagram 4} \right\rangle_L \right)$$

$$+\frac{1}{2}\nu d \left\langle \left(\text{diagram} \right) \middle| \text{diagram} \right\rangle_{\varepsilon^{-1}} \right) . \quad (8.1)$$

The MOPE coefficient is

$$\left(\text{diagram} \right) = -\nu^2 d \left(\mathbf{b} \mathbf{b}^{-D} - \mathbf{c} \mathbf{c}^{-D} \right)^2 \left(a^{2\nu} + g^{2\nu} \right)^{-d/2-1} . \quad (8.2)$$

The non-trivial diagram in (8.1) is

$$\left\langle \text{diagram} \right\rangle_L = \int_{a,b,c,g < L} \left(\text{diagram} \right) . \quad (8.3)$$

Apply $L\partial/\partial L$ and map onto $a = L = 1$:

$$\begin{aligned} & \left\langle \text{diagram} \right\rangle_L \\ &= \frac{1}{\varepsilon} \int_{\substack{a=L \\ b,c,g}} \left(\text{diagram} \right) \max(a, b, c, g)^{-\varepsilon} \\ &= -\frac{\nu d}{\varepsilon} \int_{\substack{a=L \\ b,c,g}} \frac{2-D}{2} \left(\mathbf{b} \mathbf{b}^{-D} - \mathbf{c} \mathbf{c}^{-D} \right)^2 \left(a^{2\nu} + g^{2\nu} \right)^{-d/2-1} \max(a, b, c, g)^{-\varepsilon} . \end{aligned} \quad (8.4)$$

The second term in (8.1) shall subtract exactly the pole term of (8.4) divided by d , *not* the pole of (8.4), which contains a factor $d = d_c + \mathcal{O}(\varepsilon)$. To verify this, note that

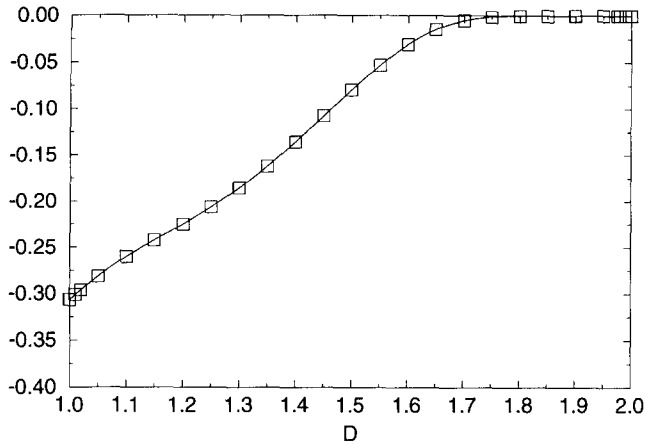
$$\int_{a=\text{fixed}, b,c} \frac{2-D}{2} \left(\mathbf{b} \mathbf{b}^{-D} - \mathbf{c} \mathbf{c}^{-D} \right)^2 = a^{2-D} , \quad (8.5)$$

which is proven by partial integration. This yields

$$\begin{aligned} & \frac{1}{\varepsilon} \int_{\substack{a=L \\ b,c,g}} \frac{2-D}{2} \left(\mathbf{b} \mathbf{b}^{-D} - \mathbf{c} \mathbf{c}^{-D} \right)^2 \left(a^{2\nu} + g^{2\nu} \right)^{-d_c/2-1} \\ &= \frac{1}{\varepsilon} \int_{\substack{a=L \\ b,c,g}} a^{2\nu} \left(a^{2\nu} + g^{2\nu} \right)^{-d_c/2-1} \\ &= \frac{1}{\varepsilon} \int_{\substack{a=L \\ b,c,g}} \frac{1}{2} \left(a^{2\nu} + g^{2\nu} \right) \left(a^{2\nu} + g^{2\nu} \right)^{-d_c/2-1} , \end{aligned} \quad (8.6)$$

where in the last step we used the invariance under conformal mapping. This is equivalent to

$$\frac{1}{2} \left\langle \text{diagram} \right\rangle_{\varepsilon^{-1}} , \quad (8.7)$$



D		D		D		D	
1.00	-0.306853	1.20	-0.225	1.50	-7.97×10^{-2}	1.80	-9.97×10^{-5}
1.01	-0.301	1.25	-0.206	1.55	-5.33×10^{-2}	1.85	-1.48×10^{-6}
1.02	-0.296	1.30	-0.185	1.60	-3.11×10^{-2}	1.90	-2.31×10^{-10}
1.05	-0.282	1.35	-0.162	1.65	-1.49×10^{-2}	1.95	-3.89×10^{-22}
1.10	-0.260	1.40	-0.136	1.70	-5.24×10^{-3}	1.975	-4.88×10^{-46}
1.15	-0.244	1.45	-0.108	1.75	-1.13×10^{-3}	2.00	0

Fig. 8.1. Numerical results for Eq. (8.8). The statistical error is 10^{-2} .

which proves the desired result. We therefore can write

$$\begin{aligned}
 & \left\langle \text{diagram} \right\rangle_L + \frac{1}{2} \nu d \left\langle \text{diagram} \right\rangle_{\varepsilon^{-1}} \\
 &= -\frac{\nu d}{\varepsilon} \int_{\substack{a=L \\ b,c,g}} \frac{2-D}{2} (bb^{-D} - cc^{-D})^2 \\
 & \quad \times \left\{ (a^{2\nu} + g^{2\nu})^{-d/2-1} \max(a, b, c, g)^{-\varepsilon} - (a^{2\nu} + g^{2\nu})^{-d_c/2-1} \right\} \\
 &= (-\nu d) \frac{1}{2} \int_{a=1; b,c,g} (bb^{-D} - cc^{-D})^2 (a^{2\nu} + g^{2\nu})^{-d_c/2-1} \\
 & \quad \times [\ln(a^{2\nu} + g^{2\nu}) - (2-D) \ln(\max(a, b, c, g))] + \mathcal{O}(\varepsilon). \quad (8.8)
 \end{aligned}$$

The method to numerically integrate (8.8) is the same as in Section 7.7. We give the results in Fig. 8.1.

In the limit $D \rightarrow 1$ (8.8) reduces to

$$-2 \int_0^\infty dg \frac{\ln(1+g)}{(1+g)^3} + 2 \int_1^\infty dg \frac{\ln(g)}{(1+g)^3} = \ln(2) - 1 = -0.306852819. \quad (8.9)$$

9. Renormalization of the wavefunction, main contribution

9.1. Derivation of an analytic expression

In this section, the calculation of \mathcal{F}_1 , defined in Eq. (4.31), will be discussed. We write

$$I(L) = 2\mathcal{F}_1 = \left\langle \text{diagram 1} \middle| \text{diagram 2} \right\rangle_L - \left\langle \text{diagram 3} \middle| \text{diagram 4} \right\rangle_L \left\langle \text{diagram 5} \middle| \text{diagram 6} \right\rangle_L - \left\langle \text{diagram 7} \middle| \text{diagram 8} \right\rangle_L \left\langle \text{diagram 9} \middle| \text{diagram 10} \right\rangle_L. \quad (9.1)$$

Let us discuss the MOPE coefficients involved. Explicit expressions are given later. The first is

$$\left(\text{diagram 1} \middle| \text{diagram 2} \right). \quad (9.2)$$

(9.2) has two different types of subdivergences, which are subtracted by the two counterterms in (9.1). Let us symbolically write down the factorization of the MOPE coefficients. If one of the dipoles is contracted first, the MOPE coefficient factorizes as

$$\begin{aligned} \left(\text{diagram 1} \middle| \text{diagram 2} \right) &= \left(\text{diagram 3} \middle| \text{diagram 4} \right) \left(\text{diagram 5} \middle| \text{diagram 6} \right) \\ &+ \left(\text{diagram 7} \middle| \text{diagram 8} \right) \left(\text{diagram 9} \middle| \text{diagram 10} \right) + \dots \end{aligned} \quad (9.3)$$

The first term is a relevant counterterm, which we did not mention explicitly in (9.1). The second subtracts the marginal subdivergence. Note that we have again to take care of the tensorial structure of the factorization.

If the two dipoles are contracted to a single dipole first, the factorization is

$$\left(\text{diagram 1} \middle| \text{diagram 2} \right) = \left(\text{diagram 3} \middle| \text{diagram 4} \right) \left(\text{diagram 5} \middle| \text{diagram 6} \right) + \dots \quad (9.4)$$

Note that any of these contractions is obtained with a combinatorial factor 2.

We now give a list of the MOPE coefficients together with the Θ -functions, which restrict each counterterm to the sector in which the divergence appears and which by integration delivers the factor $1/2$ from the nested integration, cf. Section 7.1. First of all

$$\left(\text{diagram 1} \middle| \text{diagram 2} \right) = A \quad (9.5)$$

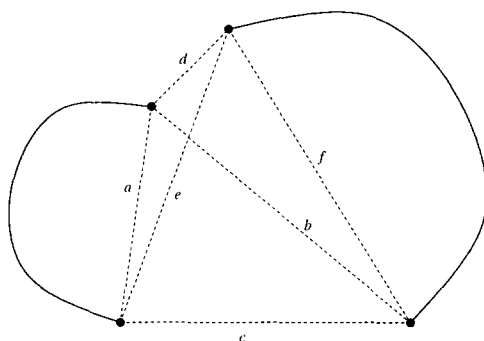


Fig. 9.1. The distances in (9.1).

with

$$A = -\frac{1}{2D} \left[f^{2\nu} a^2 + a^{2\nu} f^2 + \frac{1}{2} (e^2 + b^2 - c^2 - d^2) (c^{2\nu} - e^{2\nu} - b^{2\nu} + d^{2\nu}) \right] \\ \times \left[a^{2\nu} f^{2\nu} - \frac{1}{4} (c^{2\nu} - e^{2\nu} - b^{2\nu} + d^{2\nu})^2 \right]^{-d/2-1}. \quad (9.6)$$

The notation for the distances follows Fig. 9.1. The two relevant counterterms which appear, when a or f is contracted first and which can symbolically be written as

$$\left(\text{loop with two dots} \right) \left(\text{loop with two dots and a cross} \right) + \left(\text{loop with two dots and a cross} \right) \left(\text{loop with two dots} \right) = B \quad (9.7)$$

are

$$B = -\frac{1}{2D} (a^{-\nu d} f^{D-\nu d} + f^{-\nu d} a^{D-\nu d}). \quad (9.8)$$

The marginal counterterm

$$\left(\text{loop with two dots and a cross} \right) \left(\text{loop with two dots and a cross} \right) = C_1, C_2, \tilde{C}_1 \text{ or } \tilde{C}_2 \quad (9.9)$$

appears when either f is contracted first

$$C_1 = \left[\frac{2-D}{8D} (b^2 + e^2 - c^2 - d^2) ((f^2 + b^2 - d^2)b^{-D} - (f^2 + c^2 - e^2)c^{-D}) \right. \\ \times a^{-\nu(d+2)} f^{-\nu(d+2)} \\ - \frac{d+2}{64D} (2-D)^2 ((f^2 + b^2 - d^2)b^{-D} - (f^2 + c^2 - e^2)c^{-D})^2 \\ \times a^{D-\nu(d+2)} f^{-\nu(d+2)} \left. \right] \\ \times \Theta(f < \max(a, b, c)), \quad (9.10)$$

$$\begin{aligned}
\tilde{C}_1 = & \left[\frac{2-D}{8D} (b^2 + e^2 - c^2 - d^2) ((f^2 + e^2 - c^2)e^{-D} - (f^2 + d^2 - b^2)d^{-D}) \right. \\
& \times a^{-\nu(d+2)} f^{-\nu(d+2)} \\
& - \frac{d+2}{64D} (2-D)^2 ((f^2 + e^2 - c^2)e^{-D} - (f^2 + d^2 - b^2)d^{-D})^2 \\
& \times a^{D-\nu(d+2)} f^{-\nu(d+2)} \left. \right] \\
& \times \Theta(f < \max(a, d, e)), \tag{9.11}
\end{aligned}$$

or when a is contracted first,

$$\begin{aligned}
C_2 = & \left[\frac{2-D}{8D} (b^2 + e^2 - c^2 - d^2) ((a^2 + b^2 - c^2)b^{-D} - (a^2 + d^2 - e^2)d^{-D}) \right. \\
& \times a^{-\nu(d+2)} f^{-\nu(d+2)} \\
& - \frac{d+2}{64D} (2-D)^2 ((a^2 + b^2 - c^2)b^{-D} - (a^2 + d^2 - e^2)d^{-D})^2 \\
& \times f^{D-\nu(d+2)} a^{-\nu(d+2)} \left. \right] \\
& \times \Theta(a < \max(b, d, f)), \tag{9.12}
\end{aligned}$$

$$\begin{aligned}
\tilde{C}_2 = & \left[\frac{2-D}{8D} (b^2 + e^2 - c^2 - d^2) ((a^2 + e^2 - d^2)e^{-D} - (a^2 + c^2 - b^2)c^{-D}) \right. \\
& \times a^{-\nu(d+2)} f^{-\nu(d+2)} \\
& - \frac{d+2}{64D} (2-D)^2 ((a^2 + e^2 - d^2)e^{-D} - (a^2 + c^2 - b^2)c^{-D})^2 \\
& \times f^{D-\nu(d+2)} a^{-\nu(d+2)} \left. \right] \\
& \times \Theta(a < \max(c, e, f)). \tag{9.13}
\end{aligned}$$

Two equivalent versions are given as one e.g. may put the counterterm for $f \rightarrow 0$ on either endpoint of the distance f .

The last class of counterterms, Eq. (9.4), appears when either $(c, d) \rightarrow 0$ or $(b, e) \rightarrow 0$. For the first contraction, the two equivalent versions are

$$\begin{aligned}
D_1 = & -\frac{1}{2D} a^{D-\nu d} (c^{2\nu} + d^{2\nu})^{-d/2} \Theta(d < a) \Theta(c < a), \\
\tilde{D}_1 = & -\frac{1}{2D} f^{D-\nu d} (c^{2\nu} + d^{2\nu})^{-d/2} \Theta(d < f) \Theta(c < f). \tag{9.14}
\end{aligned}$$

For the second contraction they are

$$D_2 = -\frac{1}{2D} a^{D-\nu d} (e^{2\nu} + b^{2\nu})^{-d/2} \Theta(b < a) \Theta(e < a),$$

$$\tilde{D}_2 = -\frac{1}{2D} f^{D-\nu d} (e^{2\nu} + b^{2\nu})^{-d/2} \Theta(b < f) \Theta(e < f). \quad (9.15)$$

We now define the integrand which has to be taken in (9.1)

$$F(a, b, c, d, e, f) := A - B - \frac{1}{2} (C_1 + \tilde{C}_1 + C_2 + \tilde{C}_2 + D_1 + \tilde{D}_1 + D_2 + \tilde{D}_2). \quad (9.16)$$

We used the symmetric version of the counterterms, but could have also taken $\lambda C_1 + (1 - \lambda) \tilde{C}_1$ instead of $\frac{1}{2} (C_1 + \tilde{C}_1)$. We will use this freedom later in order to simplify the calculations. As usual this expression has to be integrated over all distances restricted to be smaller than L . Applying $L\partial/\partial L$ and mapping onto $c = L = 1$ results in

$$J(L) = L \frac{\partial}{\partial L} I(L) = \int_{c=1; a, b, d, e, f} F(a, b, c, d, e, f) \max(a, b, c, d, e, f)^{-2\varepsilon}. \quad (9.17)$$

The integral $J(L)$ is convergent as can be seen from a somehow tedious generalized Taylor expansion for the domains of possible divergences ($a \rightarrow 0$; $f \rightarrow 0$; $(c, d) \rightarrow 0$, or as c is fixed for all the other distances to ∞ ; $(b, e) \rightarrow 0$). So the term $\max(a, b, c, d, e, f)^{-2\varepsilon}$ can be dropped and the limit $\varepsilon \rightarrow 0$, $d \rightarrow d_c$ can be performed.

We furthermore have checked that the subtracted terms C_1 , \tilde{C}_1 , C_2 , \tilde{C}_2 , D_1 and D_2 are up to subdominant contributions in ε equivalent to the terms given in equation (9.1), i.e. that the changes in the domain of integration do not matter (the so-called “two-loop miracle”). This seems to be familiar by now, but nevertheless has to be checked.

9.2. Analytic continuation of the measure

Now $F(a, b, c, d, e, f)$ will be integrated numerically. The main problem is again, that the measure already used in Section 7 and defined in (7.19) has to be improved by partial integration. As in Subsection 7.2 we have to calculate the partial derivative applied to A , B , C_1 , \tilde{C}_1 , C_2 , \tilde{C}_2 , D_1 and D_2 , i.e. \mathbf{R} , given by Eq. (7.22) applied to these terms. Hereby \mathbf{R} will also act on the Θ -functions yielding terms proportional to the δ -distribution. We will first discuss some ingenious methods to analytically calculate these “non-diagonal” terms, which work well for D_1 , D_2 and C_1 , but fail for C_2 or equivalently \tilde{C}_2 . We then discuss another method to analytically continue the integral, which cannot be used for the numerics neither.

The problem is finally solved by brute force: As in Section 7 we change the prescription for the sectors so that the corresponding Θ -functions commute with \mathbf{R} . The corrections are calculated numerically.

To analyze the problem, we first write down \mathbf{R} applied to each term. We study especially the contributions proportional to the δ -distributions, which cannot be calculated numerically. In order to simplify these formulas, we use the identity $\nu d_c = 2D$,

$$\begin{aligned}
\mathbf{R}A = & -\frac{1}{2D} \left[(2-D)a^2 f^{-D} + 2a^{2\nu} + \frac{2-D}{2} (e^2 + b^2 - c^2 - d^2) (d^{-D} - e^{-D}) \right] \\
& \times \left[a^{2\nu} f^{2\nu} - \frac{1}{4} (c^{2\nu} - e^{2\nu} - b^{2\nu} + d^{2\nu})^2 \right]^{-d_c/2-1} \\
& + \frac{D+2}{2D} \left[f^{2\nu} a^2 + a^{2\nu} f^2 + \frac{1}{2} (e^2 + b^2 - c^2 - d^2) (c^{2\nu} - e^{2\nu} - b^{2\nu} + d^{2\nu}) \right] \\
& \times \left[a^{2\nu} f^{-D} - \frac{1}{2} (c^{2\nu} - e^{2\nu} - b^{2\nu} + d^{2\nu}) (d^{-D} - e^{-D}) \right] \\
& \times \left[a^{2\nu} f^{2\nu} - \frac{1}{4} (c^{2\nu} - e^{2\nu} - b^{2\nu} + d^{2\nu})^2 \right]^{-d_c/2-2}, \tag{9.18}
\end{aligned}$$

$$\mathbf{R}B = \frac{1}{2} a^{-2D} f^{-D-2} + a^{-D} f^{-2D-2}, \tag{9.19}$$

$$\begin{aligned}
\mathbf{R}C_1 = & \left[-\frac{(2-D)(2+D)}{8D} (b^2 + e^2 - c^2 - d^2) \right. \\
& \times ((f^2 + b^2 - d^2)b^{-D} - (f^2 + c^2 - e^2)c^{-D}) a^{-D-2} f^{-D-4} \\
& + \frac{(2-D)(2+D)^2}{32D} ((f^2 + b^2 - d^2)b^{-D} - (f^2 + c^2 - e^2)c^{-D})^2 a^{-2} f^{-D-4} \left. \right] \\
& \times \Theta(f < \max(a, b, c)) \\
& - \left[\frac{2-D}{8D} (b^2 + e^2 - c^2 - d^2) ((f^2 + b^2 - d^2)b^{-D} - (f^2 + c^2 - e^2)c^{-D}) \right. \\
& \times a^{-D-2} f^{-D-2} \\
& - \frac{(2-D)(2+D)}{32D} ((f^2 + b^2 - d^2)b^{-D} - (f^2 + c^2 - e^2)c^{-D})^2 a^{-2} f^{-D-2} \left. \right] \\
& \times \frac{1}{f} [\delta(f-a)\Theta(f>b)\Theta(f>c) + \delta(f-b)\Theta(f>a)\Theta(f>c) \\
& + \delta(f-c)\Theta(f>a)\Theta(f>b)], \tag{9.20}
\end{aligned}$$

$$\begin{aligned}
\mathbf{R}\tilde{C}_1 = & \left[-\frac{2-D}{8D} (b^2 + e^2 - c^2 - d^2) a^{-D-2} f^{-D-2} \right. \\
& \times (D(f^2 + e^2 - c^2)e^{-D-2} - D(f^2 + d^2 - b^2)d^{-D-2} - 4e^{-D} + 4d^{-D}) \\
& - \frac{(2-D)(2+D)}{8D} (b^2 + e^2 - c^2 - d^2) \\
& \times ((f^2 + e^2 - c^2)e^{-D} - (f^2 + d^2 - b^2)d^{-D}) a^{-D-2} f^{-D-4} \\
& + \frac{(2-D)(2+D)}{16D} ((f^2 + e^2 - c^2)e^{-D} - (f^2 + d^2 - b^2)d^{-D}) a^{-2} f^{-D-2} \left. \right]
\end{aligned}$$

$$\begin{aligned}
& \times \left(D(f^2 + e^2 - c^2)e^{-D-2} - D(f^2 + d^2 - b^2)d^{-D-2} - 4e^{-D} + 4d^{-D} \right) \\
& + \frac{(2-D)(2+D)^2}{32D} \left((f^2 + e^2 - c^2)e^{-D} - (f^2 + d^2 - b^2)d^{-D} \right)^2 a^{-2} f^{-D-4} \Big] \\
& \times \Theta(f < \max(a, d, e)) \\
& - \left[\frac{2-D}{8D} (b^2 + e^2 - c^2 - d^2) \left((f^2 + e^2 - c^2)e^{-D} - (f^2 + d^2 - b^2)d^{-D} \right) \right. \\
& \times a^{-D-2} f^{-D-2} \\
& \left. - \frac{(2-D)(2+D)}{32D} \left((f^2 + e^2 - c^2)e^{-D} - (f^2 + d^2 - b^2)d^{-D} \right)^2 a^{-2} f^{-D-2} \right] \\
& \times \frac{1}{f} \delta(a-f) \Theta(f > d) \Theta(f > e), \tag{9.21}
\end{aligned}$$

$$\begin{aligned}
\mathbf{RC}_2 = & \left[\frac{2-D}{8} (b^2 + e^2 - c^2 - d^2) (a^2 + d^2 - e^2) d^{-D-2} a^{-D-2} f^{-D-2} \right. \\
& - \frac{(2-D)(2+D)}{8D} (b^2 + e^2 - c^2 - d^2) \\
& \times \left((a^2 + b^2 - c^2)b^{-D} - (a^2 + d^2 - e^2)d^{-D} \right) a^{-D-2} f^{-D-4} \\
& - \frac{(2-D)(2+D)}{16} \left((a^2 + b^2 - c^2)b^{-D} - (a^2 + d^2 - e^2)d^{-D} \right) a^{-D-2} f^{-2} \\
& \times (a^2 + d^2 - e^2) d^{-D-2} \\
& \left. + \frac{(2-D)(2+D)}{16D} \left((a^2 + b^2 - c^2)b^{-D} - (a^2 + d^2 - e^2)d^{-D} \right)^2 a^{-D-2} f^{-4} \right] \\
& \times \Theta(a < \max(b, d, f)) \\
& + \left[\frac{2-D}{8D} (b^2 + e^2 - c^2 - d^2) \left((a^2 + b^2 - c^2)b^{-D} - (a^2 + d^2 - e^2)d^{-D} \right) \right. \\
& \times a^{-D-2} f^{-D-2} \\
& \left. - \frac{(2-D)(2+D)}{32D} \left((a^2 + b^2 - c^2)b^{-D} - (a^2 + d^2 - e^2)d^{-D} \right)^2 f^{-2} a^{-D-2} \right] \\
& \times \left[\frac{1}{d} \delta(a-d) \Theta(a > b) \Theta(a > f) + \frac{1}{f} \delta(a-f) \Theta(a > b) \Theta(a > d) \right], \tag{9.22}
\end{aligned}$$

$$\begin{aligned}
\mathbf{RC}_2 = & \left[-\frac{2-D}{8} (b^2 + e^2 - c^2 - d^2) (a^2 + e^2 - d^2) e^{-D-2} a^{-D-2} f^{-D-2} \right. \\
& - \frac{(2-D)(2+D)}{8D} (b^2 + e^2 - c^2 - d^2) \\
& \times \left((a^2 + e^2 - d^2)e^{-D} - (a^2 + c^2 - b^2)c^{-D} \right) a^{-D-2} f^{-D-4}
\end{aligned}$$

$$\begin{aligned}
& + \frac{(2-D)(2+D)}{16} \left((a^2 + e^2 - d^2)e^{-D} - (a^2 + c^2 - b^2)c^{-D} \right) a^{-D-2} f^{-2} \\
& \times (a^2 + e^2 - d^2)e^{-D-2} \\
& + \frac{(2-D)(2+D)}{16D} \left((a^2 + e^2 - d^2)e^{-D} - (a^2 + c^2 - b^2)c^{-D} \right)^2 a^{-D-2} f^{-4} \Big] \\
& \times \Theta(a < \max(c, e, f)) \\
& + \left[\frac{2-D}{8D} (b^2 + e^2 - c^2 - d^2) \right. \\
& \times \left((a^2 + e^2 - d^2)e^{-D} - (a^2 + c^2 - b^2)c^{-D} \right) a^{-D-2} f^{-D-2} \\
& \left. - \frac{(2-D)(2+D)}{32D} \left((a^2 + e^2 - d^2)e^{-D} - (a^2 + c^2 - b^2)c^{-D} \right)^2 a^{-D-2} f^{-2} \right] \\
& \times \left[\frac{1}{e} \delta(a-e) \Theta(a > c) \Theta(a > f) + \frac{1}{f} \delta(a-f) \Theta(a > c) \Theta(a > e) \right], \quad (9.23)
\end{aligned}$$

$$\begin{aligned}
\mathbf{RD}_1 &= a^{-D} (c^{2\nu} + d^{2\nu})^{-d_c/2-1} d^{-D} \Theta(d < a) \Theta(c < a) \\
&+ \frac{1}{2D} a^{-D} (c^{2\nu} + d^{2\nu})^{-d_c/2} \frac{1}{d} \delta(d-a) \Theta(c < a), \quad (9.24)
\end{aligned}$$

$$\begin{aligned}
\mathbf{R}\tilde{D}_1 &= \left(\frac{1}{2} f^{-D-2} (c^{2\nu} + d^{2\nu})^{-d_c/2-1} + f^{-D} (c^{2\nu} + d^{2\nu})^{-d_c/2-1} d^{-D} \right) \\
&\times \Theta(c < f) \Theta(d < f) - \frac{1}{2D} f^{-D} (c^{2\nu} + d^{2\nu})^{-d_c/2} \frac{1}{f} \delta(c-f) \Theta(d < f), \quad (9.25)
\end{aligned}$$

$$\begin{aligned}
\mathbf{RD}_2 &= a^{-D} (e^{2\nu} + b^{2\nu})^{-d_c/2-1} e^{-D} \Theta(b < a) \Theta(e < a) \\
&+ \frac{1}{2D} a^{-D} (e^{2\nu} + b^{2\nu})^{-d_c/2} \frac{1}{e} \delta(e-a) \Theta(b < a), \quad (9.26)
\end{aligned}$$

$$\begin{aligned}
\mathbf{R}\tilde{D}_2 &= \left(\frac{1}{2} f^{-D-2} (e^{2\nu} + b^{2\nu})^{-d_c/2} + f^{-D} (e^{2\nu} + b^{2\nu})^{-d_c/2-1} e^{-D} \right) \\
&\times \Theta(b < f) \Theta(e < f) - \frac{1}{2D} f^{-D} (e^{2\nu} + b^{2\nu})^{-d_c/2} \frac{1}{f} \delta(e-a) \Theta(b < a). \quad (9.27)
\end{aligned}$$

First we show that in this parametrization the terms proportional to the δ -distribution in (9.24) and (9.26) can be calculated analytically. We demonstrate that for (9.24).

We use the standard measure of Eq. (7.19). The vectors over which the integration will be performed are a and d . The integration over d_3 has been improved by partial integration. Let us apply that to the last term in (9.24), i.e. to

$$\frac{1}{2D} a^{-D} (c^{2\nu} + d^{2\nu})^{-d_c/2} \frac{1}{d} \delta(d-a) \Theta(c < a). \quad (9.28)$$

The integration over a is standard and can easily be performed, resulting in

$$\frac{1}{2D} (c^{2\nu} + d^{2\nu})^{-d_c/2} \frac{1}{d^2} \Theta(c < d). \quad (9.29)$$

The former integral over $\mathbf{d} = (x, y, z, 0, \dots)$ was

$$\frac{S_{D-2}}{S_D} \int_{-\infty}^{\infty} dx \int_{-\infty}^{\infty} dy \int_0^{\infty} dz z^{D-3} F(a, b, c, d, e, f) \quad (9.30)$$

and is changed to

$$\frac{1}{2-D} \frac{S_{D-2}}{S_D} \int_{-\infty}^{\infty} dx \int_{-\infty}^{\infty} dy \int_0^{\infty} dz z^{D-1} \mathbf{R}F(a, b, c, d, e, f). \quad (9.31)$$

Reversing the derivation of the measure we recognize the invariant measure in $D+2$ dimensions:

$$\frac{1}{2-D} \frac{S_{D-2} S_{D+2}}{S_D^2} \int_{d \in \mathbf{R}^{D+2}} = -\frac{1}{D} \int_{d \in \mathbf{R}^{D+2}}. \quad (9.32)$$

This can be summarized in the following formula, valid as long as the integral over \mathbf{d} factorizes from the integral over a, b and c :

$$\int_{d \in \mathbf{R}^D} F(a, b, c, d, e, f) = -\frac{1}{D} \int_{d \in \mathbf{R}^{D+2}} \mathbf{R}F(a, b, c, d, e, f). \quad (9.33)$$

The final result is given by the integral

$$-\frac{1}{2D^2} \int_1^{\infty} \frac{dd}{d} d^D (1 + d^{2\nu})^{-d_c/2} = -\frac{1}{4D^2(2-D)} \mathbf{B}\left(\frac{D}{2-D}, \frac{D}{2-D}\right), \quad (9.34)$$

where \mathbf{B} is the standard Beta-function. It is worth to mention that this is equivalent to



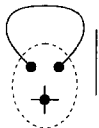

$$\frac{1}{D} \frac{1}{2} \left\langle \left(\text{diagram 1} \right) \middle| \text{diagram 2} \right\rangle_{\epsilon} \left\langle \left(\text{diagram 3} \right) \middle| \text{diagram 4} \right\rangle_{\epsilon}. \quad (9.35)$$

The factor $1/D$ is due to the measure, the factor $1/2$ due to the fact that the \mathbf{R} -operation is acting on half of the bounded distances only. The concerned reader will be able to reconstruct the factor $1/D$ from the identity

$$\int_d \frac{d_3^2}{d^2} F(d) = \frac{1}{D} \int_d F(d). \quad (9.36)$$

The analogous term in (9.26) gives the same result. It nevertheless is somehow harder to calculate. As a first step a mapping has to be performed, which exchanges b with c and d with e . This mapping is possible, although the measure is not invariant, as this mapping does not affect the height of the tetrahedron.

Equivalently it is possible to calculate the diagonal term of \mathbf{RC}_1 , Eq. (9.20). We find

$$\frac{1}{D} \left\langle \left(\text{diagram 1} \right) \middle| \text{diagram 2} \right\rangle_{\varepsilon} \left\langle \left(\text{diagram 3} \right) \middle| \text{diagram 4} \right\rangle_{\varepsilon}. \quad (9.37)$$





This time no factor $1/2$ appears, since \mathbf{R} was acting on all the distances.

The non-diagonal part of C_2 or \tilde{C}_2 *cannot* be calculated by these methods. (The concerned reader is encouraged to try this himself.) Nor is it possible to arrange the counterterms in such a way that the non-diagonal terms cancel. (Warning: The measure is not invariant by the conformal mapping, as the partial integration by f_3 has been performed.)

Regarding the problems with the \mathbf{R} -operation one may ask whether it is not better to use an alternative prescription for the analytic continuation. One might think of replacing the crucial integral

$$\int df_3 f_3^{D-3} F(a, b, c, d, e, f) \quad (9.38)$$

by

$$\int df_3 f_3^{D-3} F(a, b, c, d, e, f) - f_3^{D-3} F(a, b, c, d_p, e_p, f_p) \quad (9.39)$$

where d_p , e_p and f_p are the projections of d , e and f onto the plane spanned by f_1 and f_2 in the standard parametrization of the measure in Eq. (7.19). Here the problem arises that even if the length of $f = (f_1, f_2, f_3)$ is large, the length of $f_p = (f_1, f_2, 0)$ may tend to 0. This is a new divergence, which is integrable, but not tractable by the standard measure in the numerical integration procedure. Thus this method cannot be used.

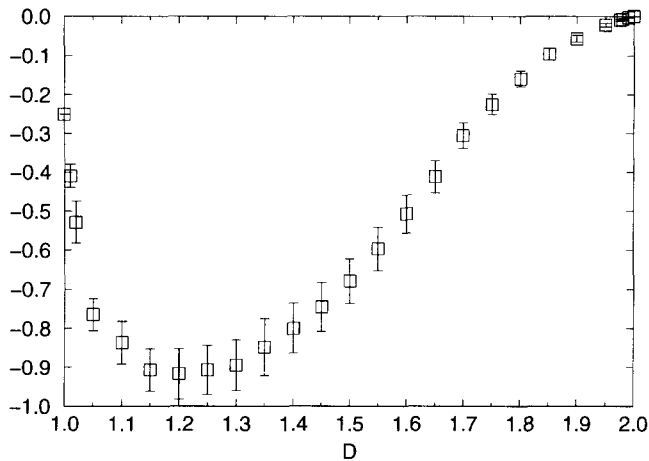
9.3. Numerical integration

We finally solve the problem by modifying as in Section 7 the Θ -functions and by calculating the corrections later. We integrate $\mathbf{R}\tilde{F}(a, b, c, d, e, f)$, where

$$\tilde{F} = A - B - \tilde{C}_1 - \tilde{C}_2 - D_1 - D_2 \quad (9.40)$$

but with modified prescriptions for the sectors: $f < d$ for \tilde{C}_1 , $a < c$ for \tilde{C}_2 , $c < a$ for D_1 and $b < a$ for D_2 . We therefore have to integrate numerically:

$$\begin{aligned}
& \mathbf{R}\tilde{F}(a, b, c, d, e, f) \\
&= -\frac{1}{2D} \left[(2-D)a^2 f^{-D} + 2a^{2\nu} + \frac{2-D}{2} (e^2 + b^2 - c^2 - d^2) (d^{-D} - e^{-D}) \right] \\
&\quad \times \left[a^{2\nu} f^{2\nu} - \frac{1}{4} (c^{2\nu} - e^{2\nu} - b^{2\nu} + d^{2\nu})^2 \right]^{-d_c/2-1} \\
&\quad + \frac{D+2}{2D} \left[f^{2\nu} a^2 + a^{2\nu} f^2 + \frac{1}{2} (e^2 + b^2 - c^2 - d^2) (c^{2\nu} - e^{2\nu} - b^{2\nu} + d^{2\nu}) \right] \\
&\quad \times \left[a^{2\nu} f^{-D} - \frac{1}{2} (c^{2\nu} - e^{2\nu} - b^{2\nu} + d^{2\nu}) (d^{-D} - e^{-D}) \right] \\
&\quad \times \left[a^{2\nu} f^{2\nu} - \frac{1}{4} (c^{2\nu} - e^{2\nu} - b^{2\nu} + d^{2\nu})^2 \right]^{-d_c/2-2} \\
&\quad - \frac{1}{2} a^{-2D} f^{-D-2} - a^{-D} f^{-2D-2} \\
&\quad + \left[\frac{2-D}{8D} (b^2 + e^2 - c^2 - d^2) a^{-D-2} f^{-D-2} \right. \\
&\quad \times (D(f^2 + e^2 - c^2)e^{-D-2} - D(f^2 + d^2 - b^2)d^{-D-2} - 4e^{-D} + 4d^{-D}) \\
&\quad + \frac{(2-D)(2+D)}{8D} (b^2 + e^2 - c^2 - d^2) \\
&\quad \times ((f^2 + e^2 - c^2)e^{-D} - (f^2 + d^2 - b^2)d^{-D}) a^{-D-2} f^{-D-4} \\
&\quad - \frac{(2-D)(2+D)}{16D} ((f^2 + e^2 - c^2)e^{-D} - (f^2 + d^2 - b^2)d^{-D}) a^{-2} f^{-D-2} \\
&\quad \times (D(f^2 + e^2 - c^2)e^{-D-2} - D(f^2 + d^2 - b^2)d^{-D-2} - 4e^{-D} + 4d^{-D}) \\
&\quad \left. - \frac{(2-D)(2+D)^2}{32D} ((f^2 + e^2 - c^2)e^{-D} - (f^2 + d^2 - b^2)d^{-D})^2 a^{-2} f^{-D-4} \right] \\
&\quad \times \Theta(f < d) \\
&\quad + \left[\frac{2-D}{8} (b^2 + e^2 - c^2 - d^2) (a^2 + e^2 - d^2) e^{-D-2} a^{-D-2} f^{-D-2} \right. \\
&\quad + \frac{(2-D)(2+D)}{8D} (b^2 + e^2 - c^2 - d^2) \\
&\quad \times ((a^2 + e^2 - d^2)e^{-D} - (a^2 + c^2 - b^2)c^{-D}) a^{-D-2} f^{-D-4} \\
&\quad - \frac{(2-D)(2+D)}{16} ((a^2 + e^2 - d^2)e^{-D} - (a^2 + c^2 - b^2)c^{-D}) a^{-D-2} f^{-2} \\
&\quad \times (a^2 + e^2 - d^2) e^{-D-2} \\
&\quad \left. - \frac{(2-D)(2+D)}{16D} ((a^2 + e^2 - d^2)e^{-D} - (a^2 + c^2 - b^2)c^{-D})^2 a^{-D-2} f^{-4} \right] \\
&\quad \times \Theta(a < c)
\end{aligned}$$



<i>D</i>		<i>D</i>		<i>D</i>	
1.00	-0.25	1.30	-0.895 ± 0.066	1.70	-0.306 ± 0.034
1.01	-0.315 ± 0.028 - 0.072	1.35	-0.848 ± 0.074	1.75	-0.225 ± 0.027
1.02	-0.446 ± 0.053 - 0.070	1.40	-0.800 ± 0.065	1.80	-0.159 ± 0.021
1.05	-0.727 ± 0.041 - 0.036	1.45	-0.746 ± 0.063	1.85	-0.096 ± 0.015
1.10	-0.831 ± 0.055 - 0.006	1.50	-0.680 ± 0.057	1.90	-0.056 ± 0.009
1.15	-0.905 ± 0.055	1.55	-0.597 ± 0.056	1.95	-0.022 ± 0.005
1.20	-0.917 ± 0.065	1.60	-0.507 ± 0.049	1.975	-0.0091 ± 0.0024
1.25	-0.907 ± 0.063	1.65	-0.412 ± 0.041	2.00	0

Fig. 9.2. Numerical results for (9.41). The first error is the statistical error, the second the correction for the systematic error as discussed in the text. The latter is only given, when it is not negligible.

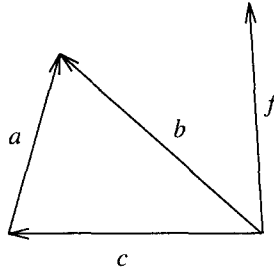
$$\begin{aligned}
 & -a^{-D}(c^{2\nu} + d^{2\nu})^{-d_c/2-1}d^{-D}\Theta(c < a) \\
 & -a^{-D}(e^{2\nu} + b^{2\nu})^{-d_c/2-1}e^{-D}\Theta(b < a).
 \end{aligned} \tag{9.41}$$

The variable transformations are the same as discussed in Sections 7.3 and 7.4. The numerical calculations are very difficult. Due to the complexity of the integrand, the numerical errors induced by the limited precision of the workstation became important too and limited the reduction of the statistical error. The total CPU time was about 1000 hours on a workstation. We obtained the numerical results summarized in Fig. 9.2.

The systematic error was corrected using Table 7.1. The error bars represent the statistical error of the AMC integration, which could not be reduced due to the lack of performance of the work-station, both in speed and in precision. The numerical results are in agreement with the analytically calculated value $-\frac{1}{4}$ for $D \rightarrow 1$, discussed later.

9.4. The correction for the first marginal counterterm

We arranged the counterterms \tilde{C}_1 and \tilde{C}_2 so that they both have the same correction. This correction is up to terms of $\mathcal{O}(\varepsilon)$ (for the notation cf. Fig. 9.3):

Fig. 9.3. The orientation of the vectors a , b , c and f .

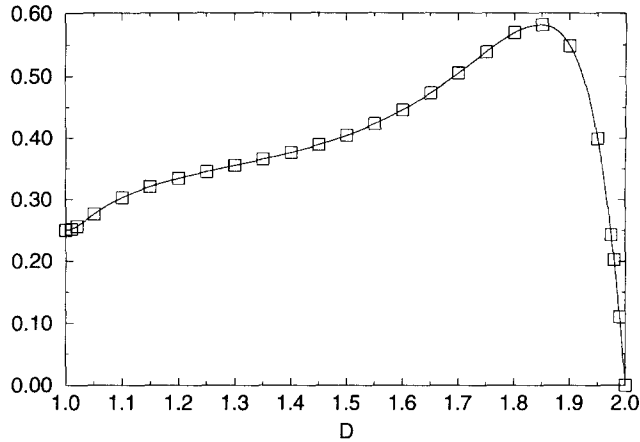
$$\begin{aligned}
 & \int_{c=1; a,b,d,e,f} \left[\frac{2-D}{2D} a f (b f b^{-D} - c f c^{-D}) a^{-\nu(d+2)} f^{-\nu(d+2)} \right. \\
 & \quad \left. - \frac{d+2}{16D} (2-D)^2 (b f b^{-D} - c f c^{-D})^2 a^{D-\nu(d+2)} f^{-\nu(d+2)} \right] \\
 & \quad \times [\Theta(f < c) - \Theta(f < \max(a, b, c))] \\
 & = \int_{a=1; b,c} \left[\frac{2-D}{2D^2} (a b b^{-D} - a c c^{-D}) a^{-\nu(d+2)} \right. \\
 & \quad \left. - \frac{(2-D)^2(2+d)}{16D^2} (b b^{-D} - c c^{-D})^2 a^{D-\nu(d+2)} \right] \\
 & \quad \times \frac{1}{\varepsilon} [c^\varepsilon - \max(a, b, c)^\varepsilon]. \tag{9.42}
 \end{aligned}$$

Expanding $\frac{1}{\varepsilon} [c^\varepsilon - \max(a, b, c)^\varepsilon] = \ln(c) - \ln(\max(a, b, c)) + \mathcal{O}(\varepsilon)$ and using the symmetry of (9.42) yields

$$\begin{aligned}
 & \int_{a=1; b,c} \left[\frac{2-D}{4D^2} (a b b^{-D} - a c c^{-D}) a^{-D-2} - \frac{(2-D)(2+D)}{16D^2} (b b^{-D} - c c^{-D})^2 a^{-2} \right] \\
 & \quad \times [\ln(c) + \ln(b) - 2 \ln(\max(a, b, c))] + \mathcal{O}(\varepsilon) \\
 & = \int_{a=1; b,c} \left[\frac{2-D}{8D^2} ((a^2 + b^2 - c^2) b^{-D} + (a^2 + c^2 - b^2) c^{-D}) a^{-D-2} \right. \\
 & \quad \left. - \frac{(2-D)(2+D)}{16D^2} (b^{2-2D} + c^{2-2D} + (a^2 - b^2 - c^2) b^{-D} c^{-D}) \right] a^{-2} \\
 & \quad \times [\ln(c) + \ln(b) - 2 \ln(\max(a, b, c))] + \mathcal{O}(\varepsilon). \tag{9.43}
 \end{aligned}$$

This integral is calculated numerically using the measure given by (7.52)–(7.57) in Section 7.7. The results are given in Fig. 9.4.

For $D \rightarrow 1$ an analytical calculation gives



D	D	D	D	D
1.00 1/4	1.15 0.321	1.40 0.376	1.65 0.473	1.90 0.548
1.01 0.252	1.20 0.334	1.45 0.389	1.70 0.505	1.95 0.399
1.02 0.256	1.25 0.345	1.50 0.405	1.75 0.539	1.975 0.244
1.05 0.276	1.30 0.355	1.55 0.423	1.80 0.570	1.99 0.110
1.10 0.303	1.35 0.365	1.60 0.446	1.85 0.581	2.00 0

Fig. 9.4. Numerical results for (9.43). The relative statistical error is 10^{-3} .

$$\frac{1}{2} \int_0^1 db \ln(b) - \frac{3}{4} \int_0^1 db \ln(b) = \frac{1}{4}. \quad (9.44)$$

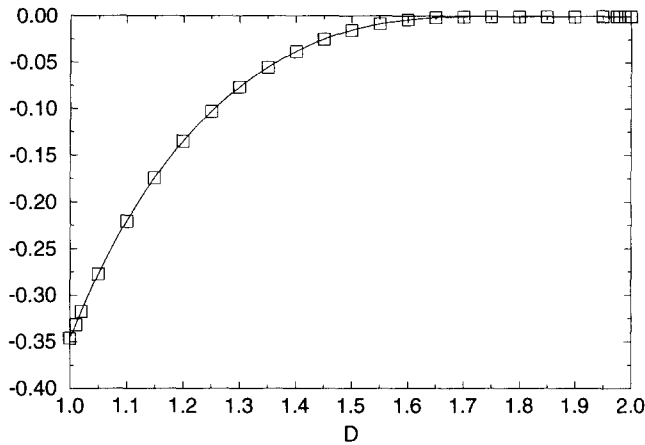
This is in agreement with the numerical data in Fig. 9.4.

9.5. The correction for the second marginal counterterm

Up to order ε for D_1 and D_2 each, the following correction has to be added:

$$\begin{aligned}
 & \frac{1}{2D} \int_{c=1; a,b,d,e,f} a^{D-\nu d} (c^{2\nu} + d^{2\nu})^{-d/2} \Theta(c < a) (\Theta(d < a) - 1) \\
 &= -\frac{1}{2D} \int_{c=1; d>c} (c^{2\nu} + d^{2\nu})^{-d/2} \frac{1}{\varepsilon} (d^e - c^e) \\
 &= \frac{1}{2D} \frac{1}{(2-D)^2} \int_0^1 \frac{dx}{x} x^{D/(2-D)} (1+x)^{-2D/(2-D)} \ln(x) + \mathcal{O}(\varepsilon). \quad (9.45)
 \end{aligned}$$

For $D \rightarrow 1$ an analytical calculation gives



D		D		D	
1.00	-3.4657×10^{-1}	1.30	-7.7076×10^{-2}	1.70	-4.7420×10^{-4}
1.01	-3.3167×10^{-1}	1.35	-5.5699×10^{-2}	1.75	-8.3621×10^{-5}
1.02	-3.1736×10^{-1}	1.40	-3.8640×10^{-2}	1.80	-6.1097×10^{-6}
1.05	-2.7766×10^{-1}	1.45	-2.5397×10^{-2}	1.85	-7.5149×10^{-8}
1.10	-2.2098×10^{-1}	1.50	-1.5529×10^{-2}	1.90	-1.0256×10^{-11}
1.15	-1.7416×10^{-1}	1.55	-8.6017×10^{-3}	1.95	-1.7552×10^{-23}
1.20	-1.3541×10^{-1}	1.60	-4.1478×10^{-3}	1.975	-2.8185×10^{-47}
1.25	-1.0338×10^{-1}	1.65	-1.6350×10^{-3}	2.00	0

Fig. 9.5. Numerical results for (9.45). The relative statistical error is 10^{-5} .

$$\frac{1}{2} \int_0^1 dx \frac{\ln(x)}{(1+x)^2} = -\frac{1}{2} \ln 2 = -0.3465735903. \quad (9.46)$$

The numerical data are given in Fig. 9.5. Numerical and analytical data fit nicely together.

9.6. Analytical calculation for $D \rightarrow 1$

We calculate now $J(L=1)$, Eq. (9.17), for $D=1$ and $\varepsilon=0$. We give the integrals and the numerical results for the different regions. The combinatorial factor 4 for every pair of integrals compensates against the factor $1/4$ from the measure. The symmetrized version of the counterterms has to be used. Otherwise the four integrals in one equivalence class may not coincide. So we have to integrate $A - B - \frac{1}{2}(C_1 + \tilde{C}_1 + C_2 + \tilde{C}_2 + D_1 + \tilde{D}_1 + D_2 + \tilde{D}_2)$. The three topologically different diagrams and the corresponding Feynman diagrams of scalar φ^4 -theory are shown in Fig. 9.6.

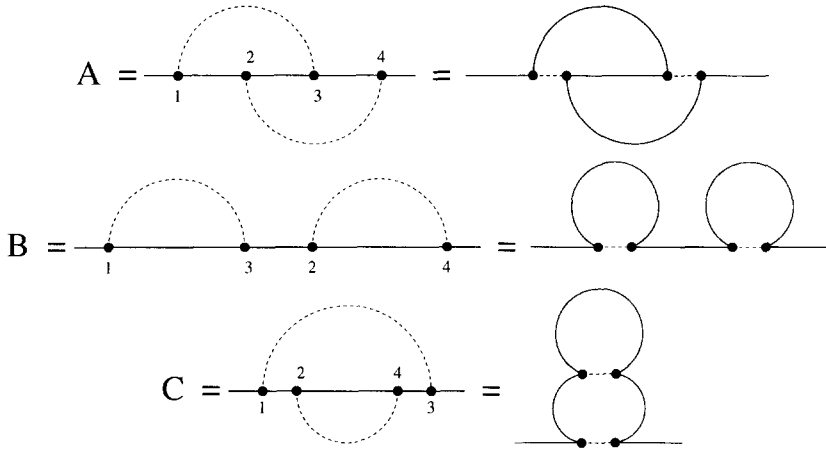


Fig. 9.6. The three topological inequivalent classes A, B and C and the corresponding Feynman diagrams of scalar φ^4 theory in the limit $N \rightarrow 0$.

$$\begin{aligned}
 \text{Diagram A} &= \int_1^\infty da \int_1^\infty df \left[-\frac{1}{2} (fa^2 + af^2 - 2af)(af - 1)^{-3} \right. \\
 &\quad + \frac{1}{2} (a^{-2}f^{-1} + a^{-1}f^{-2}) \\
 &\quad + \frac{1}{4} a^{-2}f^{-1} \Theta(a - f) + \frac{1}{4} a^{-1}(a + f - 2)^{-2} \Theta(a - f + 1) \\
 &\quad \left. + \frac{1}{4} a^{-1}f^{-2} \Theta(f - a) + \frac{1}{4} f^{-1}(a + f - 2)^{-2} \Theta(f - a + 1) \right] \\
 &= -\frac{1}{2} \ln(2) + \frac{3}{4}, \tag{9.47}
 \end{aligned}$$

$$\begin{aligned}
 \text{Diagram B} &= \int_0^\infty da \int_0^\infty df 0 \\
 &= 0, \tag{9.48}
 \end{aligned}$$

$$\begin{aligned}
 \text{Diagram C} &= \int_1^\infty da \int_0^{a-1} df \left[-\frac{1}{2} af^{-2}(a - f)^{-2} + \frac{1}{2} (a^{-2}f^{-1} + f^{-2}a^{-1}) \right. \\
 &\quad + \frac{1}{2} a^{-2}f^{-1} + \frac{1}{4} (a^{-1}(a - f)^{-2} + a^{-1}(a + f)^{-2}) \\
 &\quad \left. + \frac{1}{4} f^{-1}(a - f)^{-2} \Theta(f - 1) \Theta(2f + 1 - a) \right] \\
 &= -\frac{1}{2} \ln(2) - \frac{1}{2}. \tag{9.49}
 \end{aligned}$$

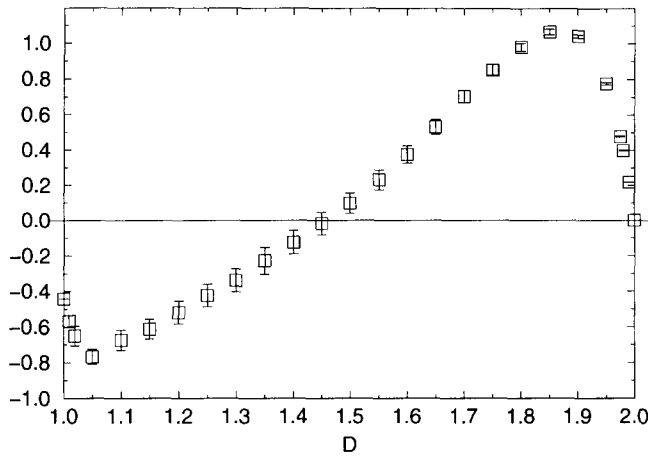


Fig. 9.7. Numerical results for $J(1)$, Eq. (9.17). Only the statistical error is given. The systematic error has been corrected.

Together this gives

$$\begin{aligned}
 & \text{[Diagram 1]} + \text{[Diagram 2]} + \text{[Diagram 3]} = -\ln(2) + \frac{1}{4} \\
 & = -0.4431 \dots \quad (9.50)
 \end{aligned}$$

9.7. The complete diagram

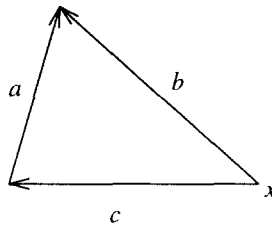
In Fig. 9.7 we show the complete results for $J(1)|_{\varepsilon=0}$, Eq. (9.17). We can verify that the limit $D \rightarrow 1$ is correctly reproduced within the error bars.

10. Second contribution to the renormalization of the wave function

The second contribution to the renormalization of the wave function is, see (4.32),

$$\begin{aligned}
 \mathcal{F}_2 = & -\frac{1}{2} \left\langle \text{[Diagram 1]} \middle| \text{[Diagram 2]} \right\rangle_{\varepsilon} \left(\left\langle \text{[Diagram 3]} \middle| \text{[Diagram 4]} \right\rangle_L + \nu(d+2) \left\langle \text{[Diagram 5]} \middle| \text{[Diagram 6]} \right\rangle_L \right. \\
 & \left. - \left\langle \text{[Diagram 7]} \middle| \text{[Diagram 8]} \right\rangle_L \left\langle \text{[Diagram 9]} \middle| \text{[Diagram 10]} \right\rangle_L \right).
 \end{aligned}$$

In order to determine \mathcal{F}_2 , we calculate

Fig. 10.1. The orientation of the vectors a , b and c and the position of the point x .

$$\left\langle \begin{array}{c} \text{loop with two dots} \\ \text{dashed circle} \end{array} \middle| \begin{array}{c} \text{dot} \\ \text{cross} \end{array} \right\rangle_L + \nu(d+2) \left\langle \begin{array}{c} \text{loop with two dots} \\ \text{dashed circle} \end{array} \middle| \begin{array}{c} \text{dot} \\ \text{cross} \end{array} \right\rangle_L - \left\langle \begin{array}{c} \text{loop with two dots} \\ \text{dashed circle} \end{array} \middle| \begin{array}{c} \text{dot} \\ \text{cross} \end{array} \right\rangle_L \left\langle \begin{array}{c} \text{two dots} \\ \text{dashed circle} \end{array} \middle| \begin{array}{c} \text{dot} \\ \text{cross} \end{array} \right\rangle_L. \quad (10.1)$$

We recall that

$$\left\langle \begin{array}{c} \text{loop with two dots} \\ \text{dashed circle} \end{array} \middle| \begin{array}{c} \text{dot} \\ \text{cross} \end{array} \right\rangle_L = \frac{\nu(d+2)}{2D} \frac{2-D}{2} \int_{a,b,c < L} (bb^{-D} - cc^{-D})^2 a^{D-\nu(d+2)} \\ - \frac{2-D}{D} \int_{a,b,c < L} (abb^{-D} - acc^{-D}) a^{-\nu(d+2)}, \quad (10.2)$$

$$\left\langle \begin{array}{c} \text{loop with two dots} \\ \text{dashed circle} \end{array} \middle| \begin{array}{c} \text{dot} \\ \text{cross} \end{array} \right\rangle_L \left\langle \begin{array}{c} \text{two dots} \\ \text{dashed circle} \end{array} \middle| \begin{array}{c} \text{dot} \\ \text{cross} \end{array} \right\rangle_L = -\frac{2-D}{D} \int_{a,c < L} a^{-\nu(d+2)} (a^2 - D(ac)^2 c^{-2}) c^{-D} \quad (10.3)$$

and

$$\nu(d+2) \left\langle \begin{array}{c} \text{loop with two dots} \\ \text{dashed circle} \end{array} \middle| \begin{array}{c} \text{dot} \\ \text{cross} \end{array} \right\rangle_L = -\frac{\nu(d+2)}{2D} \int_{a < L} a^{D-\nu d}. \quad (10.4)$$

First of all one easily convinces oneself that the integral equals 0 for $D = 1$. In the following we give two independent derivations, which were both integrated numerically and which were found to coincide. This gives an additional check that the global prefactor, which cannot be checked analytically, is correct.

We start with the first derivation: In order to subtract (10.4) from the first term in (10.2) we use the fact that (for the notation see Fig. 10.1)

$$\frac{2-D}{2} \int_{a=\text{fixed}; b,c} (bb^{-D} - cc^{-D})^2 = a^{2-D}. \quad (10.5)$$

Therefore the first contribution is

$$\frac{\nu(d+2)}{2D} \frac{2-D}{2} \left[\int_{a,b,c < L} - \int_{a < L} \right] (bb^{-D} - cc^{-D})^2 a^{D-\nu(d+2)}. \quad (10.6)$$

Applying $\frac{1}{\varepsilon} L \frac{\partial}{\partial L}$ and mapping onto $a = 1$ yields

$$\frac{\nu(d+2)}{2D} \frac{2-D}{2} \int_{a=1; b,c} (bb^{-D} - cc^{-D})^2 a^{D-\nu(d+2)} \frac{1}{\varepsilon} (\max(a, b, c)^{-\varepsilon} - a^{-\varepsilon}). \quad (10.7)$$

In the limit $\varepsilon \rightarrow 0$ this expression simplifies to

$$-\frac{(2-D)(2+D)}{4D} \int_{a=1; b,c} (bb^{-D} - cc^{-D})^2 a^{-D-2} \times (\ln(\max(a, b, c)) - \ln(a)) + \mathcal{O}(\varepsilon). \quad (10.8)$$

The second contribution is

$$\begin{aligned} & -\frac{2-D}{D} \int_{a,b,c < L} (abb^{-D} - acc^{-D}) a^{-\nu(d+2)} \\ & + \frac{2-D}{D} \int_{a,c < L} (a^2 - D(ac)^2 c^{-2}) c^{-D} a^{-\nu(d+2)} \\ & = -\frac{2-D}{D} \int_{a,b,c < L} [(abb^{-D} - acc^{-D}) - (a^2 - D(ac)^2 c^{-2}) c^{-D}] a^{-\nu(d+2)} \\ & + \frac{2-D}{D} \left[\int_{a,c < L} - \int_{a,b,c < L} \right] (a^2 - D(ac)^2 c^{-2}) c^{-D} a^{-\nu(d+2)}. \end{aligned} \quad (10.9)$$

The last term becomes after application of $\frac{1}{\varepsilon} L \frac{\partial}{\partial L}$ and mapping onto $a = 1$:

$$\frac{2-D}{D} \int_{a=1; b,c} (a^2 - D(ac)^2 c^{-2}) c^{-D} a^{-\nu(d+2)} \frac{1}{\varepsilon} (\max(a, c)^{-\varepsilon} - \max(a, b, c)^{-\varepsilon}). \quad (10.10)$$

In the limit $\varepsilon \rightarrow 0$ it reduces to

$$\begin{aligned} & \frac{2-D}{D} \int_{a=1; b,c} (a^2 - D(ac)^2 c^{-2}) c^{-D} a^{-D-2} (\ln(\max(a, b, c)) - \ln(\max(a, c))) \\ & + \mathcal{O}(\varepsilon). \end{aligned} \quad (10.11)$$

The other term in (10.9) is

$$-\frac{2-D}{D} \int_{a,b,c < L} [(\mathbf{a} \mathbf{b} \mathbf{b}^{-D} - \mathbf{a} \mathbf{c} \mathbf{c}^{-D}) - (a^2 - D(\mathbf{a} \mathbf{c})^2 c^{-2}) c^{-D}] a^{-\nu(d+2)}. \quad (10.12)$$

By power counting, a pole in $\frac{1}{\varepsilon}$ can appear for $a \rightarrow 0$. In this limit however the terms in the square brackets cancel and make the integral finite. Let us apply $L \frac{\partial}{\partial L}$ and map onto $a = 1$:

$$-\frac{2-D}{D} \int_{a=1; b,c} [(\mathbf{a} \mathbf{b} \mathbf{b}^{-D} - \mathbf{a} \mathbf{c} \mathbf{c}^{-D}) - (a^2 - D(\mathbf{a} \mathbf{c})^2 c^{-2}) c^{-D}] \times a^{-D-2} a^\varepsilon \max(a, b, c)^{-\varepsilon}. \quad (10.13)$$

This integral is a function of ε , which has the form

$$c_1 \varepsilon + \mathcal{O}(\varepsilon^2). \quad (10.14)$$

Especially it vanishes for $\varepsilon = 0$. The integral thus does not change if we subtract its value for $\varepsilon = 0$. Eq. (10.12) then becomes – remember that a factor $\frac{1}{\varepsilon}$ has to be reintroduced:

$$-\frac{2-D}{D} \int_{a=1; b,c} [(\mathbf{a} \mathbf{b} \mathbf{b}^{-D} - \mathbf{a} \mathbf{c} \mathbf{c}^{-D}) - (a^2 - D(\mathbf{a} \mathbf{c})^2 c^{-2}) c^{-D}] a^{-D-2} \times \frac{1}{\varepsilon} (a^\varepsilon \max(a, b, c)^{-\varepsilon} - 1). \quad (10.15)$$

In the limit $\varepsilon \rightarrow 0$ this simplifies to

$$\frac{2-D}{D} \int_{a=1; b,c} [(\mathbf{a} \mathbf{b} \mathbf{b}^{-D} - \mathbf{a} \mathbf{c} \mathbf{c}^{-D}) - (a^2 - D(\mathbf{a} \mathbf{c})^2 c^{-2}) c^{-D}] a^{-D-2} \times (\ln(\max(a, b, c)) - \ln(a)) + \mathcal{O}(\varepsilon). \quad (10.16)$$

The final result is the sum of (10.8), (10.11) and (10.16):

$$\begin{aligned} & \left\langle \text{diagram 1} \right\rangle_L + \nu(d+2) \left\langle \text{diagram 2} \right\rangle_L - \left\langle \text{diagram 3} \right\rangle_L \left\langle \text{diagram 4} \right\rangle_L \\ &= -\frac{(2-D)(2+D)}{4D} \int_{a=1; b,c} (b^{2-2D} + c^{2-2D} + (a^2 - b^2 - c^2) b^{-D} c^{-D}) a^{-D-2} \\ & \quad \times (\ln(\max(a, b, c)) - \ln(a)) \\ & \quad + \frac{2-D}{2D} \int_{a=1; b,c} \left[(a^2 - D/4 (a^2 + c^2 - b^2)^2 c^{-2}) c^{-D} (\ln(a) - \ln(\max(a, c))) \right. \\ & \quad \left. + (a^2 - D/4 (a^2 + b^2 - c^2)^2 b^{-2}) b^{-D} (\ln(a) - \ln(\max(a, b))) \right] \end{aligned}$$

$$\begin{aligned}
& + \left((a^2 + b^2 - c^2)b^{-D} + (a^2 + c^2 - b^2)c^{-D} \right) \left(\ln(\max(a, b, c)) - \ln(a) \right) \Big] \\
& \times a^{-D-2} + \mathcal{O}(\varepsilon). \quad (10.17)
\end{aligned}$$

Another way to treat the second term in (10.2) is to perform a partial integration (for the notation see Fig. 10.1):

$$\begin{aligned}
& \frac{1}{D} \int_{a < L} \int_x \Theta(L-b) \Theta(L-c) \mathbf{a} \nabla_x (b^{2-D} - c^{2-D}) a^{-\nu(d+2)} \\
& = -\frac{1}{D} \int_{a < L} \int_x \mathbf{a} \nabla_x [\Theta(L-b) \Theta(L-c)] (b^{2-D} - c^{2-D}) a^{-\nu(d+2)} \\
& = -\frac{1}{D} \int_{a < L} \int_x \mathbf{a} (\delta(L-b) b b^{-2} \Theta(L-c) + \Theta(L-b) \delta(L-c) c c^{-2}) \\
& \quad \times (b^{2-D} - c^{2-D}) a^{-\nu(d+2)} \\
& = -\frac{1}{D} \int_{a, c < b=L} \mathbf{a} b b^{-2} (b^{2-D} - c^{2-D}) a^{-\nu(d+2)} \\
& \quad - \frac{1}{D} \int_{a, b < c=L} \mathbf{a} c c^{-2} (b^{2-D} - c^{2-D}) a^{-\nu(d+2)} \\
& = -\frac{2}{D} \int_{a, b < c=L} \mathbf{a} c c^{-2} (b^{2-D} - c^{2-D}) a^{-\nu(d+2)}. \quad (10.18)
\end{aligned}$$

The pole in (10.3) has to be subtracted. It can be written as

$$-\frac{2-D}{D} \int_{a < L; c=L} (\mathbf{a} c)^2 a^{-\nu(d+2)} c^{-2-D} \quad (10.19)$$

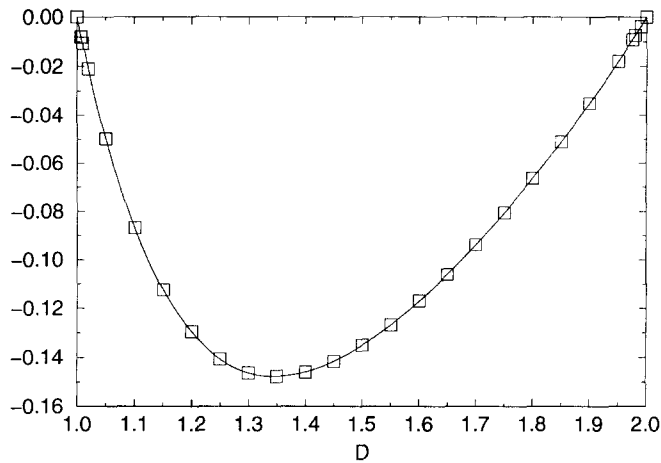
and is split into two parts,

$$-\frac{2-D}{D} \left[\int_{a, b < c=L} + \int_{a < c=L < b} \right] (\mathbf{a} c)^2 a^{-\nu(d+2)} c^{-2-D}, \quad (10.20)$$

which are mapped onto the same sector as in (10.18):

$$\begin{aligned}
& -\frac{2-D}{D} \int_{a, b < c=L} (\mathbf{a} c)^2 a^{-\nu(d+2)} c^{-2-D} \\
& + (\mathbf{a} b)^2 a^{-\nu(d+2)} b^{-2-D} (b/c)^{-\varepsilon} \Theta(a < b). \quad (10.21)
\end{aligned}$$

The complete expression, i.e. (10.18)–(10.21) is



D		D		D	
1.0	0	1.30	-1.46×10^{-1}	1.75	-8.05×10^{-2}
1.007	-8.15×10^{-3}	1.35	-1.48×10^{-1}	1.80	-6.63×10^{-2}
1.01	-1.06×10^{-2}	1.40	-1.46×10^{-1}	1.85	-5.12×10^{-2}
1.02	-2.10×10^{-2}	1.45	-1.42×10^{-1}	1.90	-3.52×10^{-2}
1.05	-4.98×10^{-2}	1.50	-1.35×10^{-1}	1.95	-1.81×10^{-2}
1.10	-8.68×10^{-2}	1.55	-1.27×10^{-1}	1.975	-9.19×10^{-3}
1.15	-1.12×10^{-1}	1.60	-1.17×10^{-1}	1.98	-7.37×10^{-3}
1.20	-1.30×10^{-1}	1.65	-1.06×10^{-1}	1.99	-3.71×10^{-3}
1.25	-1.41×10^{-1}	1.70	-9.38×10^{-2}	2.00	0

Fig. 10.2. Numerical results for (10.17). The relative statistical error is 10^{-3} .

$$\begin{aligned}
 & -\frac{1}{D} \int_{a,b < c=L} \left\{ 2acc^{-2} (b^{2-D} - c^{2-D}) \right. \\
 & \left. - (2-D) \left[(ac)^2 c^{-2-D} + (ab)^2 b^{-2-D} (b/c)^{-\varepsilon} \Theta(a < b) \right] \right\} a^{-\nu(d+2)}.
 \end{aligned} \tag{10.22}$$

One checks that the integral is locally convergent and that the limit $\varepsilon \rightarrow 0$ can be taken. Of course this derivation is not systematic but the final result is easier to integrate numerically and will therefore be used in the following. It is

$$\begin{aligned}
 & -\frac{1}{D} \int_{a,b < c=L} \left\{ 2acc^{-2} (b^{2-D} - c^{2-D}) \right. \\
 & \left. - (2-D) \left[(ac)^2 c^{-2-D} + (ab)^2 b^{-2-D} \Theta(a < b) \right] \right\} a^{-D-2}
 \end{aligned}$$

$$\begin{aligned}
&= \frac{1}{D} \int_{a,b < c=L} \left\{ (a^2 + c^2 - b^2) c^{-2} (b^{2-D} - c^{2-D}) + \frac{(2-D)}{4} \right. \\
&\quad \times \left[(a^2 + c^2 - b^2)^2 c^{-2-D} + (a^2 + b^2 - c^2)^2 b^{-2-D} \Theta(a < b) \right] \Big\} a^{-D-2}.
\end{aligned} \tag{10.23}$$

The numerical integration is performed using the measure given in Eqs. (7.52)–(7.57) in Section 7.7. The results are shown in Fig. 10.2. We verify that for $D \rightarrow 1$ and for $D \rightarrow 2$ the analytically predicted value 0 is correctly reproduced.

11. Contribution to the wavefunction renormalization from the one-loop coupling constant renormalization

We will calculate the last diagram, Eq. (4.33),

$$\mathcal{F}_3 = \frac{1}{2} \left\langle \text{diagram} \right\rangle_{\varepsilon^{-1}} \left\langle \text{diagram} \right\rangle_{\varepsilon^0}. \tag{11.1}$$

We expand up to first order in ε the following term:

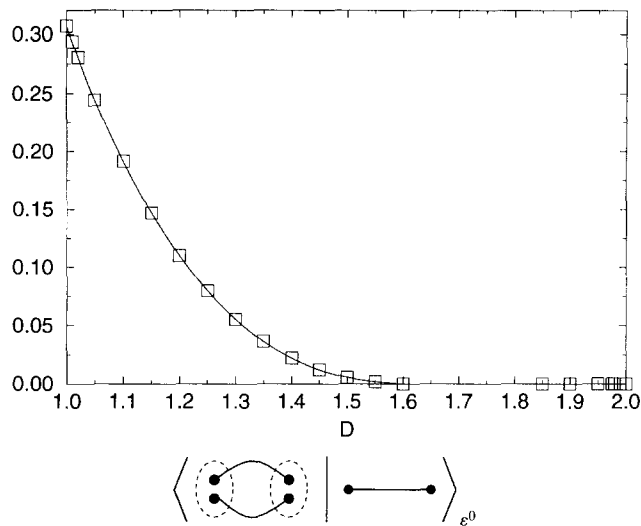
$$\left\langle \text{diagram} \right\rangle_L = \int_{s < L} \int_{t < L} (s^{2\nu} + t^{2\nu})^{-d/2}. \tag{11.2}$$

We apply $L \frac{\partial}{\partial L} |_{L=1}$ and map onto $s = L = 1$:

$$\begin{aligned}
&\int_0^\infty \frac{dt}{t} t^D (1 + t^{2\nu})^{-d/2} \max(1, t)^{-\varepsilon} \\
&= \int_0^\infty \frac{dt}{t} t^D (1 + t^{2\nu})^{-d/2} + \int_1^\infty \frac{dt}{t} t^D (1 + t^{2\nu})^{-d/2} (t^{-\varepsilon} - 1) \\
&= \frac{1}{2-D} \frac{\Gamma\left(\frac{D}{2-D}\right) \Gamma\left(\frac{D-\varepsilon}{2-D}\right)}{\Gamma\left(\frac{2D-\varepsilon}{2-D}\right)} \\
&\quad + \frac{\varepsilon}{(2-D)^2} \int_0^1 \frac{dt}{t} t^{D/(2-D)} (1+t)^{-2D/(2-D)} \ln(t).
\end{aligned} \tag{11.3}$$

This expression can still be expanded as

$$\frac{1}{2-D} \frac{\Gamma\left(\frac{D}{2-D}\right)^2}{\Gamma\left(\frac{2D}{2-D}\right)} \left[1 + \varepsilon \left(\Psi\left(\frac{2D}{2-D}\right) - \Psi\left(\frac{D}{2-D}\right) \right) \right]$$



D		D		D		D	
1.00	3.0685×10^{-1}	1.20	1.1009×10^{-1}	1.50	5.6359×10^{-3}	1.80	-5.5019×10^{-6}
1.01	2.9345×10^{-1}	1.25	7.9770×10^{-2}	1.55	1.9633×10^{-3}	1.85	-9.5846×10^{-8}
1.02	2.8050×10^{-1}	1.30	5.5395×10^{-2}	1.60	2.8999×10^{-4}	1.90	-1.7933×10^{-11}
1.05	2.4419×10^{-1}	1.35	3.6373×10^{-2}	1.65	-1.8953×10^{-4}	1.95	-4.2091×10^{-23}
1.10	1.9136×10^{-1}	1.40	2.2143×10^{-2}	1.70	-1.5855×10^{-4}	1.975	-8.0880×10^{-47}
1.15	1.4701×10^{-1}	1.45	1.2116×10^{-2}	1.75	-4.9540×10^{-5}	2.00	0

Fig. 11.1. Numerical results for Eq. (11.5). The relative statistical error is 10^{-5} .

$$+ \frac{\varepsilon}{(2-D)^2} \int_0^1 \frac{dt}{t} t^{D/(2-D)} (1+t)^{-2D/(2-D)} \ln(t). \quad (11.4)$$

The final result is

$$\begin{aligned} \left\langle \begin{array}{c} \text{diagram} \end{array} \right\rangle_{\varepsilon^0} &= \frac{1}{2-D} \frac{\Gamma\left(\frac{D}{2-D}\right)^2}{\Gamma\left(\frac{2D}{2-D}\right)} \left(\Psi\left(\frac{2D}{2-D}\right) - \Psi\left(\frac{D}{2-D}\right) \right) \\ &+ \frac{1}{(2-D)^2} \int_0^1 \frac{dt}{t} t^{D/(2-D)} (1+t)^{-2D/(2-D)} \ln(t). \end{aligned} \quad (11.5)$$

The numerical results are given in Fig. 11.1. For $D = 1$, Eq. (11.5) is analytically calculated to be

$$1 - \ln(2) = 0.30685281944 \dots \quad (11.6)$$

12. Extrapolations and calculation of critical exponents

12.1. The renormalization-group functions

As we already discussed in Section 3, the renormalization group β -function and the anomalous scaling dimension ν of r are in the MS scheme that we use obtained from the variation of the coupling constant and the field with respect to the renormalization scale μ , keeping the bare couplings fixed. Written in terms of Z and Z_b they are

$$\beta(b) = \mu \frac{\partial}{\partial \mu} \Big|_{b_0} b = \frac{-\varepsilon b}{1 + b \frac{\partial}{\partial b} \ln Z_b + \frac{d}{2} b \frac{\partial}{\partial b} \ln Z}, \quad (12.1)$$

$$\nu(b) = \frac{2-D}{2} - \frac{1}{2} \mu \frac{\partial}{\partial \mu} \Big|_{b_0} \ln Z = \frac{2-D}{2} - \frac{1}{2} \beta(b) \frac{\partial}{\partial b} \ln Z. \quad (12.2)$$

We recall the form of Z and Z_b from Eqs. (4.7), (4.26) and (4.27):

$$\begin{aligned} Z &= 1 + \frac{e_1}{\varepsilon} b + \left(\frac{\tilde{f}_1}{\varepsilon} + \frac{\tilde{f}_2(\varepsilon)}{\varepsilon^2} \right) b^2 + \mathcal{O}(b^3), \\ Z_b &= 1 + \frac{a_1}{\varepsilon} b + \left(\frac{\tilde{c}_1}{\varepsilon} + \frac{\tilde{c}_2(\varepsilon)}{\varepsilon^2} \right) b^2 + \mathcal{O}(b^3). \end{aligned} \quad (12.3)$$

Using Eqs. (4.25), (5.20), (4.12) and (4.13) we obtain

$$\beta(b) = -\varepsilon b + \left(a_1 + 1 - \frac{\varepsilon}{2D} \right) b^2 + 2 \frac{2D\tilde{f}_1 - D\tilde{c}_1 - \tilde{f}_1\varepsilon + 2\tilde{c}_1}{2-D} b^3 + \mathcal{O}(b^4) \quad (12.4)$$

and

$$\nu(b) = \frac{2-D}{2} + \frac{2-D}{4D} b + \tilde{f}_1 b^2 + \mathcal{O}(b^3). \quad (12.5)$$

For $\varepsilon > 0$, the β -function has a non-trivial IR-attractive fixed point for $\beta(b^*) = 0$. Up to second order in ε , b^* is

$$b^*(\varepsilon) = \frac{1}{1+a_1} \varepsilon + \frac{(2-D)(1+a_1) - 4D(2-D)\tilde{c}_1 - 8D^2\tilde{f}_1}{2D(2-D)(1+a_1)^3} \varepsilon^2 + \mathcal{O}(\varepsilon^3). \quad (12.6)$$

Plugging in (12.6) in (12.5) yields

$$\begin{aligned} \nu^* &= \frac{2-D}{2} + \frac{2-D}{4D(1+a_1)} \varepsilon \\ &\quad + \frac{8D^2a_1\tilde{f}_1 - 4D(2-D)\tilde{c}_1 + (2-D)(1+a_1)}{8D^2(1+a_1)^3} \varepsilon^2 + \mathcal{O}(\varepsilon^3). \end{aligned} \quad (12.7)$$

\tilde{c}_1 and \tilde{f}_1 were both calculated numerically as a function of D in the interval $1 \leq D \leq 2$.

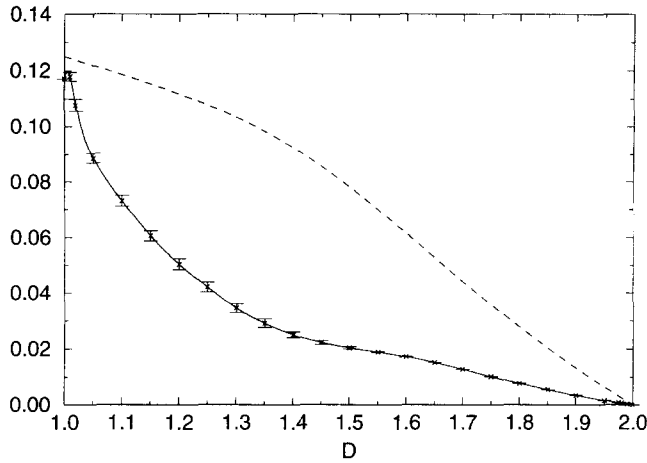


Fig. 12.1. The functions $\nu_1(D)$ (dashed line) and $\nu_2(D)$. The latter is given with the corresponding error bars of the statistical error.

12.2. The exponent ν

We can rewrite (12.7) as an ε -expansion for the critical exponent ν in terms of ε and D ,

$$\nu^* = \nu(D, d) = \nu_0(D) + \nu_1(D)\varepsilon(D, d) + \nu_2(D)\varepsilon^2(D, d) + \dots, \quad (12.8)$$

$$\varepsilon(D, d) = 2D - \frac{2-D}{2}d. \quad (12.9)$$

The result for the coefficients is given in Fig. 12.1. In order to proceed, we shall use a polynomial interpolation for $\tilde{f}_1(D)$ and for $\tilde{c}_1(D)/a_1(D)$. (A polynomial interpolation for $\tilde{c}_1(D)$ is bad as this term vanishes exponentially with $1/(2-D)$.)

We now have to use these two-loop results to calculate the critical exponent ν for self-avoiding two-dimensional membranes ($D = 2$) as a function of the dimension d of space and to compare the results with the previous one-loop results for ν .

As already stressed in previous works, the ε -expansion given by (12.8) cannot be used directly for membranes, as it can be done for polymers. There one fixes $D = 1$ and uses sophisticated resummation methods to evaluate ν for $d = 3$ ($\varepsilon = 1/2$) and even for $d = 2$ ($\varepsilon = 1$). Indeed, directly setting $D = 2$ in the ε -expansion for ν gives a trivial, but absurd, result, since all the terms $\nu_n(2)$ of the ε -expansion vanish! Moreover when $D = 2$, $\varepsilon = 4$ irrespective of the value of d . This simply means that the point $D = 2$, $\varepsilon = 0$ (which corresponds to $d_c = \infty$) is a singular point and that it is not possible to perform a direct ε -expansion around it. Instead, one may perform a similar expansion, starting from another point ($D_0, d_0 = \frac{4D_0}{2-D_0}$) on the critical curve ($\varepsilon = 0$). This approach has already been used in [30] to extrapolate the one-loop results. It introduces two different kinds of arbitrariness in the extrapolations. Firstly one is a priori free to choose any starting point on the critical curve $\varepsilon = 0$ (or at least any point in some subset of this curve). Secondly there is an arbitrariness in the “path of extrapolation” which goes from

the critical curve to the physical point ($D = 2, d$). Of course, if one knows an exact resummation procedure of the full series in ε , one should obtain the same result for any starting point and for any path of extrapolation. However, if one has a finite number of terms of the ε -expansion, even for an adequate resummation method, the final result will depend on this arbitrariness.

In [30] a minimal sensitivity method was introduced by Hwa to analyze the one-loop results. He chose a given extrapolation method and selected the starting point (D_0, d_0) on the critical curve which gives an estimate for ν , $\nu(D_0)$ which is the less sensitive to the choice of the starting point. This method works well for polymers and gives interesting results for membranes. However, when one goes to two loops, it delivers largely varying or even diverging estimates for $\nu(D_0)$ and in addition his choice for the extrapolation path is somewhat arbitrary.

We shall use a generalization of the methods introduced in [30]. Note that the expansion (12.8) is exact in D and of order 2 in ε , thus it can be expanded up to order 2 both in $D - D_0$ and ε . Now we can change our extrapolation path through any invertible transformation $\{x, y\} = \{x(D, \varepsilon), y(D, \varepsilon)\}$. One can express D and ε as function of x and y and re-expand ν up to order 2 in x and y around the point (x_0, y_0) on the critical curve.

$$\begin{aligned} \nu(D, \varepsilon) &= \tilde{\nu}(x, y) \\ &= \tilde{\nu}_{0,0}(x_0, y_0) + \Delta x \tilde{\nu}_{1,0}(x_0, y_0) + \Delta y \tilde{\nu}_{0,1}(x_0, y_0) \\ &\quad + (\Delta x)^2 \tilde{\nu}_{2,0}(x_0, y_0) + 2\Delta x \Delta y \tilde{\nu}_{1,1}(x_0, y_0) + (\Delta y)^2 \tilde{\nu}_{0,2}(x_0, y_0) + \dots \\ \Delta x &= x - x_0, \quad \Delta y = y - y_0. \end{aligned} \tag{12.10}$$

The goal is to find an optimal choice of variables $\{x, y\}$. Our guidelines for such a choice are the following: (i) the estimate for ν should depend “the least” on the choice of the expansion point on the critical curve, (ii) it should reproduce well the known result for polymers ($D = 1$), (iii) for membranes ($D = 2$) the $d \rightarrow \infty$ limit should not be singular and we should get results close to those obtained by a Gaussian variational approximation. This last point is not arbitrary and will be justified below. It turns out to be quite stringent.

Finally, we must choose some resummation procedure to extrapolate ν from the knowledge of the series (12.10) up to order 2. Since we have only a few terms and since we do not have insight in the large order behavior of these series or in the analytical structure of the resummed series, we cannot use sophisticated resummation methods (for instance those based on Borel transforms). Therefore we shall always use the truncated series at order 2 and boldly sum its terms.

Let us now discuss possible extrapolation variables. The simplest choice is to take D and ε . This works well for polymers ($D = 1$), since both at one- and two-loop order we get results which are quite stable with respect to D_0 . However, this gives very poor results for membranes ($D = 2$), since both at one- and two-loop order the results depend very much on D_0 . This could be expected, since in this case $\varepsilon = 4$ independent of d .

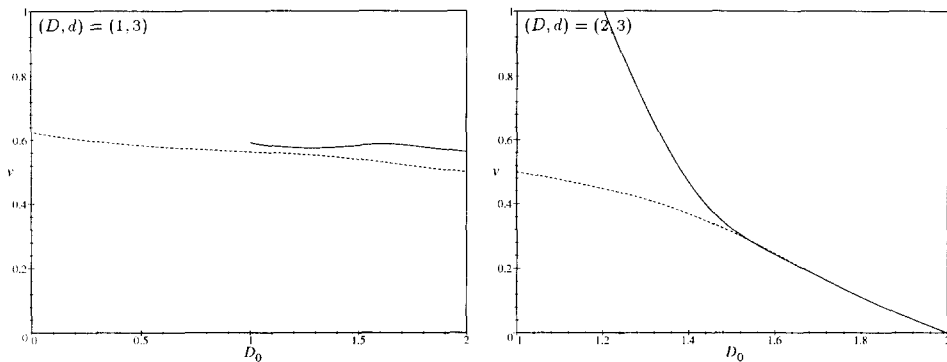


Fig. 12.2. Extrapolation of ν in D and ε to $(D, d) = (1, 3)$ and $(2, 3)$. The dashed line is the one-loop result, the full line the two-loop result. The exponent ν is plotted as function of the expansion point D_0 .

See Fig. 12.2. In the case of the membrane, no prediction is possible.

Another possibility is to expand in D and d . This expansion gives reasonable results for polymers, but poor results for membranes. This can be seen by looking at the results of Fig. 12.3 and is not surprising, since if we apply this extrapolation method to the Gaussian variational estimate $\nu_{\text{var}} = 2D/d$ it also gives poor results, although the result ν_{var} is expected to be close to the exact ν at large d (as argued in Subsection 12.3).

A more interesting choice is to use D and $D_c(d) = 2d/(4 + d)$ or equivalently D and $1/(d + 4)$. This expansion has the advantage to represent the critical curve $D_0, d_c(D_0)$ as a straight line. For polymers in three dimensions this method delivers a remarkable broad plateau, i.e. the extrapolated value of ν is relatively independent of the expansion point D_0 . For polymers in two and one dimensions we still have a plateau when $D_0 \rightarrow 2$, which delivers two-loop extrapolations close to the exact results ($\nu = 0.75$ and $\nu = 1$ respectively) (see Fig. 12.4). For membranes, this method also delivers interesting results (see Fig. 12.5). For large d , we find a stable plateau at two loops when $D_0 \rightarrow 2$, which gives for ν a result very close to the variational estimate $\nu_{\text{var}} = 4/d$, while at smaller D_0 , the plateau stops and the two-loop estimate for ν

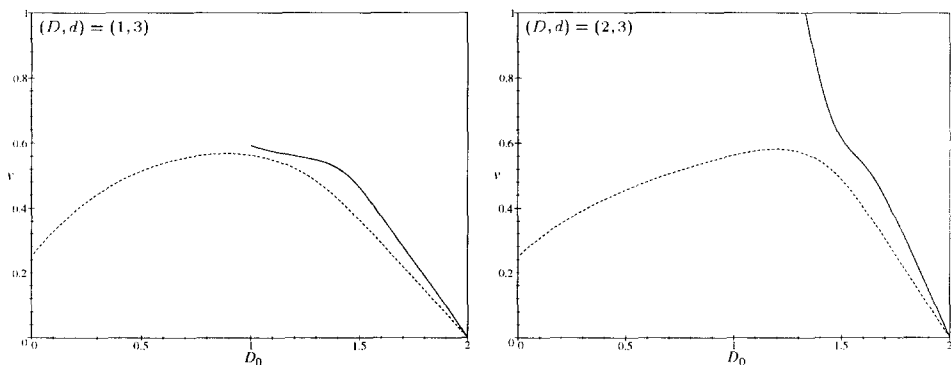


Fig. 12.3. Extrapolation in D and d to $(D, d) = (1, 3)$ and $(2, 3)$.

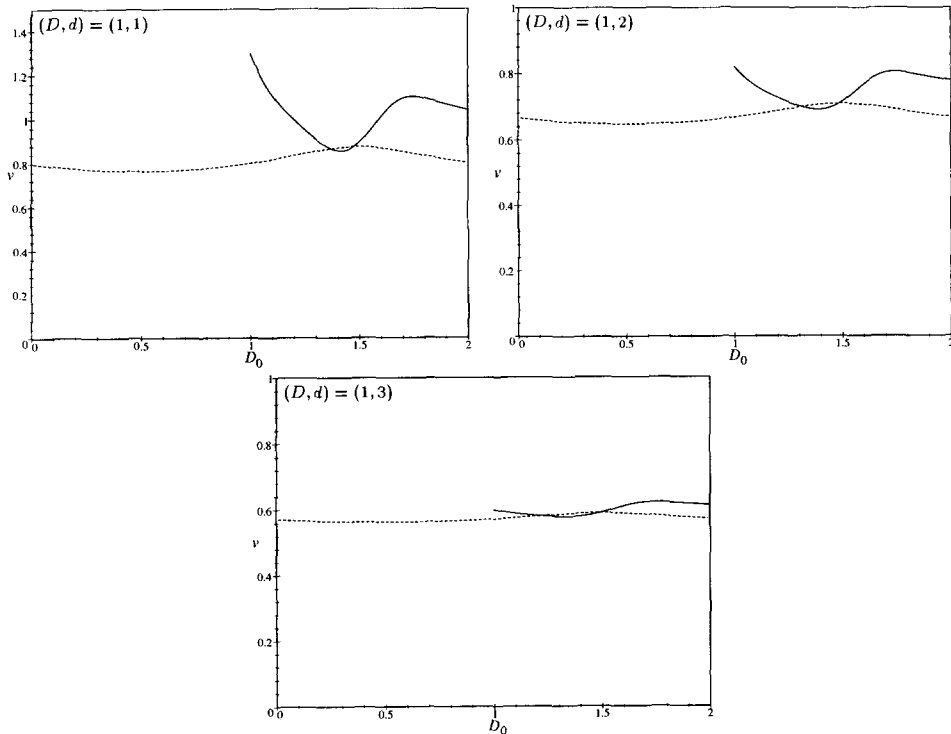


Fig. 12.4. Extrapolation for polymers in D and $D_c(d)$ to $(D, d) = (1, 1), (1, 2), (1, 3)$.

increases sharply as $D_0 \rightarrow 1$. For small d , the $D_0 \rightarrow 2$ plateau becomes an oscillatory region, still followed by a sharp increase for $D_0 \rightarrow 1$. In this case, to calculate ν , we use the minimum and the maximum of $\nu(D_0)$. Whereas the first is expected to be an underestimation, the second is expected to be an overestimation. We also give their mean value, cf. Table 12.1 and Fig. 12.5. One might think of developing in D and $1/(d+c)$, with $c \neq 4$. $c = 0$ is suggested by the variational ansatz. In fact we prefer to take $c = 2$, which is suggested by the prediction of the Flory argument (see Subsection 12.4). We obtain similar estimates as above for d large, but larger variations for smaller d . For this case we evaluated ν by the request that the second order corrections should vanish. We give the results in Table 12.1 and Fig. 12.6. The predictions for ν are good in the known cases and reasonable for membranes in three dimensions.

Another promising method is the expansion in ε and $D_c(d)$. This expansion is also regular for $D \rightarrow 2$ and is perhaps more in the spirit of an ε -expansion. Let us discuss the features of this expansion in more detail. See Figs. 12.7 and 12.8. For polymers in three dimensions we find the flattest plateau of all extrapolation methods. For membranes in three dimensions the prediction at one-loop order (dashed line) is essentially independent of the expansion point. For membranes in large dimension, at two-loop order the estimate starts from the one-loop result at $D = 2$, grows until it reaches a plateau, where $\nu \approx \nu_{\text{var}}$ and then grows rapidly again. For smaller d , there is

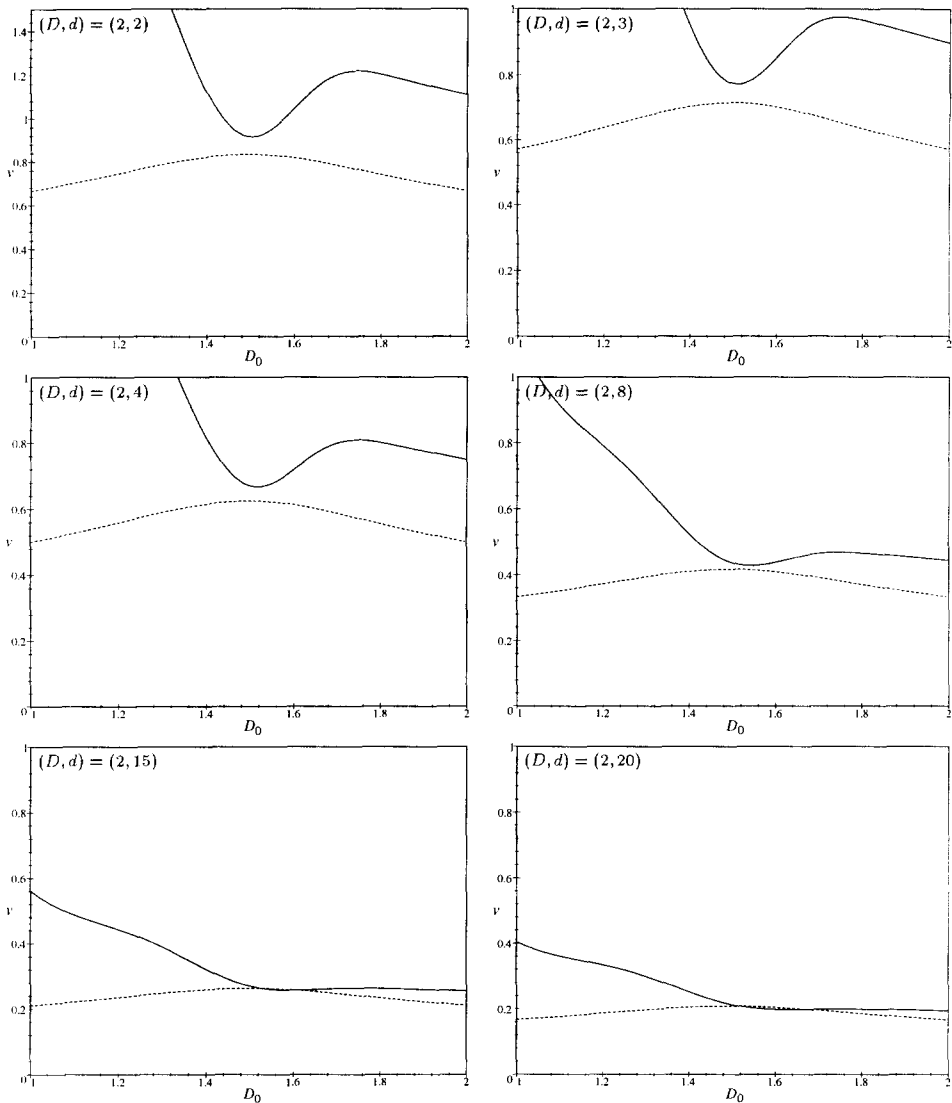


Fig. 12.5. Extrapolation for membranes in D and $D_c(d)$ to $(D, d) = (2, 2)$, $(2, 3)$, $(2, 4)$, $(2, 8)$, $(2, 15)$ and $(2, 20)$.

still a plateau and in order to extract ν from Fig. 12.8, one uses the maximum and the minimum of the plateau. Their mean is an estimate for ν , their difference an estimate of the error in *this* expansion scheme.

The results for ν from the various extrapolations are summarized in Table 12.1.

Table 12.1

Results of the numerical extrapolations for ν . If not stated otherwise the error is ± 1 in the last digit. (x, y) indicates the expansion parameters x and y as discussed in the text. min, max and mean are the minimum and the maximum of the plateau and their mean value respectively

$(x, y); (D, d)$	(1, 1)	(1, 2)	(1, 3)	(2, 2)	(2, 3)	(2, 4)	(2, 8)	(2, 20)
exact	1	0.75	0.586(4)	1	—	—	—	—
Flory	1	3/4	3/5	1	4/5	2/3	2/5	2/11
variational	2	1	2/3	2	4/3	1	1/2	1/5
$D, (d+2)^{-1}$	1.0	0.75	0.59	0.99	0.81	0.68	0.43	0.198
$D, D_c(d)$ min	0.85	0.69	0.57	0.91	0.77	0.67	0.43	0.198
$D, D_c(d)$ max	1.10	0.81	0.62	1.22	0.98	0.81	0.47	0.199
$D, D_c(d)$ mean	0.98	0.75	0.60	1.08	0.88	0.78	0.45	0.198
$D_c(d), \varepsilon$ min	0.83	0.68	0.58	0.83	0.72	0.64	0.42	0.196
$D_c(d), \varepsilon$ max	0.91	0.73	0.60	0.90	0.76	0.66	0.42	0.198
$D_c(d), \varepsilon$ mean	0.87	0.71	0.59	0.87	0.74	0.65	0.43	0.197

12.3. Variational method and perturbation expansion

In the various extrapolation schemes that we used, we have seen that the plateau structure for $D_0 \rightarrow 2$ becomes clearer when the space dimension d is large and that the corresponding estimates for ν are close to the value $\nu_{\text{var}} = 4/d$ obtained from a variational ansatz. In order to understand this phenomenon and to have a better understanding of the plateau structure of the extrapolations, we shall discuss the status of the variational method.

Using a Gaussian variational ansatz [39], the exponent ν for the crumpled phase of a self-avoiding D -dimensional tethered membrane is found to be

$$\nu_{\text{var}} = \frac{2D}{d}. \quad (12.11)$$

It was noticed in [31] that in the case of membranes with long-range interactions the variational estimate for ν is exact and can be reproduced easily by simply assuming that there is no coupling constant renormalization, i.e. that one can take $Z_b = 1$ in the renormalized Hamiltonian (3.13). This last assumption can be proven for membranes with long-range forces [31,32]. Let us rewrite the full dimension $\nu(b)$ in a way which makes this point clear. Starting from the definitions of the RG functions $\beta(b)$ (12.1) and $\nu(b)$ (12.2), we reexpress $\frac{\partial}{\partial b} \ln Z$ in terms of $\beta(b)$ and $\frac{\partial}{\partial b} \ln Z_b$,

$$\frac{\partial}{\partial b} \ln Z = -\frac{2}{db} \left(\frac{\varepsilon b}{\beta(b)} + 1 + b \frac{\partial}{\partial b} \ln Z_b \right). \quad (12.12)$$

Inserting this into (12.2) gives

$$\nu(b) = \frac{2D}{d} + \frac{\beta(b)}{db} + \frac{\beta(b)}{d} \frac{\partial}{\partial b} \ln Z_b. \quad (12.13)$$

At the IR-fixed point $b = b^*$, the second term of the r.h.s. of (12.13) vanishes. The last one does not vanish in general, but vanishes if $Z_b = 1$. In this case, we get the

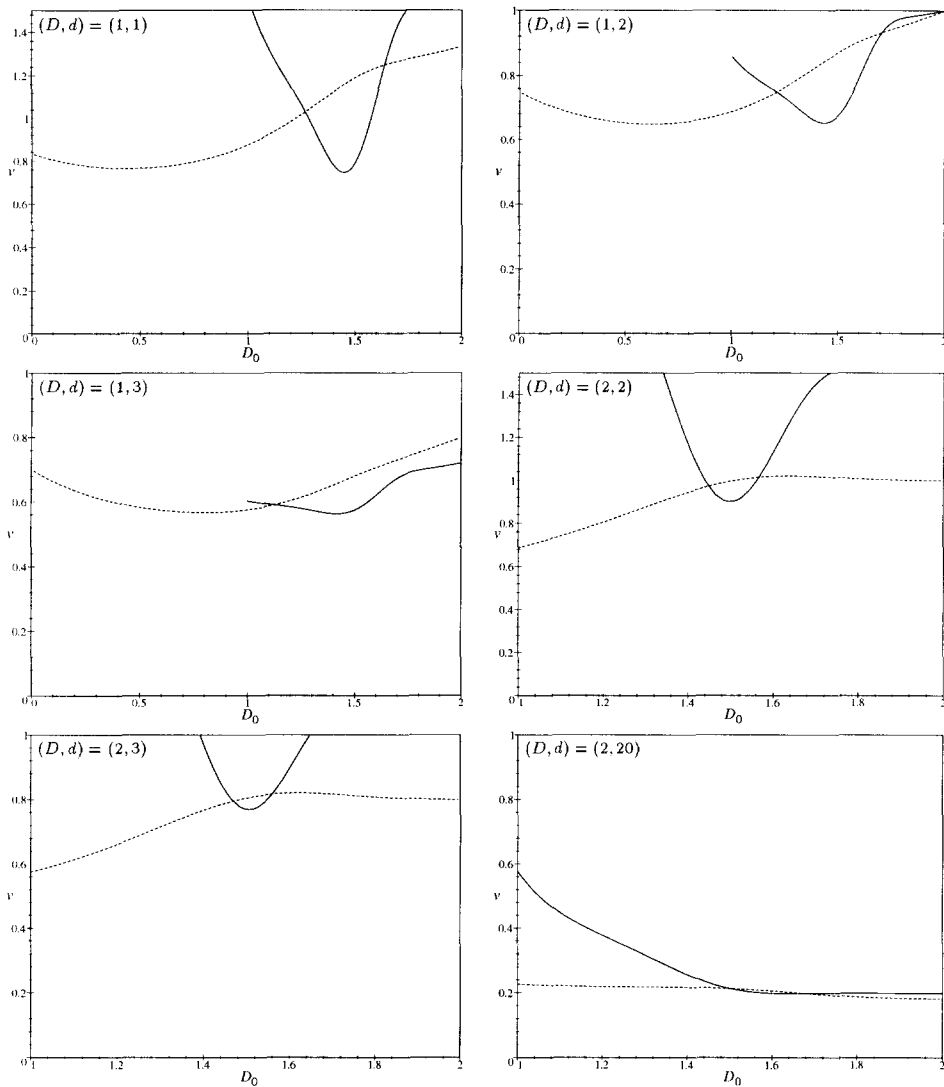


Fig. 12.6. Extrapolation in D and $1/(d+2)$ to $(D, d) = (1, 1)$, $(1, 2)$, $(1, 3)$, $(2, 2)$, $(2, 3)$ and $(2, 20)$.

variational result (12.11).

Using this observation, one can understand why the one-loop and two-loop extrapolations for ν coincide with ν_{var} for large d . Taking $d_0 \rightarrow \infty$ on the critical line amounts to take $D_0 \rightarrow 2$. The limit $d \rightarrow \infty$ corresponds thus to the limit $D \rightarrow 2$ for the counterterms. The one-loop wave-function counterterm is given by the residue

$$\left\langle \text{diagram} \right\rangle_{\epsilon} \approx 1 \quad \text{as } D \rightarrow 2 \quad (12.14)$$

while the one-loop coupling constant counterterm is given by the residue

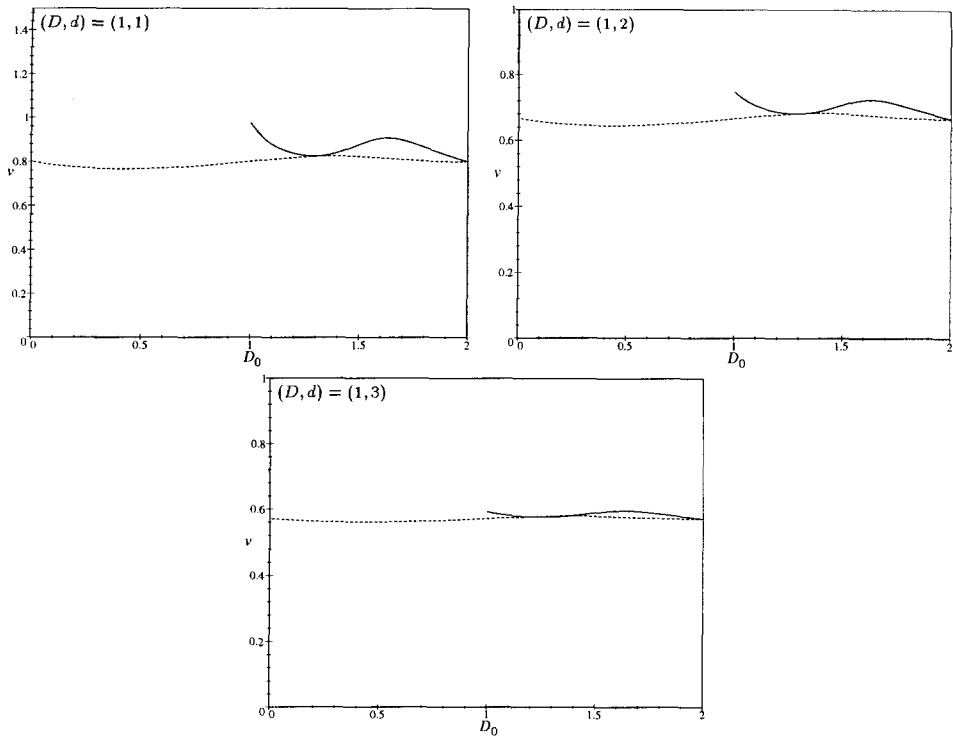


Fig. 12.7. Extrapolation for polymers in $D_c(d)$ and ε to $(D, d) = (1, 1)$, $(1, 2)$ and $(1, 3)$.

$$\left\langle \begin{array}{c} \bullet \\ \bullet \end{array} \begin{array}{c} \bullet \\ \bullet \end{array} \right| \bullet \text{---} \bullet \right\rangle_{\varepsilon} \approx 2^{-2D/(2-D)} \quad \text{as } D \rightarrow 2. \quad (12.15)$$

which is exponentially smaller than (12.14) when $D \rightarrow 2$. A similar exponential factor appears for the two-loop coupling constant counterterm compared to the two-loop wave-function counterterm (this can be checked from the analytical expressions and the numerical results).

When looking at the general structure of the divergent diagrams at N -loop order, we can argue that this phenomenon will persist, but we have no rigorous proof. However, if this exponential bound $\ln Z_b \ll \ln Z$ as $D \rightarrow 2$ is correct, this means that $\nu - \nu_{\text{var}} \sim \exp(-\text{cst.}/d)$ when $d \rightarrow \infty$.

Assuming the variational estimate (12.11) to be a good approximation for large d , it is interesting to test the various extrapolation methods that we have used to get the two-loop results. The principle is to start from the exact formula for ν_{var} , to write an ε -like expansion around the critical curve $\varepsilon = 0$, to truncate it at a fixed order and to resum the result as done previously. The results of such a resummation, using the extrapolation in $\{x, y\}$, are presented in Fig. 12.9. Let us note the following points:

- (i) The extrapolations at one- and two-loop orders of ν_{var} are indeed very similar to the extrapolations of ν at large d . In particular one recovers the same plateau

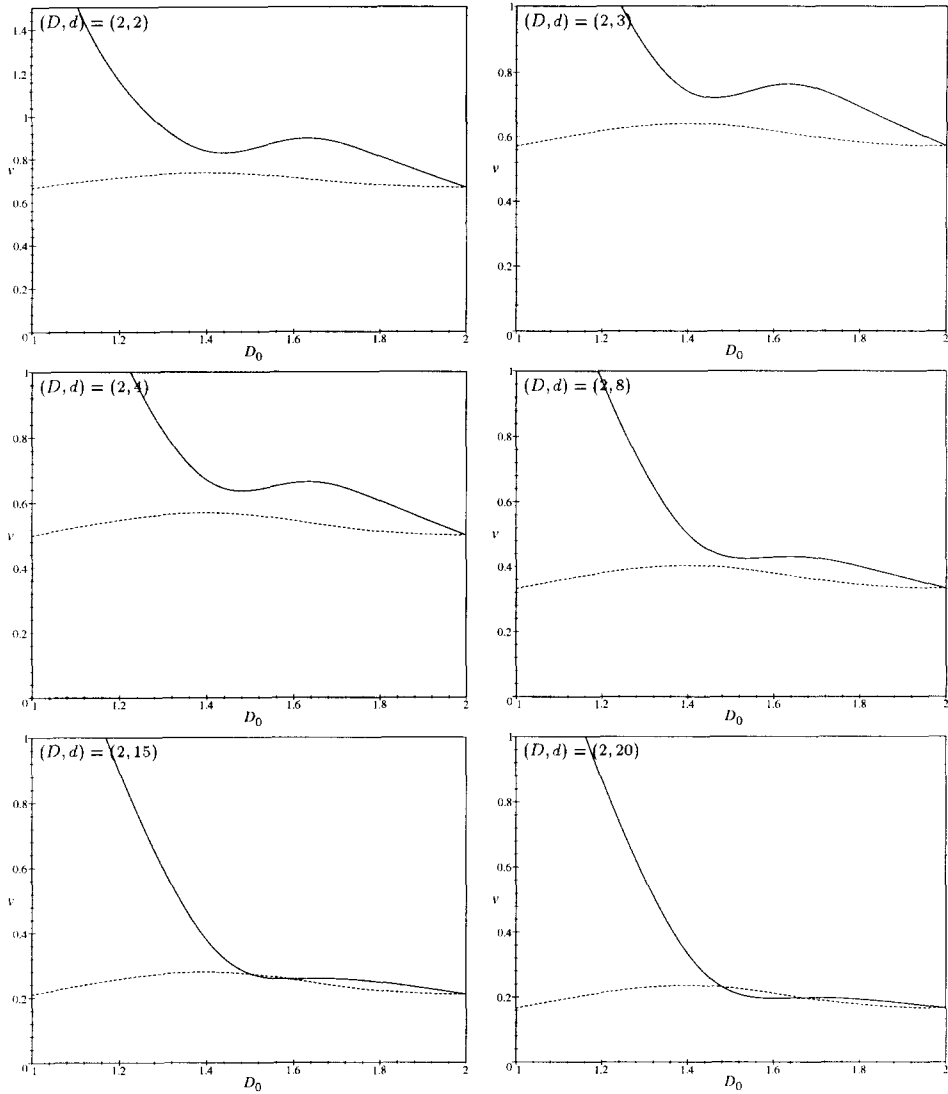


Fig. 12.8. Extrapolation in $D_c(d)$ and ϵ to $(D, d) = (2, 2)$, $(2, 3)$, $(2, 4)$, $(2, 8)$, $(2, 15)$ and $(2, 20)$.

structure and it should be noted that already the two-loop optimal estimate for ν_{var} , obtained by the minimal sensitivity method, gives the exact ν_{var} ! This is a strong point for this method, when applied for smaller d .

- (ii) One should note that the ϵ -expansion for ν_{var} is convergent, but that it has a finite radius of convergence. As a consequence, one can show that the N -loop extrapolations for ν_{var} converge towards the exact result when $N \rightarrow \infty$ only in a finite range of starting points D_0 on the critical curve. This range is explicitly

$$\frac{2d}{8+d} < D_0 < 2. \quad (12.16)$$

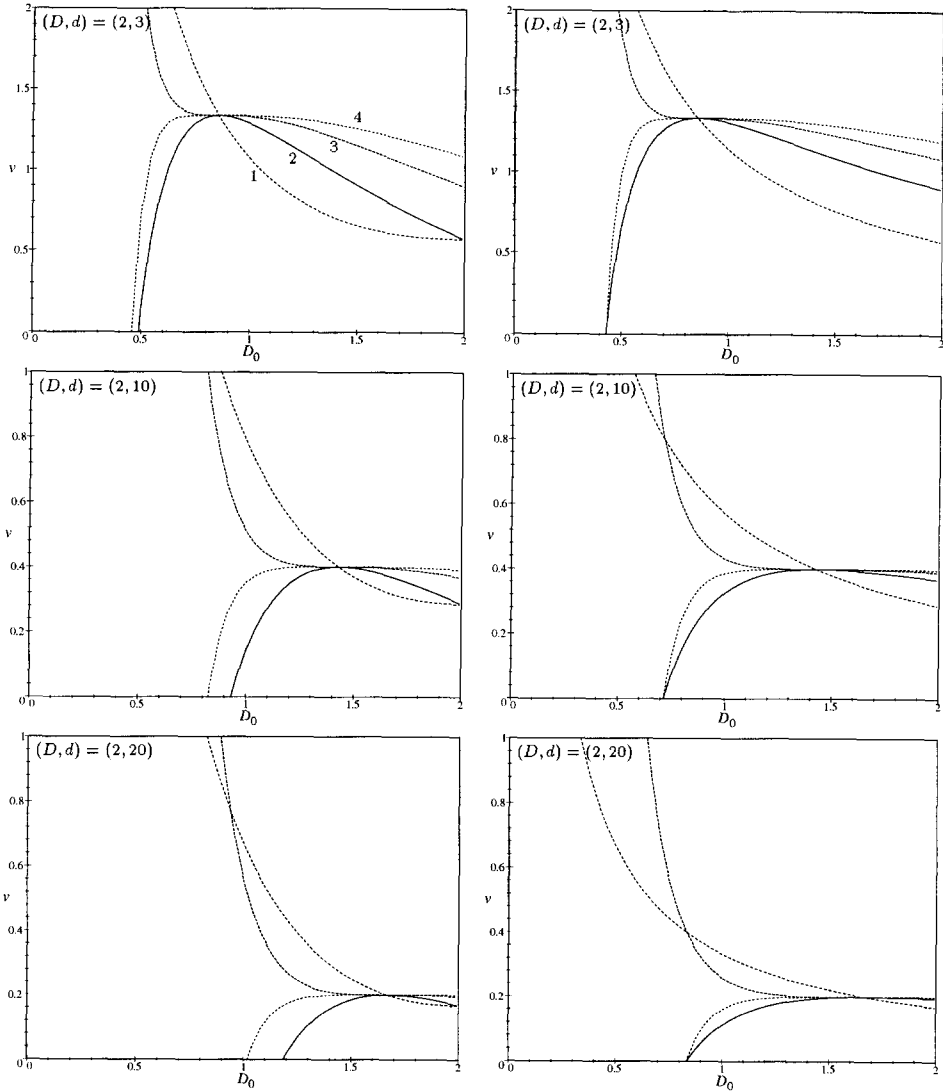


Fig. 12.9. Extrapolation of $\nu_{\text{var}} = 2D/d$ for membranes in $\{D_c(d), \varepsilon\}$ (left), and $\{D_c(D), D\}$ (right), to $(D, d) = (2, 3)$, $(2, 10)$ and $(2, 20)$. On the first figure, the labels 1–4 indicate the order of the ε -expansion i.e. $\mathcal{O}(\varepsilon^1)$ – $\mathcal{O}(\varepsilon^4)$. On all figures, the full line is the result at order ε^2 , the other lines are the results at order ε , ε^3 and ε^4 .

- (iii) The large variation of the two-loop estimates for ν as D_0 becomes small reflects the fact that we are outside of the range of convergence of the ε -expansion. This is clear when one compares the two-loop estimate with the three- and four-loop estimates in Fig. 12.9. We expect that this is still true for smaller d and that the optimal values for D_0 are still in the domain of confidence of the ε -expansion.

We now present a new ε -expansion, well suited to large d , which is suggested by

Table 12.2

Results for ν using the numerical extrapolations for νd . If not stated otherwise the error is ± 1 in the last digit

$(x, y); (D, d)$	(1, 1)	(1, 2)	(1, 3)	(2, 2)	(2, 3)	(2, 4)	(2, 8)	(2, 20)
exact	1	3/4	0.586(4)	1	—	—	—	—
Flory	1	3/4	3/5	1	4/5	2/3	2/5	2/11
variational	2	1	2/3	2	4/3	1	1/2	1/5
$D, D_c(d)$ left crossing	1.09	0.69	0.58	0.97	0.797	0.80	0.45	0.20
$D, D_c(d)$ right crossing	2.08	0.76	0.60	1.05	0.82	1.00	0.50	0.20
$D, D_c(d)$ mean crossing	1.59	0.73	0.59	1.01	0.80	0.90	0.48	0.20

the expression (12.13) for $\nu(b)$. Indeed, when evaluating the exponent $\nu^* = \nu(b^*)$ by (12.13), we see that what we really expand in ε is not ν but νd :

$$\begin{aligned} \nu^* d &= 2D + \left(\beta(b) \frac{\partial}{\partial b} \ln Z_b(b) \right) \bigg|_{b=b^*} \\ &= 2D + \mathcal{O}(\varepsilon) \end{aligned} \quad (12.17)$$

Thus we may perform the ε -expansion for νd rather than for ν . This new expansion has the advantage that it starts at order ε^0 from the result predicted by the variational ansatz. The same extrapolation methods used for ν can be used for νd .

The results are given in Table 12.2 and Fig. 12.10. We find that for polymers ($D = 1$), when using the $(D, D_c(d))$ variables, the minimal sensitivity method gives poor results, but that the criterion to take as optimal D_0 the point where the second-order correction vanishes gives good results. We use the same criterion for membranes ($D = 2$).

12.4. Expansion around Flory's estimation

In the last section we have seen that the ε -expansion for νd is in fact an ε -expansion around the variational ansatz, $\nu d = 2D + \mathcal{O}(\varepsilon)$. Another stimulating idea is to perform a similar expansion around the prediction made by Flory's argument. It is well known that the Flory result for polymers $\nu_{\text{Flory}} = 3/(2 + d)$ is simply obtained by assuming that the elastic term and the contact interaction term in the Edwards Hamiltonian scale in the same way with the internal size of the polymer. The same scaling assumption for membranes leads to the prediction

$$\nu_{\text{Flory}} = \frac{2 + D}{2 + d}. \quad (12.18)$$

It is possible to perform an ε -expansion around ν_{Flory} by simply expanding $\nu(d + 2)$. Indeed, we can set

$$Z_{\text{Flory}} = \sqrt{Z} Z_b, \quad Z_\varepsilon = \sqrt{Z/Z_b} \quad (12.19)$$

and eliminate Z_{Flory} from the system of equations (12.1) and (12.2). We obtain

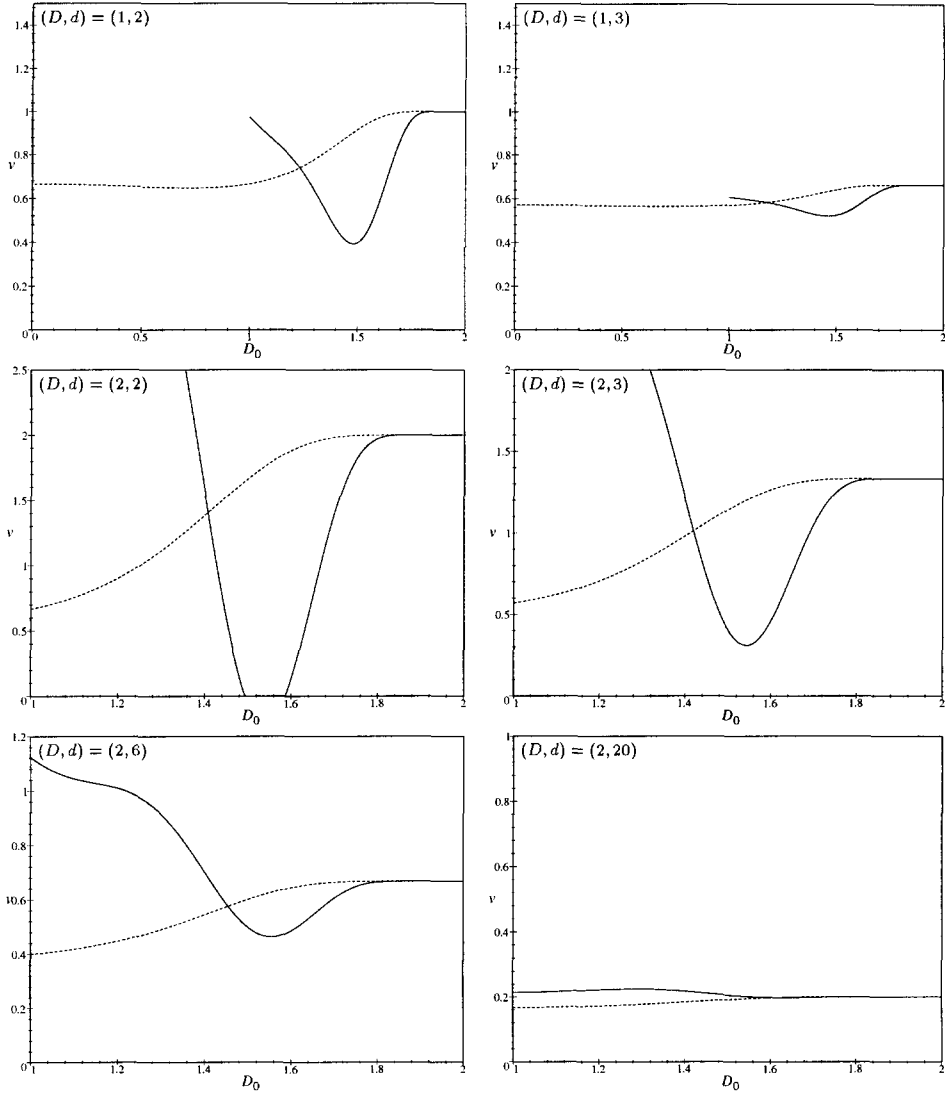


Fig. 12.10. Extrapolation of νd in D and $D_c(d)$ to $(D, d) = (1, 2), (1, 3), (2, 2), (2, 3), (2, 6), (2, 20)$.

$$\nu^*(d+2) = D + 2 + \left(\beta(b) \frac{\partial}{\partial b} \ln \left(\frac{Z_b}{Z} \right) \right) \bigg|_{b=b^*}. \quad (12.20)$$

This makes clear that if the wave-function and coupling-constant renormalizations are the same (more precisely, if Z_b/Z stays finite at the IR-fixed point b^*) the Flory result becomes exact. Moreover, the ε -expansion of $\nu(d+2)$ is clearly an ε -expansion around ν_{Flory} .

This expansion seems to be the most satisfying numerically. In particular, the method of minimal sensitivity and that of minimizing the second-order term give generally

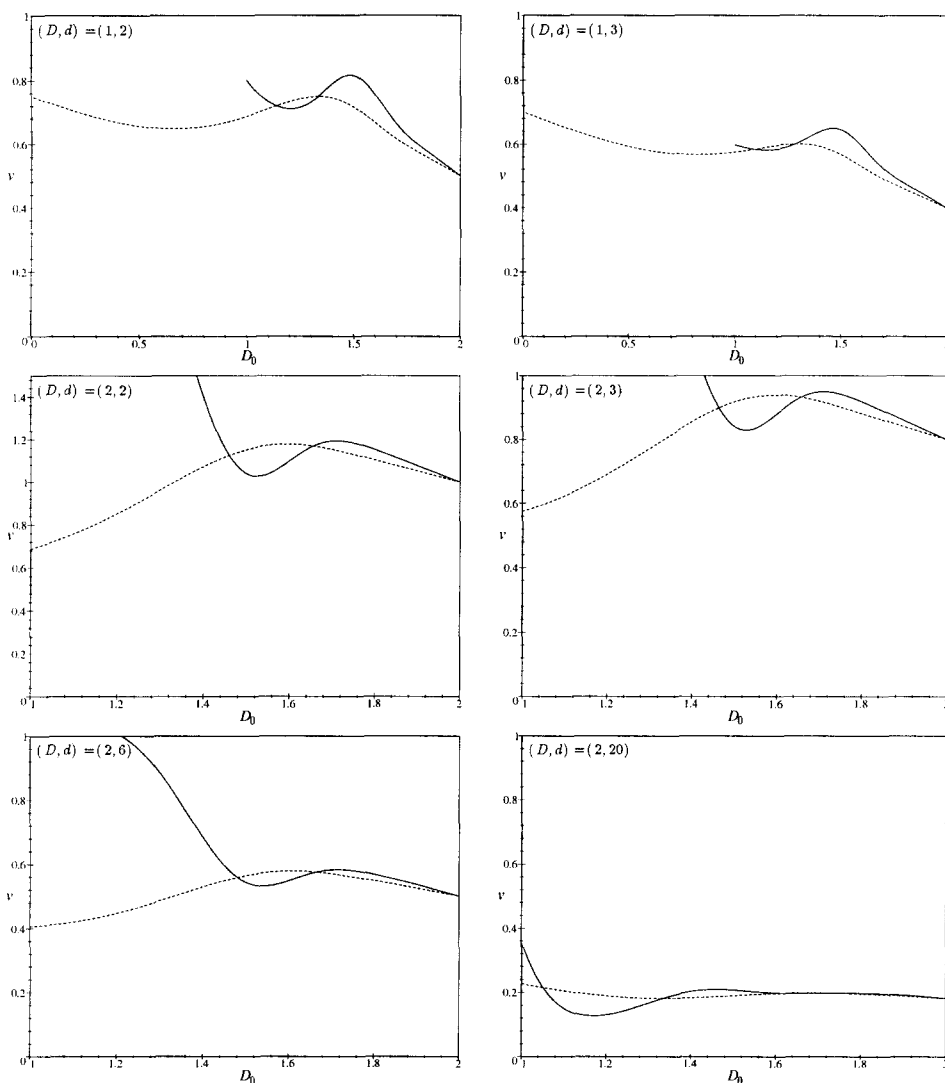


Fig. 12.11. Extrapolation of $\nu(d+2)$ in D and d to $(D, d) = (1, 2), (1, 3), (2, 2), (2, 3), (2, 6), (2, 20)$.

close results. We therefore give in the following plots for all interesting combinations of variables and dimensions (D, d) , see Figs. (12.11) to (12.14). Let us stress that good expansion parameters for ν are not necessarily good for $\nu(d+2)$ and vice versa. For example, the expansion in D and d is bad for ν but works quite well (although not optimal) for $\nu(d+2)$. We study the expansion in (D, d) , (d, ε) , $(D, D_c(d))$ and $(D_c(d), \varepsilon)$. The results of the extrapolations are collected in Table 12.3.

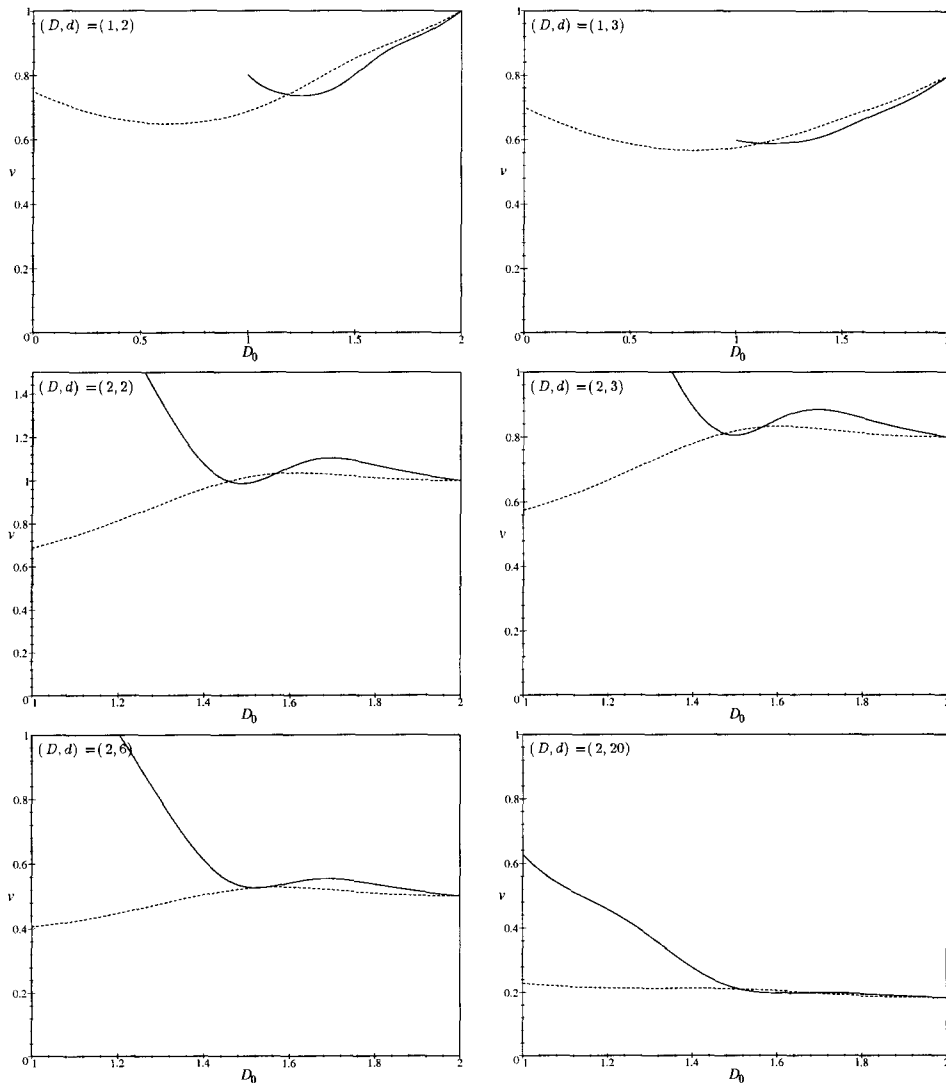


Fig. 12.12. Extrapolation of $\nu(d+2)$ in d and ε to $(D, d) = (1, 2), (1, 3), (2, 2), (2, 3), (2, 6), (2, 20)$.

12.5. Summary of the two-loop extrapolations for ν

Let us summarize. In Fig. 12.15 we represent the results of a two-loop extrapolation for ν in the case of membranes ($D = 2$) in d dimensions ($2 \leq d \leq 20$). We see that for $d \rightarrow \infty$ the prediction of the Gaussian variational method becomes exact, as argued above. For small d , the prediction made by Flory's argument is close to our results. This is a non-trivial statement, since the membrane case corresponds to $\varepsilon = 4$ and in comparison with polymers in $d = 3$, where $\varepsilon = 1/2$, the two-loop corrections were expected to be large. In fact we have found that the two-loop corrections are small

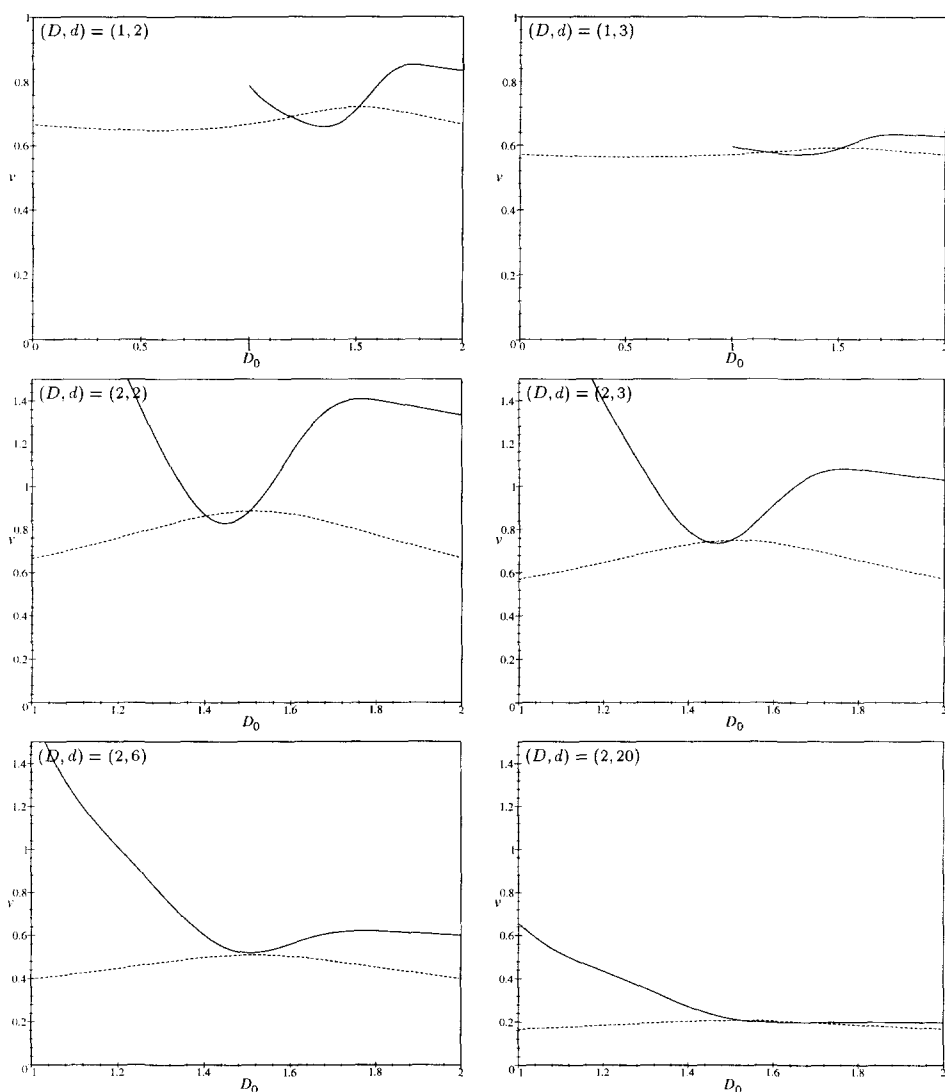


Fig. 12.13. Extrapolation of $\nu(d+2)$ in $D_c(d)$ and ε to $(D, d) = (1, 2), (1, 3), (2, 2), (2, 3), (2, 6), (2, 20)$.

when one expands around the critical curve $\varepsilon = 0$ for an adequate range of $D \approx 1.5$ (depending slightly on d and on the choice of variables) and a suitable choice of extrapolation variables. In this case the two-loop corrections are even smaller than the one-loop corrections and allow for more reliable extrapolations to $\varepsilon = 4$.

12.6. Other critical exponents

The two-loop calculations presented in this paper allow in principle to compute other scaling exponents for self-avoiding tethered membranes. The first exponent is the so-

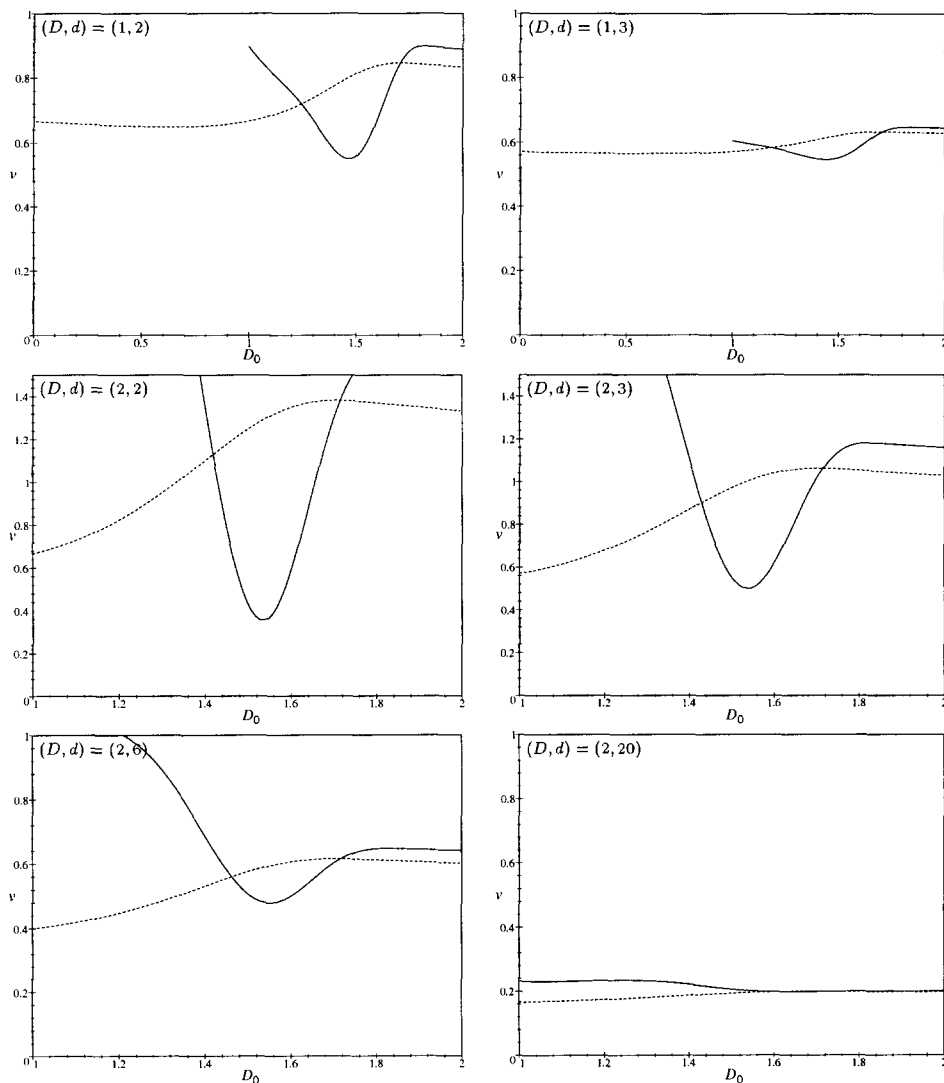


Fig. 12.14. Extrapolation of $\nu(d+2)$ in D and $D_c(d)$ to $(D, d) = (1, 2), (1, 3), (2, 2), (2, 3), (2, 6), (2, 20)$.

called correction to scaling exponent ω which governs the corrections to the large L scaling behaviour. It is known that this exponent is given by the slope of the β -function at the IR-fixed point b^*

$$\omega = \left. \frac{\partial}{\partial b} \beta(b) \right|_{b=b^*}. \quad (12.21)$$

Its ε -expansion is given by

Table 12.3

Results for ν from the numerical extrapolations for $\nu(d+2)$ at second order. “min”, “max” and “mean” denote respectively the estimate at the minimum of the plateau, at the maximum of the plateau and their mean value. “left crossing”, “right crossing” and “mean crossing” denote respectively the estimate at the leftmost point where the second order correction vanishes, at the rightmost point and their mean value. If not stated otherwise the error is ± 1 in the last digit

$(x, y); (D, d)$	(1, 1)	(1, 2)	(1, 3)	(2, 2)	(2, 3)	(2, 4)	(2, 8)	(2, 20)
exact	1	3/4	0.586(4)	1	—	—	—	—
Flory	1	3/4	3/5	1	4/5	2/3	2/5	2/11
variational	2	1	2/3	2	4/3	1	1/2	1/5
D, d min	0.93	0.71	0.58	1.02	0.83	0.70	0.43	0.20
D, d max	1.09	0.82	0.65	1.20	0.95	0.79	0.46	0.19
D, d mean	1.01	0.76	0.62	1.11	0.89	0.75	0.45	0.20
D, d left crossing	0.95	0.72	0.59	1.12	0.90	0.75	0.44	0.20
D, d right crossing	1.00	0.75	0.60	1.16	0.93	0.78	0.45	0.20
D, d mean crossing	0.97	0.73	0.59	1.14	0.91	0.76	0.44	0.20
d, ε min	0.98	0.74	0.59	0.98	0.80	0.68	0.42	0.19
d, ε max	—	—	—	1.10	0.88	0.73	0.44	0.20
d, ε mean	—	—	—	1.04	0.84	0.70	0.43	0.20
d, ε left crossing	1.00	0.74	0.59	0.99	0.81	0.73	0.44	0.20
d, ε right crossing	—	—	—	1.03	0.83	0.68	0.42	0.20
d, ε mean crossing	—	—	—	1.01	0.82	0.71	0.43	0.20
$D_c(d), \varepsilon$ min	0.75	0.56	0.57	0.83	0.74	0.64	0.43	0.20
$D_c(d), \varepsilon$ max	1.24	0.86	0.64	1.40	1.08	0.86	0.48	0.20
$D_c(d), \varepsilon$ mean	0.99	0.76	0.60	1.12	0.91	0.75	0.45	0.20
$D_c(d), \varepsilon$ left crossing	0.84	0.69	0.58	0.86	0.74	0.64	—	0.21
$D_c(d), \varepsilon$ right crossing	0.91	0.72	0.60	0.63	0.75	0.64	—	0.20
$D_c(d), \varepsilon$ mean crossing	0.88	0.70	0.59	0.87	0.74	0.64	—	0.20
$D, D_c(d)$ min	0.35	0.55	0.55	—	0.49	0.52	0.41	0.20
$D, D_c(d)$ max	1.39	0.90	0.65	—	1.18	0.85	0.50	0.20
$D, D_c(d)$ mean	0.87	0.72	0.60	—	0.84	0.68	0.45	0.20
$D, D_c(d)$ left crossing	0.95	0.72	0.58	1.12	0.90	0.74	0.45	0.20
$D, D_c(d)$ right crossing	1.27	0.84	0.63	1.38	1.06	0.85	0.47	0.20
$D, D_c(d)$ mean crossing	1.06	0.78	0.61	1.25	0.98	0.80	0.46	0.20

$$\omega = \varepsilon + \frac{(2-D)\tilde{c}_1(D) + 2D\tilde{f}_1(D)}{(2-D) \left(\frac{1}{2-D} \frac{\Gamma^2\left(\frac{D}{2-D}\right)}{\Gamma\left(\frac{2D}{2-D}\right)} \right)^2} \varepsilon^2 + \mathcal{O}(\varepsilon^3). \quad (12.22)$$

(For the definition of $\tilde{c}_1(D)$ and $\tilde{f}_1(D)$, see (4.34) and (4.28).)

We have tried to use the extrapolation methods that we have developed for ν to get two-loop estimates for ω . Unfortunately, it turns out that the term of order ε^2 is always very large compared to the term of order ε and there is no domain along the critical curve where a reliable estimate can be extracted from the ε -expansion. Thus the situation for the exponent ω seems to be very different from that for ν .

Another scaling exponent which can be obtained from our calculations is the so-called bulk contact exponent θ_2 . For a general introduction to contact exponents for polymers and membranes we refer to Ref. [41]. A detailed discussion of the calculation of contact exponents within the Edwards model for self-avoiding membranes will be given

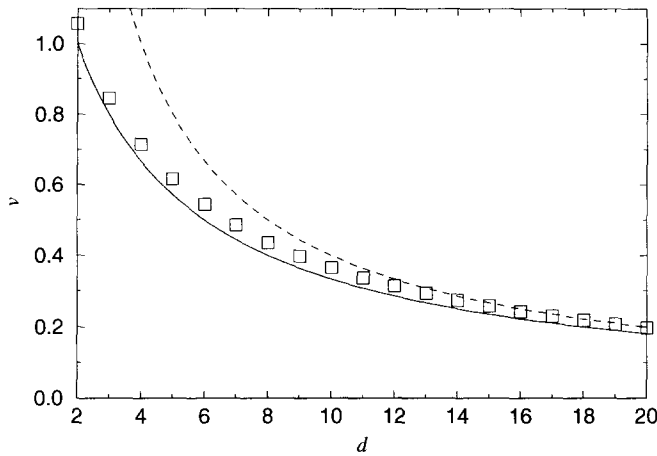


Fig. 12.15. Extrapolation of the two-loop results in d and ε for membranes $D = 2$ in d dimensions, using (12.20) (squares). The solid line is the prediction made by Flory's theory, the dashed line by the variational ansatz.

in [32]. We simply recall the basic results here. The contact exponent θ_2 is related to the probability to find two *fixed* points x_1 and x_2 inside the membrane at a relative distance $r = |\mathbf{r}|$ in external d -dimensional space:

$$P(r; x_1, x_2) = \left\langle \tilde{\delta}^d(\mathbf{r} - (\mathbf{r}(x_1) - \mathbf{r}(x_2))) \right\rangle. \quad (12.23)$$

For a large membrane, P is expected to take the scaling form

$$P(r; x_1, x_2) = R_{12}^{-d} F(r/R_{12}), \quad (12.24)$$

where R_{12} is the mean distance between x_1 and x_2 ,

$$R_{12}^2 = \frac{1}{2} \left\langle (\mathbf{r}(x_1) - \mathbf{r}(x_2))^2 \right\rangle. \quad (12.25)$$

The contact exponent θ_2 is given by the small r behavior of the scaling function F

$$F\left(\frac{r}{R_{12}}\right) \sim \left(\frac{r}{R_{12}}\right)^{\theta_2} \quad \text{when } r \rightarrow 0. \quad (12.26)$$

θ_2 is simply related to the scaling dimension ω_{12} of the two-membrane contact operator

$$\delta_{12}(x_1, x_2) = \tilde{\delta}^d(\mathbf{r}_1(x_1) - \mathbf{r}_2(x_2)) \quad (12.27)$$

in the model of two independent self-avoiding membranes. This model is described by the Hamiltonian

$$\mathcal{H} = \left(\int_{x_1 \in M_1} \frac{1}{2} (\nabla \mathbf{r}_1(x_1))^2 + \int_{x_2 \in M_2} \frac{1}{2} (\nabla \mathbf{r}_2(x_2))^2 \right)$$

$$\begin{aligned}
& +b \left(\int_{x_1 \in M_1} \int_{y_1 \in M_1} \tilde{\delta}^d(\mathbf{r}_1(x_1) - \mathbf{r}_1(y_1)) + \int_{x_2 \in M_2} \int_{y_2 \in M_2} \tilde{\delta}^d(\mathbf{r}_2(x_2) - \mathbf{r}_2(y_2)) \right) \\
& + 2t \int_{x_1 \in M_1} \int_{y_2 \in M_2} \tilde{\delta}^d(\mathbf{r}_1(x_1) - \mathbf{r}_2(y_2)) . \quad (12.28)
\end{aligned}$$

This model can be made UV-finite at $\varepsilon = 0$ by the same renormalization factors for \mathbf{r} and b as the one-membrane model, i.e. by replacing in (12.28) $\mathbf{r} \rightarrow Z(b)^{1/2}\mathbf{r}$ and $b \rightarrow bZ_b(b)Z(b)^{d/2}\mu^\varepsilon$, but with an additional renormalization for the inter-membrane coupling $t \rightarrow tZ_t(b, t)Z(b)^{d/2}\mu^\varepsilon$. The new counterterm Z_t can be calculated in terms of the same divergent diagrams as those which contribute to Z_b , but with different numerical factors. In particular, one can show that when $t = b$, $Z_t(b, t = b) = Z_b(b)$, so that the symmetric two-membrane model reduces to the one-membrane model.

As a consequence of this formalism, one can define a new RG function, β_t ,

$$\beta_t(b, t) = \mu \frac{\partial}{\partial \mu} t \Big|_{\substack{\text{bare } b, t \\ \text{fixed}}} \quad (12.29)$$

to calculate the RG flow in the (b, t) plane and check that $(b, t) = (b^*, b^*)$ is the IR-stable fixed point which governs the scaling behavior of a large membrane. It turns out that the θ_2 contact exponent and the anomalous dimension ω_{12} of the contact operator δ_{12} are related to the t -derivative of the β_t function at the IR-fixed point by

$$\omega_{12} = -\nu^* \theta_2 = \frac{\partial}{\partial t} \beta_t \Big|_{b=t=b^*} . \quad (12.30)$$

As a result, the ε -expansion for θ_2 involves the same diagrams as ω and ν , but in a different combination. The result is somehow complicated, so let us simply write the counterterm Z_t and compare it with Z_b (already given in Sections 3 and 4).

$$\begin{aligned}
Z_b(b) &= 1 + \frac{a_1}{\varepsilon} b + \left(\frac{a_1(a_1 - 1/2)}{\varepsilon^2} + \frac{a_1/4D + C_1 + C_2 + C_3}{\varepsilon} \right) b^2 + \dots , \\
Z_t(b, t) &= 1 + \frac{a_1}{\varepsilon} t + \left(\frac{a_1^2}{\varepsilon} + \frac{C_1}{\varepsilon} \right) t^2 + \left(-\frac{a_1/2}{\varepsilon^2} + \frac{a_1/4D + C_2 + C_3}{\varepsilon} \right) bt + \dots \quad (12.31)
\end{aligned}$$

We have tried to use the extrapolation methods that we have developed for ν to get two-loop estimates for θ_2 . As for ω , it turns out that the term of order ε^2 is always very large compared to the term of order ε and that there is no domain along the critical curve where a reliable estimate can be extracted from the ε -expansion.

12.7. Scaling for membranes at the θ -point (tri-critical point)

In [34] it was shown that the scaling behavior of membranes at the tri-critical θ -point is dominated by the modified two-point interaction $\tilde{\delta}''(\mathbf{r}(x) - \mathbf{r}(y))$, which is repulsive

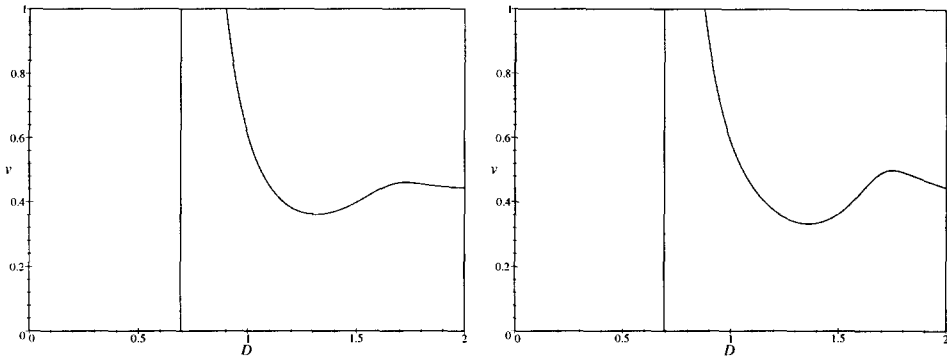


Fig. 12.16. Extrapolation for ν at the tri-critical point in $(D_c(d), \varepsilon')$ and in $(D, D_c(d))$ to $D = 2$ and $d = 3$, one-loop results.

at short distance but attractive at larger distance. Membranes at the θ -point are thus quite different from polymers, where the three-point repulsive interactions dominate. As a consequence, the scaling exponent ν^θ at the θ -point has a different ε -expansion, which can be computed analytically at first order and is found to be [32,34]

$$\nu^\theta(D, \varepsilon') = \frac{2-D}{2} + \frac{2-D}{4D \left(1 + \frac{1}{2} \frac{(10D-D^2-8)\Gamma^2\left(\frac{D}{2-D}\right)}{(2-D)^3\Gamma\left(\frac{2D}{2-D}\right)} \right)} \varepsilon' + \mathcal{O}(\varepsilon'^2) \quad (12.32)$$

with

$$\varepsilon' = 3D - 2 - d \frac{(2-D)}{2}. \quad (12.33)$$

This expansion is again correct up to first order in d or ε' and exact in D . We can use the extrapolation methods developed in this paper to evaluate the exponent ν from the one-loop results. The extrapolation method proposed by Hwa [30] does not work in this case. Two variants of our method deliver reasonable results: The expansion in ε' and $D_c(d)$ and the expansion in D and $D_c(d)$. The one-loop estimate for membranes in three dimensions is (cf. Fig. 12.16):

$$\nu^\theta = 0.42 \pm 0.08. \quad (12.34)$$

Due to our experiences with the former extrapolations, we expect that the one-loop results will be an underestimation. They may be compared to the Flory result

$$\nu_{\text{Flory}}^\theta = \frac{2+D}{4+d}, \quad (12.35)$$

which evaluates to 0.57 in the case of membranes in three dimensions.

12.8. Comparison with numerical simulations and experiments

The numerical study of two-dimensional self-avoiding tethered membranes imbedded into three dimensions was started in 1986 by Kantor, Kardar and Nelson [11,12]. They found for the exponent ν a value close to the prediction made by Flory's argument. These simulations as most of the following use a system composed of balls and springs (spring and bead model). Self-avoidance is effective between the balls. It was a surprise when it was found [14,9] that the simulations of larger membranes obtain a flat phase. Abraham and Nelson [10] explained this result by suggesting that an effective bending rigidity is induced by the geometric constraints of the model (there is a maximal angle for which neighbouring faces can bend due to the finite size of the balls). If this induced effective rigidity is larger than the critical rigidity, where the crumpling transition (transition to a flat phase induced by the bending rigidity *without* self-avoidance) occurs, the membrane will always be in the flat phase.

After these studies, several attempts were made to reduce the effective rigidity of the membrane in order to observe a crumpled phase, by using smaller balls [15] or by bond dilution [22,23]. None of these attempts was successful. Another possibility to reduce the rigidity is to impose self-avoidance not between balls but between faces of the lattice. Using this method Baumgärtner et al. found a crumpled swollen phase. Kroll and Gompper later declared that also in this model the membrane is flat [19]. Finally let us remark that a crumpled phase has been found by balancing the induced rigidity by long-range attractive interactions [16,17]. We still want to mention the simulations of self-avoiding tethered membranes in a space of four, five, six and eight dimensions. Grest [20] found that in four dimensions, the membrane is flat, but is crumpled in dimensions higher than 4. Subsequent simulations by Barsky and Plischke [21] confirm this conclusion.

To summarize: For three dimensions most numerical simulations indicate that the membrane is in the flat phase, but the results are still not fully conclusive. The simulations which find a crumpled phase give values for ν which are close to our analytical estimates. The situation seems to be similar in four dimensions.

A few experimental studies of tethered membranes have also been performed, but the situation is not clear neither. The best studied system is graphite oxide, i.e. a monolayer of carbon atoms. The first experiments by Hwa et al. [24] found a phase with fractal dimension $d_f = 2.4$. This result is contested in [25] by direct electron microscopy methods, although the latter authors obtain within the error bars the same data from their diffraction experiments. It is not clear if these membranes are sloppy enough or if their internal stiffness is sufficiently large to induce in itself the transition towards a flat phase. Another system studied is the spectrin network of red blood cells [26], but the role of disorder (which may induce a wrinkling transition) seems here important. In summary, the experiments are not yet helpful to clarify the situation.

12.9. A possible scenario for low dimensions

The fact that most numerical simulations only find a flat phase (with $\nu = 1$) for self-avoiding tethered membranes in three dimensions, while our analytical estimates lead to $\nu < 1$, has still to be explained. As mentioned above, a possible explanation is that the analytical calculations apply to floppy membranes (with very small bending rigidity), while “real systems” studied numerically or experimentally are rigid enough to cross the crumpling transition barrier and to stay in the flat phase.

However, the fact that reducing the rigidity does not induce the crumpling transition suggest another, more drastic possibility. It is known that for phantom tethered membranes, the lower critical dimension d_l , below which the crumpled phase does not exist, lies between 1 and 2 ($1 < d_l < 2$). It is possible that, when self-avoidance is taken into account, the lower critical dimension d_l for the crumpling transition moves upwards to about 3. In this case self-avoiding tethered membranes are always flat, however small the rigidity is.

Let us give heuristic arguments that this is indeed the case in three dimensions. Let us start from phantom membranes (without self-avoidance). The fractal exponent ν is then 0 in the crumpled phase, 1 in the flat phase, and equal to

$$\nu_c = 1 - \frac{1}{d} + \mathcal{O}\left(\frac{1}{d^2}\right) \quad (12.36)$$

at the crumpling transition [42]. This last estimate is the result of a large d expansion. Its applicability to low dimensions is thus not clear a priori, but numerical simulations [8] show that even in three dimensions this approximation is reasonable ($\nu_c = 2/3$). Let us now ask whether self-avoidance is relevant at the crumpling transition. By naive power counting we find that this is the case if

$$\mathcal{D} = 2 \cdot 2 - \nu_c d > 0, \quad (12.37)$$

i.e. with (12.36) for

$$d < 5. \quad (12.38)$$

For $\mathcal{D} > 0$ we expect that the fractal exponent ν_c at the crumpling transition is different with or without self-avoidance. But let us assume that self-avoidance does not change drastically the exponent ν_c at the crumpling transition, i.e. that

$$\nu_c \approx \nu_{c+SA}, \quad (12.39)$$

where the second exponent is the exponent ν at the crumpling transition in the presence of self-avoidance. This is certainly true for \mathcal{D} small. As we expect that the radius of gyration of a self-avoiding membrane with rigidity is an increasing function of the bending rigidity modulus κ , until we reach the crumpling transition, it is simple to deduce the inequality between the fractal exponent of self-avoiding membranes in the crumpled phase ν_{SA} and at the crumpling transition ν_{c+SA}

$$\nu_{c+SA} \leq \nu_{SA} . \quad (12.40)$$

Assuming that (12.39) holds, using the estimate (12.36) for ν_{c+SA} and our two-loop estimates for ν_{SA} , we find that this basic inequality is violated if

$$d < d_l \approx 3.8 . \quad (12.41)$$

Our interpretation is that d_l is nothing but the lower critical dimension of the crumpling transition with self-avoidance, and that for $d < d_l$ the membrane is always in the flat, rigid phase.

We want to emphasize that this line of arguments is still somehow speculative. It is however tempting to compare our crude estimate of $d_l \approx 3.8$ with the numerical simulations in three, four and five dimensions which yield $4 \leq d_l \leq 5$. To confirm or disapprove this scenario, one must take into account the effect of the bending rigidity in our renormalization group calculations.

13. Conclusions

In this article we presented the first renormalization group calculation at two-loop order for self-avoiding flexible tethered membranes. These second order corrections were found to be surprisingly small if one uses an adequate extrapolation scheme.

We were able to clarify the status of the Gaussian variational method and to show that it becomes exact for $d \rightarrow \infty$. For low dimensions the two-loop results are in good agreement with the prediction made by Flory's approximation, although *systematically* slightly larger.

In order to improve these results, one should understand if the plateau phenomenon observed at two-loop order persists to higher orders, and one should control the general large order behavior of perturbation theory for this model. Another important issue is whether the IR-fixed point studied here is stable towards perturbation by bending rigidity. Indeed, for small enough d this might destabilize the crumpled phase and explain why numerical simulations in $d = 3$ normally see a flat phase. We gave additional arguments which corroborate this scenario.

Acknowledgments

We thank E. Guitter, G.S. Grest, T. Hwa and J. Zinn-Justin for useful discussions and J.-M. Drouffe for a careful reading of the manuscript.

Appendix A. Normalizations

We use peculiar normalizations in order to simplify the calculations. First of all, we normalize the integration measure of the internal space as (S_D is the volume of the D -dimensional unit sphere)

$$\int_x = \frac{1}{S_D} \int d^D x, \quad S_D = 2 \frac{\pi^{D/2}}{\Gamma(D/2)}. \quad (\text{A.1})$$

This provides

$$\int_x |x|^{\varepsilon-D} \Theta(|x| - L) = \frac{1}{\varepsilon} L^\varepsilon. \quad (\text{A.2})$$

The δ -distribution is normalized according to

$$\tilde{\delta}^d(r(x) - r(y)) = (4\pi)^{d/2} \delta^d(r(x) - r(y)) = \int_p e^{ip(r(x)-r(y))} \quad (\text{A.3})$$

with

$$\int_p = \pi^{-d/2} \int d^d p \quad (\text{A.4})$$

to have

$$\int_p e^{-p^2 a} = a^{-d/2}. \quad (\text{A.5})$$

Using for the free Hamiltonian

$$\mathcal{H}_0 = \frac{1}{2-D} \int_x \frac{1}{2} (\nabla r(x))^2 \quad (\text{A.6})$$

yields

$$\left\langle \frac{1}{2} (r_i(x) - r_j(y))^2 \right\rangle_0 = \delta_{ij} |x - y|^{2-D}. \quad (\text{A.7})$$

Appendix B. Example of the MOPE

We give as an explicit example of the MOPE the derivation of (6.2).

$$\begin{array}{c} x_1 \text{---} y_1 \quad x_2 \text{---} y_2 \quad x_3 \text{---} y_3 \\ = \int_k \int_p \int_q : e^{ikr(x_1)} :: e^{ipr(x_2)} :: e^{iqr(x_3)} :: e^{-ikr(y_1)} :: e^{-ipr(y_2)} :: e^{-iqr(y_3)} : . \end{array} \quad (\text{B.1})$$

These exponentials shall be contracted like

$$\text{---} \bullet \text{---} \bullet \text{---} \bullet \text{---} \bullet \longrightarrow \left(\begin{array}{c} \bullet \text{---} \bullet \\ \bullet \text{---} \bullet \\ \bullet \text{---} \bullet \end{array} \right) . \quad (\text{B.2})$$

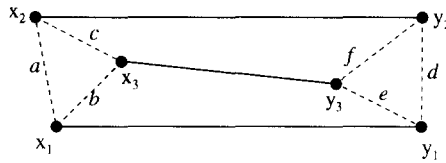


Fig. B.1. The distances and the points in (B.1).

We therefore use the OPE for the points x_1 , x_2 and x_3 , supposed the differences between these points become small:

$$: e^{ikr(x_1)} :: e^{ipr(x_2)} :: e^{iqr(x_3)} := e^{ikr(x_1)+ipr(x_2)+iqr(x_3)} : e^{kp a^{2\nu} + kq b^{2\nu} + pq c^{2\nu}}. \quad (\text{B.3})$$

The new variables for the distances between the points are given in Fig. B.1. An analogous expansion is valid for y_1 , y_2 and y_3 . In order to retain only the most important contribution, we expand

$$: e^{ikr(x_1)+ipr(x_2)+iqr(x_3)} := e^{i(k+p+q)r((x_1+x_2+x_3)/3)} (1 + \mathcal{O}(\nabla r)) : \quad (\text{B.4})$$

and neglect the contributions of order $\mathcal{O}(\nabla r)$ because they are proportional to irrelevant operators. After a shift in the integration variable q ,

$$q \longrightarrow q - k - p,$$

Eq. (B.1) becomes

$$\begin{aligned} & \int_q : e^{iqr((x_1+x_2+x_3)/3)} :: e^{-iqr((y_1+y_2+y_3)/3)} : \\ & \times \int_k \int_p e^{kp(a^{2\nu}+d^{2\nu})+k(q-k-p)(b^{2\nu}+e^{2\nu})+p(q-k-p)(c^{2\nu}+f^{2\nu})}. \end{aligned} \quad (\text{B.5})$$

The integral over q yields the δ -distribution plus higher derivatives of this distribution. The latter are irrelevant operators and can be neglected. As they come from the expansion of the last exponential factor in q , we only have to retain the last factor, evaluated at $q = 0$. This gives

$$\begin{aligned} & \int_k \int_p e^{kp(a^{2\nu}+d^{2\nu})-k(k+p)(b^{2\nu}+e^{2\nu})-p(k+p)(c^{2\nu}+f^{2\nu})} \\ & = \left[(b^{2\nu} + e^{2\nu})(c^{2\nu} + f^{2\nu}) - \frac{1}{4} (b^{2\nu} + e^{2\nu} + c^{2\nu} + f^{2\nu} - a^{2\nu} - d^{2\nu}) \right]^{-d/2}. \end{aligned} \quad (\text{B.6})$$

This can still be factorized as is known from ancient Heron:

$$\left(\left(\begin{array}{c} \bullet \\ \bullet \\ \bullet \end{array} \right) \left(\begin{array}{c} \bullet \\ \bullet \\ \bullet \end{array} \right) \right) = \left[\frac{1}{4} \left(\sqrt{a^{2\nu} + d^{2\nu}} + \sqrt{b^{2\nu} + e^{2\nu}} + \sqrt{c^{2\nu} + f^{2\nu}} \right) \right]$$

$$\begin{aligned}
& \times \left(\sqrt{b^{2\nu} + e^{2\nu}} + \sqrt{c^{2\nu} + f^{2\nu}} - \sqrt{a^{2\nu} + d^{2\nu}} \right) \\
& \times \left(\sqrt{a^{2\nu} + d^{2\nu}} + \sqrt{c^{2\nu} + f^{2\nu}} - \sqrt{b^{2\nu} + e^{2\nu}} \right) \\
& \times \left(\sqrt{a^{2\nu} + d^{2\nu}} + \sqrt{b^{2\nu} + e^{2\nu}} - \sqrt{c^{2\nu} + f^{2\nu}} \right) \Big]^{-d/2}.
\end{aligned} \tag{B.7}$$

Appendix C. Equation of motion

The equation of motion reflects the invariance of the functional integral under a change of variables for the fields. The expectation value of an observable \mathcal{O} in the free theory is

$$\langle \mathcal{O} \rangle_0 = \frac{\int \mathcal{D}[r] \mathcal{O} e^{-\frac{1}{2-D} \int_x \star}}{\int \mathcal{D}[r] e^{-\frac{1}{2-D} \int_x \star}}. \tag{C.1}$$

We now perform a global rescaling of $r(x)$:

$$r(x) \longrightarrow (1 + \kappa) r(x). \tag{C.2}$$

The expectation value of \mathcal{O} , Eq. (C.1) is unchanged. The explicit form becomes up to first order in κ

$$\langle \mathcal{O} \rangle_0 = \frac{\int \mathcal{D}[r] \mathcal{O} (1 + \kappa [\mathcal{O}]_r) \left(1 - \frac{2\kappa}{2-D} \int_x \star \right) e^{-\frac{1}{2-D} \int_x \star}}{\int \mathcal{D}[r] \left(1 - \frac{2\kappa}{2-D} \int_x \star \right) e^{-\frac{1}{2-D} \int_x \star}}. \tag{C.3}$$

$[\mathcal{O}]_r$ is the canonical dimension of the operator \mathcal{O} , measured in units of r , i.e. that $[r]_r = 1$. Calculating the difference of (C.1) and (C.3) gives

$$\left\langle \mathcal{O} \int \star \right\rangle_0^{\text{conn}} = \nu [\mathcal{O}]_r \left\langle \mathcal{O} \right\rangle_0^{\text{conn}}. \tag{C.4}$$

For several operators we have

$$\left\langle \mathcal{O}_1 \mathcal{O}_2 \int \star \right\rangle_0^{\text{conn}} = \nu ([\mathcal{O}_1]_r + [\mathcal{O}_2]_r) \left\langle \mathcal{O}_1 \mathcal{O}_2 \right\rangle_0^{\text{conn}} \tag{C.5}$$

and in particular

$$\left\langle \text{---} \int \star \right\rangle_0^{\text{conn}} = -\nu d \left\langle \text{---} \right\rangle_0^{\text{conn}}, \tag{C.6}$$

$$\left\langle \mathcal{O} \int \star \right\rangle_0^{\text{conn}} = (2 + [\mathcal{O}]_r) \nu \left\langle \mathcal{O} \right\rangle_0^{\text{conn}}. \tag{C.7}$$

These relations are equivalently valid for non-connected expectation values. (To prove this, note that $\langle \text{---} \oplus \text{---} \rangle_0 = 0$.)

We can now apply these equations to calculate the pole term of

$$\left\langle \left(\text{---} \oplus \text{---} \right) \left| \text{---} \oplus \text{---} \right. \right\rangle_L.$$

The equation of motion yields

$$\left\langle \int \int \int \int \int \text{---} \oplus \text{---} \right\rangle_0 = -2vd \left\langle \int \int \int \int \text{---} \oplus \text{---} \right\rangle_0. \quad (\text{C.8})$$

On the l.h.s. the possible divergences proportional to $\text{---} \oplus \text{---}$ come from the following integrals:

$$4 \left\langle \int \int \int \int \int \left(\text{---} \oplus \text{---} \right) \right\rangle_0 + 2 \left\langle \int \int \int \int \int \left(\text{---} \oplus \text{---} \right) \right\rangle_0. \quad (\text{C.9})$$

In the second term, $\text{---} \oplus \text{---}$ has to have some distance L from the endpoints of $\text{---} \oplus \text{---}$.

The pole terms proportional to $\text{---} \oplus \text{---}$ appearing on the r.h.s. of (C.8) and in (C.9) are

$$\begin{aligned} \left\langle \int \int \int \int \text{---} \oplus \text{---} \right\rangle_0 &= \left(2 \left\langle \left(\text{---} \oplus \text{---} \right) \left| \text{---} \oplus \text{---} \right. \right\rangle_{\varepsilon^{-1}} + \mathcal{O}(\varepsilon^0) \right) \\ &\quad \times \left\langle \int \int \text{---} \oplus \text{---} \right\rangle_0, \end{aligned} \quad (\text{C.10})$$

$$\begin{aligned} \left\langle \int \int \int \int \int \left(\text{---} \oplus \text{---} \right) \right\rangle_0 &= \left(\left\langle \left(\text{---} \oplus \text{---} \right) \left| \text{---} \oplus \text{---} \right. \right\rangle_{\varepsilon^{-1}} + \mathcal{O}(\varepsilon^0) \right) \\ &\quad \times \left\langle \int \int \text{---} \oplus \text{---} \right\rangle_0, \end{aligned} \quad (\text{C.11})$$

$$\begin{aligned} \left\langle \int \int \int \int \int \left(\text{---} \oplus \text{---} \right) \right\rangle_0 &= -vd \left(\left\langle \left(\text{---} \oplus \text{---} \right) \left| \text{---} \oplus \text{---} \right. \right\rangle_{\varepsilon^{-1}} + \mathcal{O}(\varepsilon^0) \right) \\ &\quad \times \left\langle \int \int \text{---} \oplus \text{---} \right\rangle_0. \end{aligned} \quad (\text{C.12})$$

In the last equation, we used that

$$\begin{aligned} \left\langle \int \int \int \int \int \left(\text{---} \oplus \text{---} \right) \right\rangle_0 &= \left\langle \int \int \int \int \left(\text{---} \oplus \text{---} \right) \right\rangle_0 \\ &\quad \times \left[\left\langle \left(\text{---} \oplus \text{---} \right) \left| \text{---} \oplus \text{---} \right. \right\rangle_{\varepsilon^{-1}} + \mathcal{O}(\varepsilon^0) \right] \end{aligned} \quad (\text{C.13})$$

and that

$$\begin{aligned} \left\langle \iiint \int \text{---} \bullet \text{---} \bullet \text{---} \bullet \right\rangle_0 &= \left\langle \iiint \int \text{---} \bullet \text{---} \bullet \right\rangle_0 \\ &\quad - 2 \left\langle \iiint \int \text{---} \bullet \text{---} \bullet \right\rangle_0. \end{aligned} \quad (\text{C.14})$$

The second term has no contribution proportional to $\bullet \text{---} \bullet$ and thus can be neglected. The first is evaluated using the equation of motion:

$$\left\langle \iiint \int \text{---} \bullet \text{---} \bullet \right\rangle_0 = -\nu d \left\langle \iint \int \text{---} \bullet \right\rangle_0. \quad (\text{C.15})$$

Together this yields (C.12).

Finally using Eqs. (C.8)–(C.12) gives

$$\left\langle \text{---} \bullet \text{---} \bullet \right\rangle_{\varepsilon^{-1}} = -\frac{\nu d}{2} \left\langle \text{---} \bullet \text{---} \bullet \right\rangle_{\varepsilon^{-1}} \mathcal{O}(\varepsilon^0). \quad (\text{C.16})$$

We further have to show that

$$\begin{aligned} \left\langle \text{---} \bullet \text{---} \bullet \right\rangle_{\varepsilon^{-1}} &= -\nu(d+2) \left\langle \text{---} \bullet \right\rangle_{\varepsilon^{-1}} \\ &\quad + \left\langle \text{---} \bullet \right\rangle_{\varepsilon^{-1}} \left\langle \text{---} \bullet \right\rangle_{\varepsilon^0}. \end{aligned} \quad (\text{C.17})$$

The equation of motion yields

$$\left\langle \iiint \int \text{---} \bullet \text{---} \bullet \right\rangle_0 = -\nu d \left\langle \iint \int \text{---} \bullet \right\rangle_0. \quad (\text{C.18})$$

The integral on the l.h.s. of (C.18) can be decomposed as

$$\left\langle \iiint \int \text{---} \bullet \right\rangle_0 + \left\langle \iiint \int \text{---} \bullet \right\rangle_0. \quad (\text{C.19})$$

The divergencies of the r.h.s. of (C.18) and of the first term in (C.19) are

$$\left\langle \iint \int \text{---} \bullet \right\rangle_0 = \left\langle \text{---} \bullet \right\rangle_{\varepsilon^{-1}} \left\langle \int \text{---} \bullet \right\rangle_0 + \mathcal{O}(\varepsilon^0), \quad (\text{C.20})$$

$$\left\langle \iiint \int \text{---} \bullet \right\rangle_0 = \left\langle \text{---} \bullet \right\rangle_{\varepsilon^{-1}} \left\langle \int \text{---} \bullet \right\rangle_0 + \mathcal{O}(\varepsilon^0). \quad (\text{C.21})$$

The divergence of the second term in (C.19) is extracted as

$$\left\langle \int \int \int \int \text{diagram} \right\rangle_0 = \left\langle \text{diagram} \right\rangle_{\epsilon^{-1}} \left\langle \int \int \text{diagram} \right\rangle_0. \quad (\text{C.22})$$

The second factor on the r.h.s. of (C.22) is

$$\begin{aligned} \left\langle \int \int \int \text{diagram} \right\rangle_0 &= \left\langle \int \int \int \text{diagram} \right\rangle_0 - \left\langle \int \int \int \text{diagram} \right\rangle_0 \\ &= 2\nu \left\langle \int \int \text{diagram} \right\rangle_0 - \left\langle \int \int \int \text{diagram} \right\rangle_0, \end{aligned} \quad (\text{C.23})$$

where again the equations of motion are used. Using (C.18) to (C.23) yields (C.17).

References

- [1] D.R. Nelson, T. Piran and S. Weinberg, eds., *Statistical Mechanics of Membranes and Surfaces*, Proceedings of the Fifth Jerusalem Winter School for Theoretical Physics (1987) World Scientific, Singapore, 1989).
- [2] L. Peliti and S. Leibler, *Phys. Rev. Lett.* 54 (1985) 1690.
- [3] D.R. Nelson and L. Peliti, *J. de Phys.* 48 (1987) 1085.
- [4] Y. Kantor, M. Kardar and D.R. Nelson, *Phys. Rev. Lett.* 57 (1986) 791; *Phys. Rev. A* 35 (1987) 3056.
- [5] M. Paczuski, M. Kardar and D.R. Nelson, *Phys. Rev. Lett.* 60 (1988) 2638.
- [6] J.A. Aronovitz and T. C. Lubensky, *Phys. Rev. Lett.* 60 (1988) 2634.
- [7] M. Paczuski and M. Kardar, *Phys. Rev. A* 39 (1989) 6086.
- [8] Y. Kantor and D. R. Nelson, *Phys. Rev. Lett.* 58 (1987) 2774; *Phys. Rev. A* 36 (1987) 4020.
- [9] F.F. Abraham, W.E. Rudge and M. Plischke, *Phys. Rev. Lett.* 62 (1989) 1757.
- [10] F. F. Abraham and D. R. Nelson, *J. de Physique* 51 (1990) 2653; *Science* 249 (1990) 393.
- [11] Y. Kantor, M. Kardar and D.R. Nelson, *Phys. Rev. Lett.* 57 (1986) 791.
- [12] Y. Kantor, M. Kardar and D.R. Nelson, *Phys. Rev. A* 35 (1987) 3056.
- [13] Y. Kantor and D.R. Nelson, *Phys. Rev. A* 36 (1987) 4020.
- [14] M. Plischke and D. Boal, *Phys. Rev. A* 38 (1988) 4943.
- [15] Y. Kantor and K. Kremer, *Phys. Rev. E* 48 (1993) 2490.
- [16] D. Liu and M. Plischke, *Phys. Rev. A* 45 (1992) 7139.
- [17] G.S. Grest and I.B. Petsche, *Phys. Rev. E* 50 (1994) 1737.
- [18] A. Baumgärtner, *J. Phys. I France* 1 (1991) 1549; A. Baumgärtner and W. Renz, *Europhys. Lett.* 17 (1992) 381.
- [19] D.M. Kroll and G. Gompper, *J. Phys. I France* 3 (1993) 1131.
- [20] G.S. Grest, *J. Phys. I France* 1 (1991) 1695.
- [21] S. Barsky and M. Plischke, *Phys. Rev. E* 50 (1994) 3911.
- [22] G.S. Grest and M. Murat, *J. de Physique* 51 (1990) 1415.
- [23] M. Plischke and B. Fourcade, *Phys. Rev. A* 43 (1991) 2056.
- [24] T. Hwa, E. Kokufuta and T. Tanaka, *Phys. Rev. A* 44 (1991) 2235; X. Wen et al., *Nature* 355 (1992) 426.
- [25] M.S. Spector, E. Naranjo, S. Chiruvolu and J.A. Zasadzinski *Phys. Rev. Lett.* 73 (1994) 2867.
- [26] C.F. Schmidt, K. Svoboda, N. Lei, I.B. Petsche, L.E. Berman, C.R. Safinya and G.S. Grest, *Science* 259 (1993) 952.
- [27] J.A. Aronowitz and T.C. Lubensky, *Europhys. Lett.* 4 (1987) 395.
- [28] M. Kardar and D. R. Nelson, *Phys. Rev. Lett.* 58 (1987) 1289; *Phys. Rev. A* 38 (1988) 966.
- [29] J. des Cloizeaux and G. Jannink, *Polymers in solution, their modelling and structure* (Clarendon Press, Oxford, 1990).

- [30] T. Hwa, *Phys. Rev. A* 41 (1990) 1751.
- [31] F. David, B. Duplantier and E. Guitter, *Phys. Rev. Lett.* 72 (1994) 311.
- [32] F. David, B. Duplantier and E. Guitter, in preparation.
- [33] F. David and K.J. Wiese, *Phys. Rev. Lett.* 76 (1996) 4564.
- [34] K.J. Wiese and F. David, *Nucl. Phys. B* 450 (1995) 495.
- [35] This point is already explained (not using the MOPE formalism) in B. Duplantier, T. Hwa and M. Kardar, *Phys. Rev. Lett.* 64 (1990) 2022.
- [36] B. Duplantier, *Phys. Rev. Lett.* 62 (1989) 2337.
- [37] F. David, B. Duplantier and E. Guitter, *Nucl. Phys. B* 394 (1993) 555.
- [38] F. David, B. Duplantier and E. Guitter, *Phys. Rev. Lett.* 70 (1993) 2205.
- [39] E. Guitter and J. Palmeri, *Phys. Rev. A* 45, (1992) 734;
M. Goulian, *J. Phys. II France* 1 (1991) 1327;
P. Le Doussal, *J. Phys. A* 25 (1992) L469.
- [40] P.G. de Gennes, *Phys. Lett.* 38 A (1972) 339.
- [41] B. Duplantier, in Ref. [1].
- [42] F. David and E. Guitter, *Europhys. Lett.* 5 (1988) 709.